Wayne State University Dissertations

January 2021

The Role Of Biomaterial Substrate In Stem Cell Fate Determination

Zhenjie Liu
Wayne State University

THE ROLE OF BIOMATERIAL SUBSTRATE IN STEM CELL FATE DETERMINATION

by

ZHENJIE LIU

DISSERTATION

Submitted to the Graduate School

of Wayne State University,

Detroit, Michigan

in partial fulfillment of the requirements

for the degree of

DOCTOR OF PHILOSOPHY

2021

MAJOR: PHYSIOLOGY

Approved By:

_____
Advisor   Date

_____

_____

_____

_____

DEDICATION

This dissertation is dedicated to my loving parents, Jingxun Liu and Xiaojing Liu, for your

guidance, support, and encouragement during my studying period; to my dear wife, Li Tao, for

your support, understanding, and love.

ACKNOWLEDGEMENTS

TABLE OF CONTENTS

LIST OF TABLES

LIST OF FIGURES

LIST OF ABBREVIATIONS

ACMFP	Aligned contiguous microfiber platform
ASMFP	Aligned sub-micro-fiber platform
BDNF	Brain-derived neurotrophic factor
BMP	Bone morphogenetic protein
CN	Cochlear nucleus
CNS	Central nerves system
DMSO	Dimethyl sulfoxide
ECM	Extracellular matrix
EGF	Epidermal growth factor
ESC	Embryonic stem cell
ESN	Embryonic stem cell-derived neurons
FDA	Food and Drug Administration
FGF	Fibroblast growth factor
GDNF	Glial cell line-derived neurotrophic factor
GFP	Green fluorescent protein
IGF-1	Insulin-like growth factor 1
LIF	Leukemia inhibitory factor
NB	Neuroblasts
NGF	Nerve growth factor
NNE	Non-neural ectoderm
NSC	Neural stem cell

NT-4	Neurotrophin-4
OPO	Otic placode and otocyst
PBS	Phosphate-buffered saline
PCL	Polycaprolactone
PDMS	Polydimethylsiloxane
PDL	Poly-D-Lysine
PFA	Paraformaldehyde
PI	Propidium Iodide
PLGA	Poly (lactic-co-glycolic acid)
PLO	Poly-L-ornithine
PNS	Peripheral nerves system
RA	Retinoic acid
SGN	Spiral ganglion neuron
SHH	Sonic hedgehog
THF	Tetrahydrofuran
TSP1	Thrombospondin 1

CHAPTER 1 – INTRODUCTION

(This chapter contains previously published material. See Appendix A.)

Embryonic stem cells (ESCs) and their development

Stem cells are widely studied as they provide a suitable cell replacement source for research and clinical therapy (Gao et al., 2018; Huang and Zhang, 2019; Mead et al., 2015). Stem cells have two properties, which are self-renewal and pluripotency (He et al., 2009; Liu et al., 2019). Stem cells are mainly divided into three types of cells by their origins: ESCs, tissue-specific stem cells, and induced pluripotent stem cells (Li et al., 2016; Lin et al., 2017; Thomson et al., 1998). In this dissertation, we mainly focus on the research of the ESCs.

Embryonic stem cells (ESCs) are collected from the inner cell mass of the blastocyst in the early stages of embryonic development, followed by cell line established and cultured *in vitro* for further study (Baldwin, 2009; Biswas and Hutchins, 2007; Thomson et al., 1998). ESCs demonstrate a high capacity for self-renewal and pluripotency, as summarized in Figure 1. Firstly, the ESCs can be kept in the undifferentiated stage *in vitro* by culture with a feeder cell layer, specific serum, or leukemia inhibitory factor (LIF) treatment (Biswas and Hutchins, 2007; Fleischmann et al., 2009; Ludwig and J, 2007; Martello and Smith, 2014; Wei et al., 2018). The undifferentiated ESCs have the ability of differentiation and proliferation. The ESCs will support a stable and abundant source of cells for further research and clinical application. Secondly, ESCs have a strong ability of pluripotency. ESCs can differentiate into primitive ectoderm cells, which can then differentiate into any of the three primary germ layer cell types (mesoderm, ectoderm, and endoderm) during gastrulation *in vivo* (Baldwin, 2009; Thomson et al., 1998). These three cell types have the incredible capacity to differentiate into approximately 220 different types of

mature cells to carry out specific functions *in vivo*. Moreover, many papers reported that similar to their *in vivo* development, ESCs can be manipulated *in vitro* to cause differentiation into various cell types, such as nerve cells, bone cells, blood cells, and immune cells (Kuhn et al., 2014; Liu et al., 2018b; Smith et al., 2015; Vanhee et al., 2015; Yang et al., 2008). In this dissertation, we mainly focus on neural regeneration from ESCs.
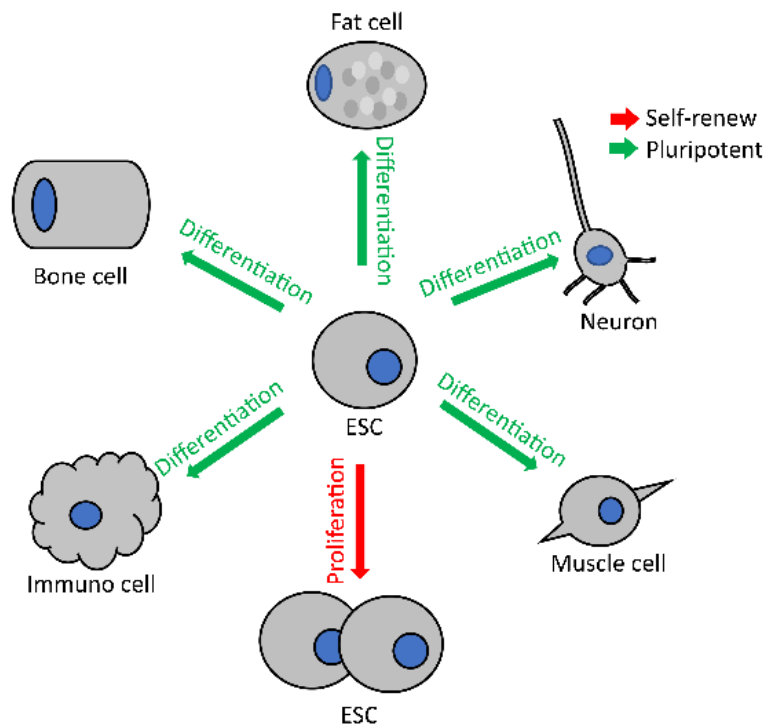
Figure 1. Diagram representing embryonic stem cell (ESC) properties. ESCs possess two unique properties, which are self-renewal and pluripotency. For self-renewal (red arrow), ESCs can be kept in the undifferentiated stage and they can proliferate into new ESCs with the properties of the previous cell (Biswas and Hutchins, 2007; Fleischmann et al., 2009; Ludwig and J, 2007; Martello and Smith, 2014; Wei et al., 2018). For the pluripotent (green arrow), ESCs can differentiate into variety of cell types, such as fat cells, neurons, muscle cells, immune cells, and bone cells (Kuhn et al., 2014; Liu et al., 2018b; Smith et al., 2015; Vanhee et al., 2015; Yang et al., 2008). The diagram was self-designed and all contents were based on studies and conclusions in the following literature (Biswas and Hutchins, 2007; Fleischmann et al., 2009; Kuhn et al., 2014; Liu et al., 2018b; Ludwig and J, 2007; Martello and Smith, 2014; Smith et al., 2015; Vanhee et al., 2015; Wei et al., 2018; Yang et al., 2008).

Neural differentiation of ESC

Newly generated ESC-derived neurons have been widely used in stem cell and neuron

replacement research (Craff et al., 2007; Han and Hu, 2020; Liu et al., 2018b). Based on the

requirements of the newly generated neurons, there are several methods used to generate

different types of neurons from the ESCs (Figure 2). The ESCs are cultured as an embryoid body
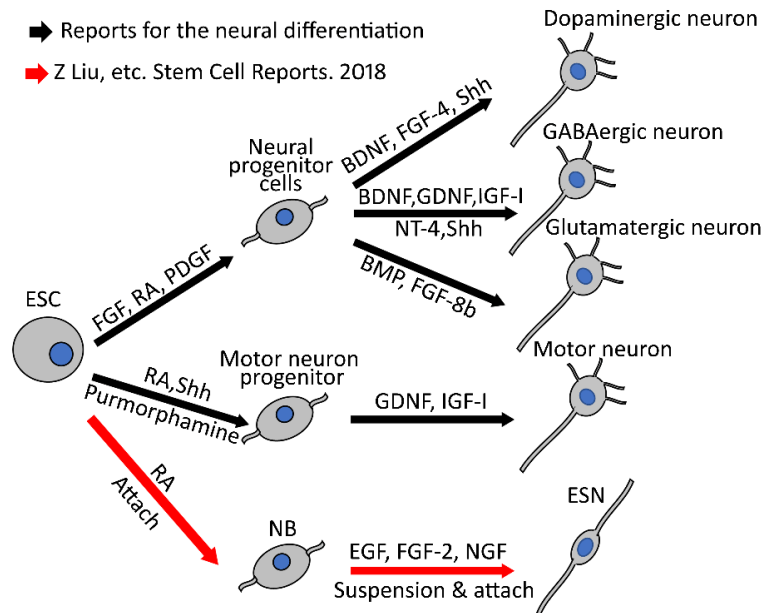
Figure 2. Diagram showing the neural differentiation of ESCs. Several methods were used to guide ESCs differentiate into different type of neurons. For example, brain-derived neurotrophic factor (BDNF), fibroblast growth factor 4 (FGF-4), and sonic hedgehog (Shh) treatment can guide the dopamine neurons generation (Alizadeh et al., 2019; Malczynska et al., 2019), insulin-like growth factor 1 (IGF-I) and glial cell line-derived neurotrophic factor (GDNF) treatment can guide the motor neurons generation (Fang et al., 2019; Rabinovsky et al., 2003), fibroblast growth factor 8b (FGF-8b) and (bone morphogenetic protein) BMP treatment can guide the glutamatergic neurons generation (Liu et al., 2018b), and BDNF, GFND, IGF-1, neurotrophin-4 (NT-4), and Shh treatment can guide the GABAergic neurons generation. Previously, we reported a novel neural differentiation method to generate glutamatergic bipolar neurons from ESCs via retinoic acid (RA), epidermal growth factor (EGF), FGF-2, and nerve growth factor (NGF) treatment (Liu et al., 2018b). The diagram was self-designed and all contents were based on studies and conclusions in the following literature (Alizadeh et al., 2019; Fang et al., 2019; Liu et al., 2018b; Malczynska et al., 2019; Rabinovsky et al., 2003).

at the early stage, followed by chemical treatments to induce the ESCs to differentiate into neural

progenitor cells (Ouyang et al., 2015; Shparberg et al., 2019). At the mid- and end-stages of the

neural differentiation, different growth factors or cytokines are used to treat the cells to generate

different neuron types. Specifically, ESCs can differentiate into the dopamine neurons via brain-

derived neurotrophic factor (BDNF), fibroblast growth factor 4 (FGF-4), and sonic hedgehog (Shh) treatments (Alizadeh et al., 2019; Malczynska et al., 2019). The ESCs can differentiate into the motor neurons via insulin-like growth factor 1 (IGF-I) and glial cell line-derived neurotrophic factor (GDNF) treatments (Fang et al., 2019; Rabinovsky et al., 2003). The ESCs can differentiate into glutamatergic neurons via fibroblast growth factor 8b (FGF-8b) and bone morphogenetic protein (BMP) treatments (Liu et al., 2018b). The ESCs can differentiate into GABAergic neurons via BDNF, GDNF, IGF-1, neurotrophin-4 (NT-4), and Shh treatments (Wang et al., 2008).

Liu and colleagues of Dr. Hu's laboratory (2018) have previously reported a novel neural differentiation method to generate bipolar glutamatergic neurons from ESCs *in vitro* (Figure 3A-
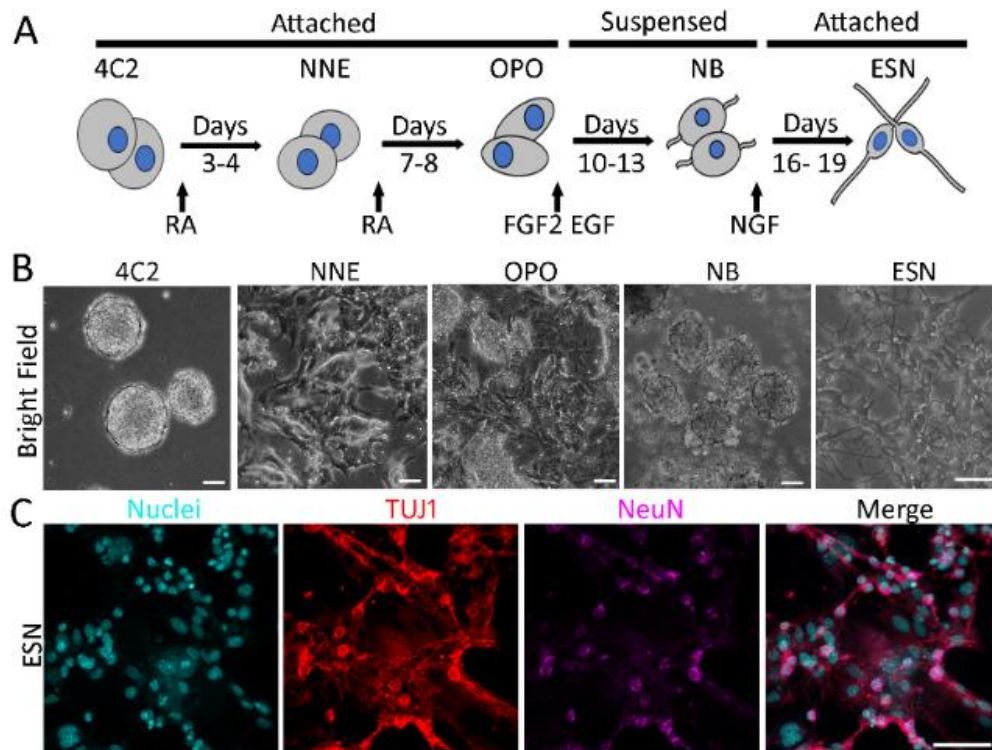
Figure 3. "Step by step" neural differentiation of the ESCs. (A) Diagram of the "step by step" neural differentiation from the ESC cell line (4C2). (B) Bright field images showed the cell morphology of the different differentiation time points, including non-neural ectoderm (NNE), otic placode and otocyst (OPO), NB, and ESN. (C) The immunofluorescence images showed the ESNs were double label by two neuron markers TUJ1 and NeuN. Diagram and figures representing a particular generation process of ESN and based on study from Liu and colleagues (Liu et al., 2018b). Scale bars in B and C are 50 μm.

B) (Liu et al., 2018b). This new neural differentiation method mimics the physiological process of neuron development. ESCs were treated with retinoic acid (RA) to form the neuroblasts (NBs) at the early stage. At the mid- and end-stage (cell differentiation period from neural stem cell to neuron was defined as mid- and end- stage) of the neural differentiation, the epidermal growth factor (EGF), FGF-2, and nerve growth factor (NGF) were used to treat the NBs to differentiate into ESC-derived neurons (ESNs). These ESNs showed bipolar morphology and expressed neuron-specific genes and proteins (Figure 3C) (Liu et al., 2018b).

The newly generated neurons need to have native neuronal function, including the ability to transmit signals between cells, if they are to be used for neuron replacement therapy. In our previous report, ESNs were showed to have the ability of making connections with endogenous neurons and sensory cells *in vitro* for signal transfer (Figure 4) (Liu et al., 2018b). The regenerated
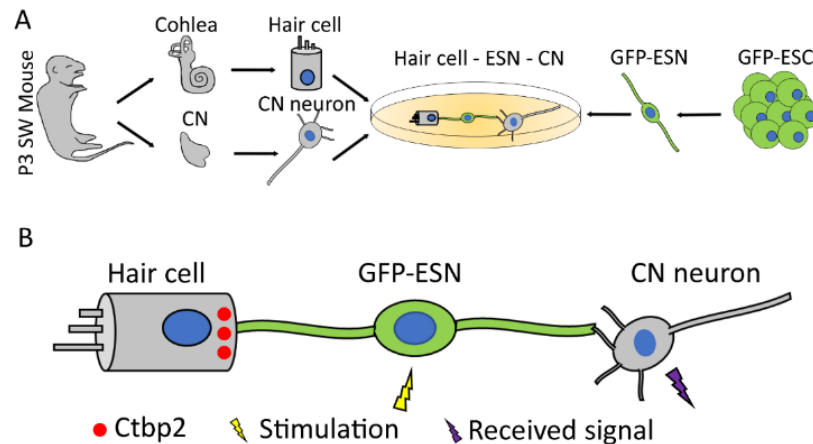
Figure 4. Diagram representing properties of ESNs connected with a hair cell and CN neuron. (A) Diagram of a tri-culture of a green fluorescent protein prelabeled ESN (GFP-ESN), a native hair cell and a CN neuron. (B) Diagram of a hair cell, ESN, and CN connection *in vitro*. Ctbp2 which is the hair cell synapse marker expressed in the ESN connected hair cell. The CN neuron can receive ESN's electrophysiological signal via ESN-CN connection *in vitro* (Liu et al., 2018b). All contents were based on study from Liu and colleagues (Liu et al., 2018b).

ESNs are a potential cell source for neuron replacement research and therapy (Craff et al., 2007; Han and Hu, 2020; Liu et al., 2018b). However, the newly generated ESNs had some

disadvantages: (1) The regeneration yield of ESNs was low, which mean less neurons were available at the end of experiments; (2) The ESNs' neurites were short and nondirective, which limited for the formation of the connection; (3) The synapses between ESNs and native neurons were immature, showing low expression of the synapse vehicle & protein markers, and low electrophysiology activity compared with native neurons. These disadvantages may limit their therapeutic effect. In this dissertation, we sought to overcome these limitations via novel methodology.

Biomaterial-induced cell growth and differentiation

Two methods exist for stimulating neural differentiation: the biochemical signal stimulation method and the physical signal stimulation method (Figure 5). The biochemical
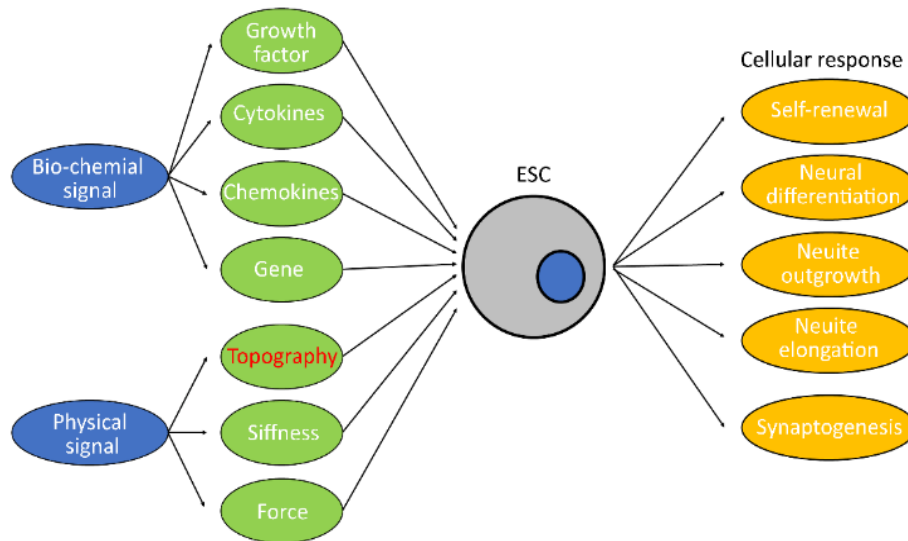
Figure 5. Diagram of the factors that induce cellular responses in ESC. Bio-chemical signals (Dong et al., 2017; Hu et al., 2019; Lau and Hudson, 2010; Li et al., 2016), which include growth factor, cytokines, chemokines, and gene editing and physical signals, which included topography, stiffness, and force, can contribute the ESC's cellular response, such as self-renewal, neural differentiation, neurite outgrowth & elongation, and synaptogenesis (Jain et al., 2020; Zhu et al., 2019; Zimmermann and Schaffer, 2019). The diagram was self-designed and all contents were based on studies and conclusions in the following literature (Dong et al., 2017; Hu et al., 2019; Jain et al., 2020; Lau and Hudson, 2010; Li et al., 2016; Zhu et al., 2019; Zimmermann and Schaffer, 2019).

Signal stimulation method uses growth factors, cytokines, chemokines, small molecular treatment, or gene editing methods to stimulate neural differentiation and neuron maturation (Dong et al., 2017; Hu et al., 2019; Lau and Hudson, 2010; Li et al., 2016). The physical signal stimulation method alters the microenvironment to stimulate cell proliferation, differentiation, and maturation (Jain et al., 2020; Zhu et al., 2019; Zimmermann and Schaffer, 2019). In this context, the microenvironment includes matrix topography, matrix stiffness, and mechanical forces. The extracellular matrix has been reported to stimulate neural differentiation from the neural stem cells via the integrin receptor (Long and Huttner, 2019; Pan et al., 2014). The micro-pattern matrix can guide neuron growth and migration (Cheng and Kisaalita, 2010; Yang et al., 2005). The micro-fluid solution can stimulate neuron growth (Neto et al., 2016). In addition, the micro-electric field can stimulate neurite elongation and synaptogenesis (Alexander et al., 2006; McCaig et al., 2000). However, there are fewer reports that micro-patterns could stimulate neural differentiation. Moreover, the range of functional sizes of the micro- (10- 1000 μm), submicro- (1- 10 μm), and nano- (0.1- 1 μm) patterns to guide neurite outgrowth and neural differentiation are not clear. In this dissertation, different sizes of micro-, submicro-, and nano-pattern platforms will be designed, fabricated, and evaluated for their capacity to stimulate neural differentiation, neurite outgrowth, and synaptogenesis.

During development, the ESCs live in a complex micro-environment *in vivo*. The micro-environment includes topographical information, physiological cues, soluble factors, and cell-cell interactions. The micro-, submicro-, and nano-pattern topography of the micro-environment play a vital role in the ESC growth, proliferate, development, and differentiation *in vivo* (Govey et al., 2013; Keung et al., 2010; Lapointe et al., 2013). To mimic the topography of the micro-

environment, different types of biomaterials have been used for the ESC *in vitro* culturing. These biomaterials can be divided into fiber, groove, gel, pore, and tube by their 3D shape (Cheng and Kisaalita, 2010; Gu et al., 2016; Onoe et al., 2016; Yang et al., 2017). They also can be divided by their material type into metal, silicon, gel, polymer (Grossemy et al., 2019; Mantecon-Oria et al., 2020; Yan et al., 2017).

The different shapes, properties, and functions of biomaterial platforms have been designed, fabricated, and applied in cell biological research, tissue assembly, and tissue implantation (Aamodt and Grainger, 2016; Chew and Danti, 2017; Gao et al., 2019). This dissertation aims to study the micro-, submicro-, and nano-pattern topography-induced neural differentiation and maturation. To achieve the aims, the biomaterial used in this dissertation needs to have the following properties: (1) The biomaterial needs to be approved by the Food and Drug Administration (FDA), which can be used in tissue implantation; (2) The material needs to have good biocompatibility, which is not toxic for the cell and tissue culture; (3) The material needs to be biodegradable, but stable during the experiment and degraded after implantation; (4) The materials need to be plastic, in which the shape and size of the materials are controllable in the micro-, submicro-, and nano-level.

Significance for cell biology and cell replacement

Biomaterial platforms are widely used and studied in stem cell research. For example, a bio-platform could be used to maintain stem cells in the undifferentiated stage *in vitro* (Fisher et al., 2010). The bio-platform has also been used to stimulate the cardiomyocytes, neurons, and epidermis cells regeneration (Haldar et al., 2019; Kim et al., 2014; Yeung et al., 2019). The bio-platform was also used in a cell-matrix interaction study and matrix-induced intracellular

pathway research (Bax et al., 2019; Cha et al., 2017). The designed, fabricated, and evaluated

micro-, submicro-, and nano-pattern platforms will open a new field of stem cell research in

neural regeneration.

The stem cell and biomaterial studies have been applied mainly to cell replacement

therapy (Bhardwaj et al., 2017; Gao et al., 2018; Huang and Zhang, 2019; Mead et al., 2015). In

this dissertation, the biomaterial-induced neural regeneration method will be studied as it may

provide a suitable approach to alleviate native neuron injury of the peripheral nerves system

(PNS) and central nerves system (CNS) (Figure 6). Stem cells are a suitable cell source for neuronal
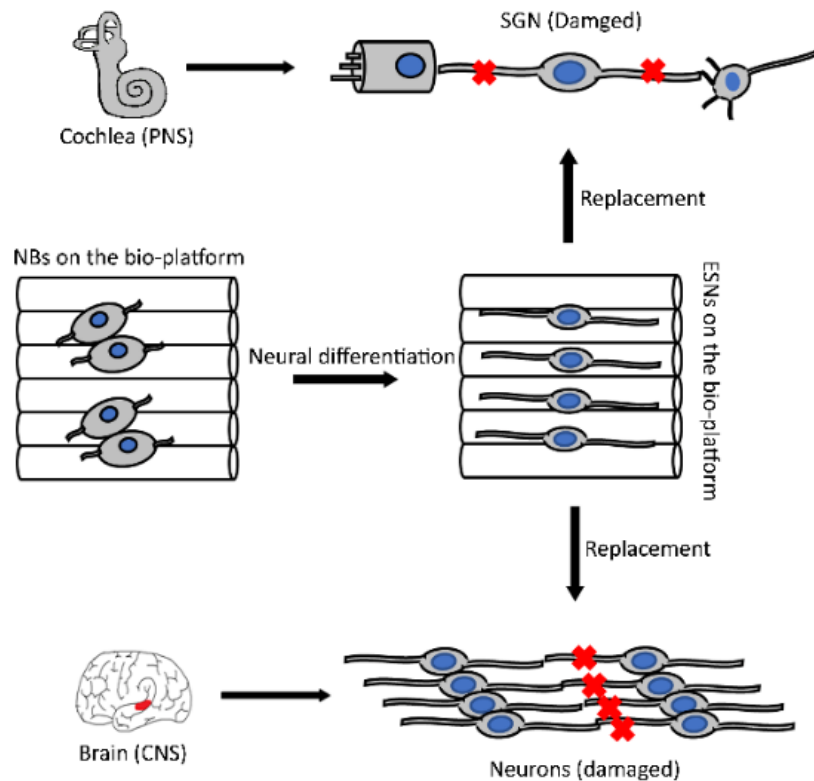
Figure 6. Diagram of expected application of the ESNs with bio-platform. The NBs were attached and differentiated on the bio-platform, which would form several ESNs on the bio-platform. The combination of ESNs and biomaterial platform could be used in the replacement of damaged spiral ganglion neurons (SGN) of the PNS and damaged neurons of the CNS.

degeneration diseases, such as cardiovascular (ischemic heart disease and heart failure) and

respiratory nerve systems (acute respiratory distress syndrome) recovery (Bagno et al., 2018;

Lanzoni et al., 2021). The bio-platform will stimulate stem cell differentiation, growth and

migration *in vitro* (Dietrich et al., 2018; Lv et al., 2017; Mashinchian et al., 2015). Stem cell

injections always result in a large amount of cell loss and off-target effects. Combining stem cells and biomaterials will improve cell viability and anchoring after the implantation *in vivo* (Ashe et al., 2020; Leach et al., 2019).

Application in the injured PNS: SGN damage-induced hearing loss

Hearing loss, which is known as hearing impairment, is the primary disability affecting approximately 10%- 15% of the population in the world (Belzner and Seal, 2009). The main symptom of hearing loss is a partial or total inability to hear. Hearing loss may happen at all stages of life. For newborn children, it is reported that 0.2%- 0.3% of children have profound hearing loss. The hearing loss that happens in this stage will influence severe consequences for children, such as the risk for irreversible speech, language, and cognitive deficits (Lieu et al., 2020). For adults (26- 69 years old), it is reported that 26 million (15%) of Americans have a high-frequency hearing loss. For the senior adults (65-74 years old and older than 74 years old), there are 30% (65-74 years old) and 47% (older than 74 years old) of Americans have impaired hearing. Hearing loss in adults induces loss of educational and employment opportunities, social withdrawal, and emotional problems (anxiety, etc.) (Contrera et al., 2016; Michels et al., 2019).

Hearing loss is usually caused by many factors, including exposure to loud sounds, noise at work, trauma, ototoxicity (overdose the ototoxic medications, such as aspirin, ibuprofen, and naproxen), aging, ear infections, developmental deficiency (Cohen et al., 2014; Mulwafu et al., 2016). Hearing loss is divided into three major types: conductive hearing loss, sensorineural hearing loss, and mixed hearing loss. Spiral ganglion neuron (SGN) damage-induced hearing loss, which is sensorineural hearing loss, is caused by SGN damage and degeneration (Epstein and Reilly, 1989; Kuhn et al., 2011). Spiral ganglion neurons play a vital role in the auditory signal

transmission pathway (Carricondo and Romero-Gomez, 2019). Spiral ganglion neurons are the "bridge" cells that connect and transmit the electrical signal between the hair cells and CNs. Partial or total damage of the SGNs will break the connections and inhibit or block the auditory pathway, respectively, which will cause sensorineural hearing loss. As the generation of SGNs only happens during early mammalian stages (embryo day 8 to postnatal day 28 of mouse), they cannot regenerate *in vivo* to cure the damaged cells. In other words, the SGN-damaged induced hearing loss is irreversible.

Our previous report showed that the newly generated ESNs could be the potential source of cells to replace the damaged SGN (Liu et al., 2018b). The ESNs can grow and differentiate on our newly designed bio-platform to get native bungee-like (highly parallel) and mature neurons (Liu and Hu, 2018). Combining the ESNs and bio-platform can be used in SGN replacement research and therapy in the future.

Application in the CNS injured: Central nervous system disease

Besides application to PNS nerve injury, the ESNs and the bio-platform system can also contribute to treatment of CNS diseases (Ashammakhi et al., 2019; Lim and Spector, 2017). CNS diseases or disorders are caused by damage of the central nerve (Cacabelos et al., 2016). These damages will affect the structure or function of the spinal cord or brain. The main signs and symptoms are loss of feeling, memory loss, tremors, slurred speech. The representative diseases are Alzheimer, Huntington, Parkinson. Many groups are currently studying bio-platform-induced cell implantation to treat spinal cord damaged. The microfiber platform can restore the damaged spinal cord by implantation with stem cell-derived neurons (Grijalvo et al., 2019). The study and usage of biomaterials will open a new avenue in CNS disease therapy.

Aims of dissertation research

Based on these new neural differentiation methods and novel findings of biomaterials, the central hypothesis to be investigated in this dissertation research is that a submicron fiber substrate can stimulate ESC-derived neural differentiation and maturation *in vitro*. There are three integrative specific aims pursued (Figure 7):
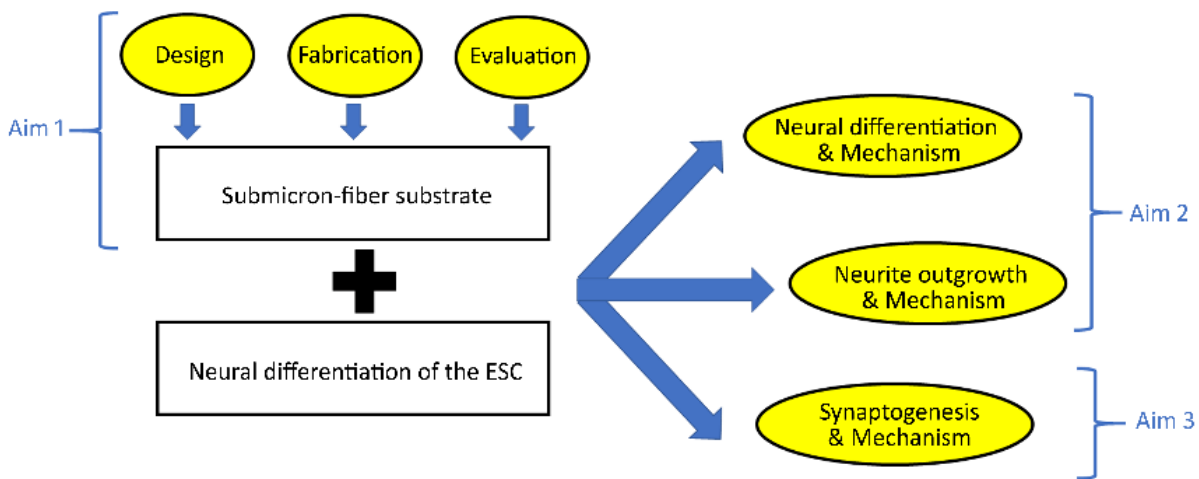
Figure 7. Road map of the specific aims. Aim 1: Fabricate the submicron fiber substrate and determine its physical, chemical, and biological properties; Aim 2: determines whether submicron fiber substrates stimulate ESN differentiation and maturation in vitro via the adhesion molecule-cytoskeleton signaling pathway; Aim 3: determines whether submicron fiber substrates can stimulate the synaptogenesis between ESNs and native CN neurons by purified TSP1 protein incorporated in the substrates.

Aim 1 is to Fabricate the submicron fiber substrate and determine its physical, chemical, and biological properties. We hypothesize that a submicron fiber substrate can be fabricated and used in the stem cell culture. The novel submicron fiber substrate will be fabricated using the micro-fluid chip system and electrospinning equipment. The physical, chemical, and biological properties of the submicron fibers, including diameter, alignment, biocompatibility, and biodegradability, will be evaluated to determine whether it is a suitable substrate for stem cell growth and differentiation.

Aim 2 will determine whether submicron fiber substrates stimulate ESN differentiation

and maturation *in vitro* via the adhesion molecule-cytoskeleton signaling pathway. We hypothesize that the submicron fiber substrate can induce ESN differentiation and maturation via the integrin receptor. ESNs will be cultured on the submicron fiber substrates, followed by evaluating neural differentiation and neurite outgrowth by immunostaining assays. Additionally, integrin receptors will be knocked down by short hairpin RNA (shRNA) technology to elucidate whether it is the critical receptor to sense the extracellular matrix signaling.

Aim 3 will determine whether submicron fiber substrates can stimulate the synaptogenesis between ESNs and native cochlear nuclei (CN) neurons by purified thrombospondin 1 (TSP1) protein incorporated in the substrates. Our previous reported that the TSP1 was a key protein which could stimulate the synaptogenesis between the ESNs and CNs *in vitro* culture (Liu et al., 2018b). Herein, we hypothesize that submicron fiber substrates incorporated with purified TSP1 protein can stimulate synaptogenesis between ESNs and native CN neurons. The purified TSP1 protein will be incorporated into the fiber substrates, which will be released into the culture medium in the co-culture containing ESNs and native CN neurons. The synaptogenesis between ESNs and native CN neurons will be evaluated using immunofluorescence to determine the role of released TSP1 in synaptogenesis.

In summary, this dissertation studies the role of submicron fiber substrates in differentiation, maturation, and synapse formation of stem cell-derived neurons, which provides a critical step for the integration of newly generated neurons into the native auditory system to rebuild the acoustic circuit *in vitro*. The success of this research will suggest the possibility of developing novel strategies to utilize ESC-derived neurons to treat hearing loss and other neurodegenerative diseases.

CHAPTER 2 – DESIGNING, FABRICATING, AND EVALUATING THE ACMFP AND ASMFP

(This chapter contains previously published material. See Appendix B.)

Abstract

clinical therapy.

Overview of the fiber platform

Biomaterial, which has a fiber-like structure, is widely used in cell biology research and clinical therapy. Different sizes, types, and protein-treated fiber platforms were designed, fabricated, and used in the research (Ong et al., 2018; Saveh-Shemshaki et al., 2019). For example, solid nano-fiber was used to stimulate stem cell differentiation *in vitro* (Silantyeva et al., 2018). The submicro-fiber was used to guide neuron growth (Kim et al., 2006). The hollow microfiber was used to rebuild the nerve tissue *in vitro* for spinal cord damage therapy (Golafshan et al., 2018; Morelli et al., 2021). In this dissertation, we mainly focus on fiber-like topography to induce stem cell fate. Different sizes of the fiber platforms were needed to be designed, fabricated, and evaluated. The size range for the fiber platform is from the micro-level to the nano-level. As the limitation about the fiber material and fabricated method, two fiber platforms were designed separately to achieve these aims, which were poly (lactic-co-glycolic acid) (PLGA)-based ACMFP (micro-level) and polycaprolactone (PCL)-based ASMFP (submicro- and nano-level).

PLGA for the ACMFP

To study the role of the micro-topography in the stem cell differentiation, an aligned and contiguous micro-pattern platform was needed. PLGA, a co-polymer material, was chosen as a biomaterial to fabricate the platform, as its multiply advantages (Astete and Sabliov, 2006; Kapoor et al., 2015). Firstly, the PLGA has good biocompatibility approved by the FDA for research and clinical usage (Zheng et al., 2018a). In addition, PLGA has little to no toxicity in cell culture and implantation (Chen et al., 2020a; Zheng et al., 2018a). Secondly, the PLGA is a biodegradable material (Du et al., 2020). It can degrade and disappear gradually *in vivo* and *in vitro*. The

degraded material of PLGA also shows good biocompatibility and metabolically (absorption and metabolism by organism) *in vivo.* The biodegradation speed is determined by its molecular weight. The biodegradation speed of PLGA, which is used in this dissertation, is 2-3 months, which does not influence the research *in vitro*. Lastly, the PLGA is plastic. It can be shaped into different structures, such as membrane, fiber, porous, tube (Lai et al., 2019; Sitt et al., 2016; Wang et al., 2019; Zheng et al., 2018b). However, the PLGA also has a disadvantage that will influence the micro-topography induced research. It is reported that PLGA fiber materials can shrink during *in vitro* culturing (Liu et al., 2018a). The reason is that the glass transition temperature (threshold temperature at which a material changes from plastic phase to glass) of the PLGA is 45-55°C, which is close to the cell culture (37°C). This low-temperature environment of the PLGA will keep the material in the plastic stage. The plastic stage of PLGA easily changes the shape and shrink spontaneously. To overcome this weakness, a method was needed to over-heat the PLGA fiber above the transaction temperature to change it into the glass stage, which can help PLGA fiber maintain a stable structure.

Micro-fluid chip-based system for the ACMFP

To fabricate the micro-pattern platform, many systems have been used widely. Micro-groove molds were used to fabricate the polydimethylsiloxane (PDMS) groove platform (Yang et al., 2017). The micro-fluid chip-based system was used to fabricate the micro-fiber (size range from 30 μm to 300 μm) (Hwang et al., 2008). In the micro-fluid chip-based system, the PLGA-DMSO solution was mixed and pumped into the chip as a micro-fluid flow. This flow would combine with the water solution in the chip. The PLGA was solidified and moved out of the chip as a fiber-like structure via the flow of PLGA solution and water solution. The different sizes of

the PLGA micro-fiber fiber can be fabricated by changing the PLGA solution and water solution flow rate. In this chapter, an updated micro-fluid chip-based system was used to fabricate the ACMFP.

PCL for the ASMFP

To study the role of submicro- and nano-topography in the stem cell differentiation, an aligned submicro-pattern platform was needed. The PLGA-based ASMFP showed that PLGA was not suitable for the submicro-level fiber platform fabrication as its fibers would break or degrade completely into small fragments in 37°C (Figure 8). To overcome this weakness, material (Goodwin et al., 2018; Vivi et al., 2019). In other words, it degrades little by little *in* cells and

Figure 8. PLGA based nano-fiber with the Pluronic F127 treatment. PLGA was used to fabricate the nano-fiber platform by electrospinning system. The nano-fiber platforms were fabricated in (A) and (C) at room temperature. All the platforms showed a fiber-like structure. After the platforms were incubated at 37 °C for 24 hours, the fiber structure of the control (B) and Pluronic F127 (D) treated groups disappeared, which indicated that PLGA-based nanofiber was hard to keep nano-fiber structure in 37 °C by the anti-shrinkage solution treatment. The data is collected using ASMFP produced by the same batch of the PCL solution. Scale bar is 10 μm in D.
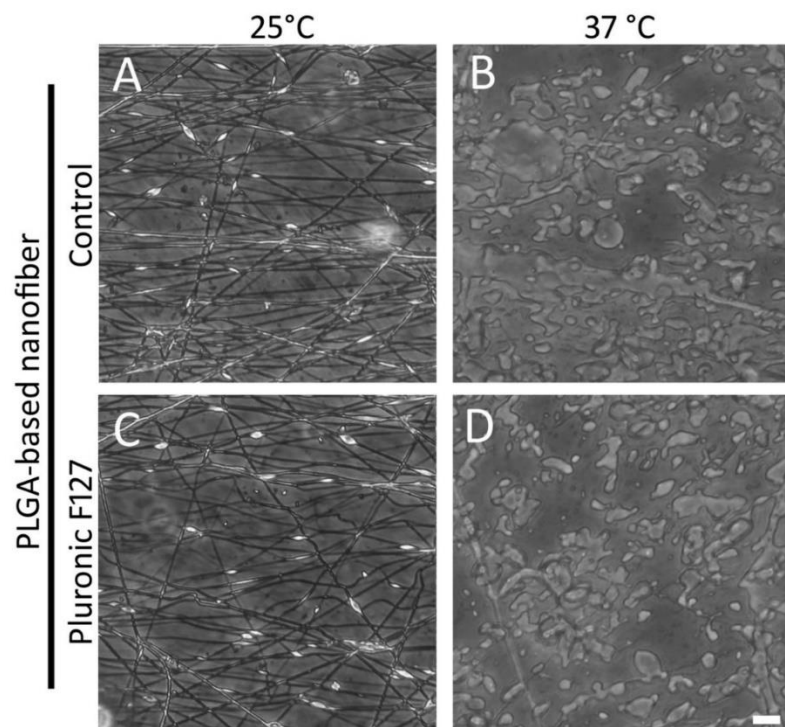
another polymer, PCL, was used to fabricate the ASMFP. PCL has lots of advantages to fabricate the ASMFP. Firstly, the PCL has good biocompatibility, which means that it is not toxic to the

tissues (Feng et al., 2019; O'Leary et al., 2020). Secondly, the PCL is a biodegradable *vivo* and *in vitro*. The biodegradation speed is determined by its molecular weight. Thirdly, the PCL is a plastic material too. It can be shaped into different kinds of structures (Chen et al., 2020b; Mo et al., 2006; Xu et al., 2018). Lastly, unlike the PLGA, the PCL has a low glass transition temperature (-60°C), which means that it will maintain in the stable glass stage after fabrication. In other words, it will not shrink in the 37°C. However, the PCL is a hydrophobic material that limits cell attachment and growth (Moran et al., 2019; Narayanan et al., 2018; Zhang et al., 2016). To overcome this weakness, a hydrophilic protein-coated method was used and evaluated in this dissertation.

Electrospinning system for the ASMFP

As the micro-fluid chip-based system only can fabricate a micro-level fiber, a nano-fiber fabrication system was needed for this dissertation. Electrospinning systems have been used widely to fabricate the submicro- and nano-level fibers (Bhardwaj and Kundu, 2010). The polymer solution is loaded with a high voltage (more than 8kV) in the electrospinning system. The polymer solidifies and changes into the submicro- and nano-level fiber-like structure in the electrospinning system. These newly generated fibers will attach to the collection unit, which loads with negative voltage. To create the aligned fiber platform, a rotating metal wheel was used to collect the fiber. The rotation speed of the wheel will determine the alignment value of the fiber platform. In addition to changing the other parameters in the system, such as micro-fluid rate, spin distance, loaded voltage, fiber platforms with different sizes were fabricated. In this dissertation, this universal electrospinning system was used to fabricate the ASMFP.

Rationale and hypothesis for Chapter 2

An aligned biomaterial-based platform was needed to apply and study the topography-induced neural differentiation. To mimic the micro-level topography, a novel platform was supposed to design and fabricate in the updated micro-fluid chip-based systems to mimic the micro-level topography. The ACMFP's physical, chemical, and biological properties would be tested, such as fiber size, alignment level, plastic, and biocompatibility. To mimic the submicro- and nano-level topography, a novel platform was supposed to design and fabricate in the electrospinning systems. Similar to the ACMFP, the ASMFP's physical, chemical, and biological properties would be tested. The chemical treatment method would be used to overcome the weakness of this platform.

Materials and Methods

Design of the ACMFP

A novel micro-fiber platform was needed to study the micro-pattern platform's role in stem cell differentiation. To achieve this aim, the ACMFP was designed, as shown in Figure 9.
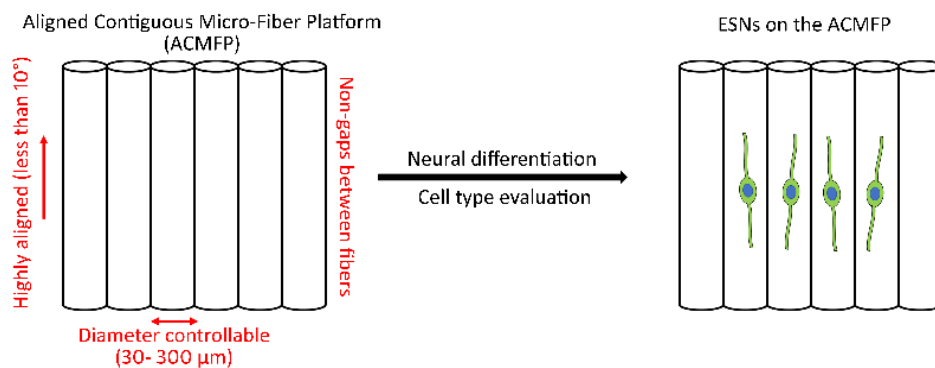
Figure 9. Designed diagram of the ACMFP. The ASMFP was designed as a platform which established by parallel (the angle between fibers were less than 10 °C) micro-fibers. These fibers, which sizes were 30- 300 μm, were fully covered the surface and show no gaps between fibers to support a fiber-like topography for the further neural differentiation experiment with cell type evaluation.

Firstly, the ACMFP was established with one layer of parallel micro-fibers. These fibers were

contiguous and parallel, which avoided the gaps between the fibers and showed high aligned

structure. In addition, the micro-fibers diameter needed to be controllable, which was used to

study the range of the functional fiber size.

ACMFP equipment set up and fabrication

The ACMFP equipment (Figure 10) was set up and updated based on the previous

Figure 10. Updated micro-fluid chip-based system for the ACMFP fabrication. (A) Diagram of the updated micro-fluid chip-based system. The core solution and sheath solution were pumped as the micro-fluid into the chip. PLGA of the core solution was solidified when met with the sheath solution and pumped out the chip as a fiber-like structure. The collecting part collected the fiber into the alignment and contiguous structure by rotation and movement. (B) Overview of the equipment, which included the fabrication unit (red box), chip (green box), and collection unit (blue box). (C) Overview of the chip, which was inserted with two solution glass pipettes. Images obtained by Z Liu and published in Liu and colleagues, 2018 (Liu and Hu, 2018).

reports (Liu and Hu, 2018). The equipment included two parts, the fabrication part and the

collection part. Two 10 mL syringes and 18 G needles were loaded on two micro-fluid pumps

separately in the fabrication part. The glass pipe connected with one pump was inserted into the

self-made PDMS fabrication chip. The other glass pipe with a puller connected with the other

pump was inserted into the output tube of the chip. The glass pipe injected the sheath solution

(50% Glycerol in distilled water; St. Louis, MO, Sigma) into the chip, while the glass pipe with a

puller injected the core solution (10% PLGA 75:25 in dimethyl sulfoxide DMSO; Sigma) into the

chip. When these two solutions combined, the PLGA began to solidify. The solidified PLGA formed

the micro-level fiber and was moved out of the chip by the output tube due to the micro-fluid pumping action. The flow rate of the two solutions controlled the size of the output PLGA fiber. To obtain fibers with diameters of from 60 to 120 μm, the core solution's and the sheath solution's flow rate were set up at 15-30 μL/min and 500 μL/min respectively. A third microfluid pump with a rotary motor was added to the equipment for the no-gap fiber collection in the collection step. The collected coverslip was loaded on the rotary motor, which was linked to the microfluid pump. The coverslip was rotated at 60 rpm and moved backward with the 40-200 μL/min fluid rate. The output microfiber was attached and rotated in the coverslips to form the no-gap and no-overlap fiber matrix. After collection, the ACMFP samples were rinsed with distilled water for 3 hours to remove the residual reagent (glycerol, water, and dimethyl sulfoxide).

To study the functional size range for the fibers, different sizes of the ACMFP needed to be fabricated. In the micro-fluid chip-based system, many parameters are controllable to generate the different sizes of the ACMFP. Table 1 showed the controllable parameters in this system, including core solution flow rate, sheath solution flow rate, rotation of the collection motor, and collection motor moving speed. By testing, this system can generate fibers with diameters from 30 μm to 300 μm. Three different fibers were chosen to study in this dissertation, which was 60 μm, 90 μm, and 120 μm. The detailed system parameters which used to fabricate three different sizes of ACMFPs were listed in the Table 1. The 60 μm ACMFP was fabricated with the 15 μL/min core solution flow rate and 40 μL/min collected pump moving speed. The 90 μm ACMFP was fabricated with the 20 μL/min core solution flow rate and 100 μL/min collected pump moving speed. The 120 μm ACMFP was fabricated with the 28 μL/min core solution flow rate and

200 μL/min collected pump moving speed.

Table 1. System parameters for the ACMFPs fabrication

Expected ACMFP fiber diameter (μm)	Core solution flow rate (μL/min)	Sheath solution flow rate (μL/min)	Rotation of the collection motor (rpm)	Collection motor move speed (μL/min)
60	15	500	60	40
90	20	500	60	100
120	28	500	60	200

PLGA flat membrane fabrication

A coverslip was designed as a mold to fabricate the PLGA flat membrane (mimic the flat topography, used as a control platform to evaluate the function of the micro-fiber topography in neural differentiation). 10% PLGA of DMSO solution was poured into the chamber. The solution was dried at room temperature overnight, following by 3 hours of distilled water rinsing to remove the residual reagent (DMSO). The PLGA flat membrane was out of the mold and cut into the proper size for the following experiments listed below.

ACMFP shrinkage assay

PLGA was in the unstable stage at 37 °C. This unstable stage of PLGA may leaded to the shape-changing and diameter shrinkage of ACMFP. Thus, the shrinkage of the ACMFP needed to be evaluated and improved here. The ACMFP was treated with 40% (m/v) Pluronic F127 solution (St. Louis, MO, Sigma) at 4 °C overnight (Figure 11). The ACMFP with Pluronic F127 solution was placed into the 70 °C incubators for 3 hours. After the solution was converted into the solid stage, the ACMFP was rinsed with ice-cold distilled water until the residual reagents (Pluronic F127) were removed. The Pluronic F127 treated and non-treated ACMFPs were sterilized with 70% alcohol for 15 minutes, followed by phosphate-buffered saline (PBS) 3-5 times rinsing. The ACMFPs were stored in the PBS in a 37 °C and 5% CO_2 incubator for 9 days. The ACMFPs were

imaged by the microscope every day (day 0 to day 12) to evaluate the shrinkage condition (the significant reduction of the fiber diameter was considered as shrinkage).
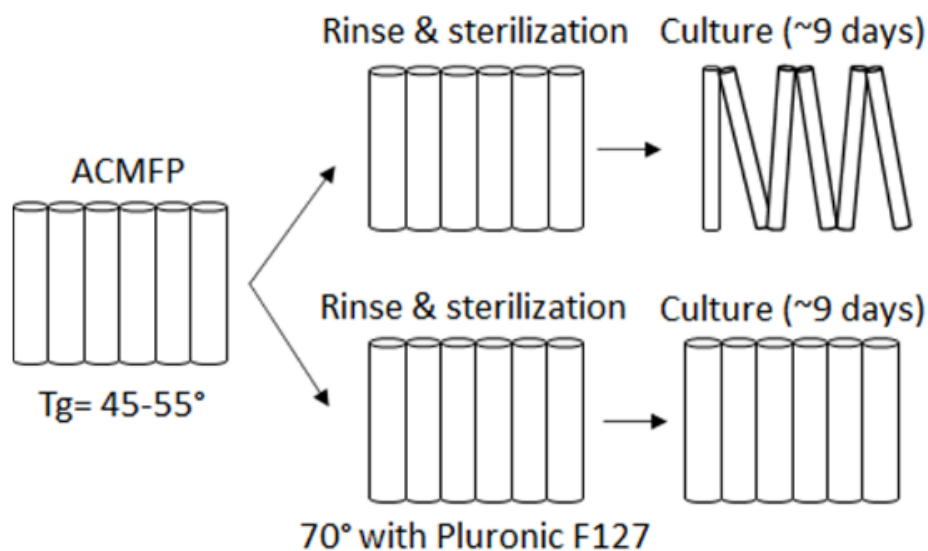
Figure 11. Diagram of the fiber shrinkage assay. The ACMFPs were rinsed and sterilized at room temperature. In the first three days, part of the ACMFPs was treated with Pluronic F127, while the left ACMFPs were treated with PBS as control. Two groups of the ACMFPs were incubated in the 37°C and 5% CO2 incubator for 9 days. All the ACMFPs were imaged and evaluated the fiber diameter and alignment value every two days, which was used to evaluate the shrinkage condition of the ACMFPs.

ACMFP biocompatibility assay

PLGA is a biocompatible material. However, the biocompatibility of the ACMFP is unclear, which is dissolved in DMSO solution and treated with Pluronic F127. The ACMFPs were sterilized with 70% alcohol for 15 minutes, followed by PBS 3-time rinsing. Next, the ACMFPs were coated with 0.1% Embryo-Max-Gelatin (Carlsbad, CA, Invitrogen) for 30 minutes and pre-treated with 10% coverslip medium in the 37 °C and 5% CO_2 incubator for 30 minutes. HEK 293 cells (universal cell line for the biocompatibility evaluation (Pospisil et al., 2016; Sun et al., 2014; Zhang et al., 2019)) were seeded on the ACMFPs and cultured with the 293T culture medium in 37°C and 5% CO_2 incubator. After 24 hours, the samples were stained with the Calcein (1:2000; live-cell marker), PI (Propidium Iodide; 1:2000; dead cell marker), and H33342 (1:3000; cell nuclei marker;

Invitrogen) in the 37 °C and 5% CO_2 incubator for 20 minutes (Figure 12). The samples were observed and imaged by Leica DMI 3000B epifluorescence microscopy. The positive signal of the Calcein, PI, and H33342 were showed in each channel of the microscopy images. The cells which doubled labeled with the Caclein and H33342 indicated that they are live cells, while the cells double-labeled with the PI and H33342 indicated that they are dead cells. The percentage of the live cells and dead cells were used to evaluate the biocompatibility of the ACMFP.
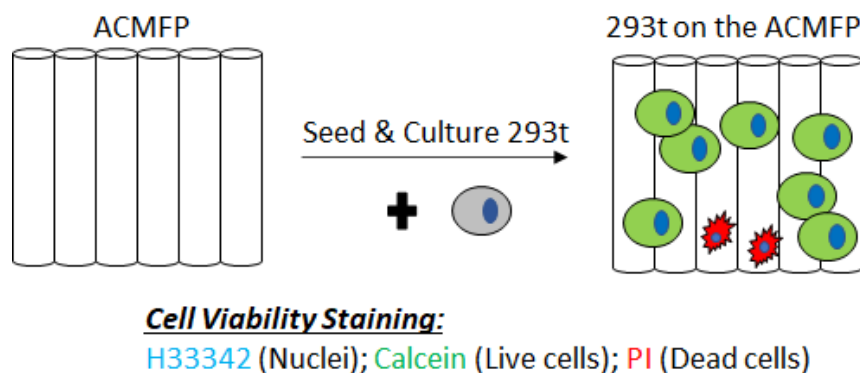
Figure 12. Diagram of the fiber biocompatibility assay. The 293T cells were seeded on the ACMFPs. After 24 hours cultured, the samples were stain with H33342 (blue, cell nuclei marker), Calcein (green, live-cell marker), and PI (Propidium Iodide; red, dead cell marker). The cell viability condition (percentage of the live & died cell) on the ACMFPs were used to evaluate the biocompatibility of the ACMFP.

Design of the ASMFP

To study the role of the submicro- and nano-pattern platform in stem cell differentiation, a novel submicro-fiber platform was needed. To achieve this aim, the ASMFP was designed, as shown in Figure 13. The ACMFP was established with multi-layers of parallel submicro-fibers. These fibers were parallel and fully covered by multi-layers which avoided the blank area between the fibers and showed a good-aligned structure. In addition, the submicro-fibers' diameter needed to be controllable, which was used to study the range of the functional fiber size.
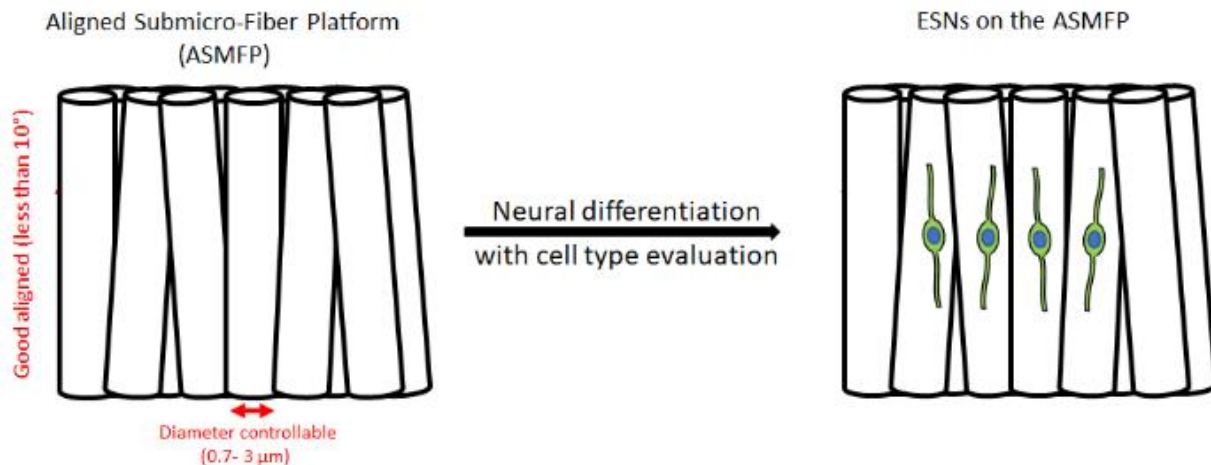
Figure 13. Design diagram of the ASMFP. The ASMFP was designed as a platform which established by parallel (the angle between fibers were less than 10 °C) submicro- or nano-fibers. These fibers, which sizes were 0.7- 3 μm, were fully covered the surface to support a fiber-like topography for the further neural differentiation experiment with cell type evaluation.

ASMFP equipment and fabrication

A standard electrospinning system (Figure 14; China, Tong Li Tech Co) was set up and calibrated as previous reports (Xue et al., 2019; Zhang et al., 2017). The PCL powder (St. Louis, MO, Sigma) was dissolved into the Chloroform /THF solution (3:1; St. Louis, MO, Sigma), with a final concentration of 30% (m/v). The 30% PCL was kept at room temperature for 24 hours to ensure all the PCL was solved. The PCL solution was loaded into the micro-fluid pump. The pump injected the solution into the electrospinning system with a fixed fluid rate (0.8 mL/h). The high voltage (8-25kV) was load into the system. The PCL solution pump needle in the electrospinning system moved from the left side to the right side at a fixed speed (2cm/s) to prevent the asymmetric thickness of the platform. The PCL fibers were pumped out of the needle and attached to the rotating metal collecting wheel, which was negatively charged. The wheel rotated at a fixed speed (2000 rpm) to ensure the fibers aligned well on the collecting wheel. After fabrication and collection, the ASMFP was rinsed with distilled water for 3 hours to remove the residual reagent (Chloroform and THF).
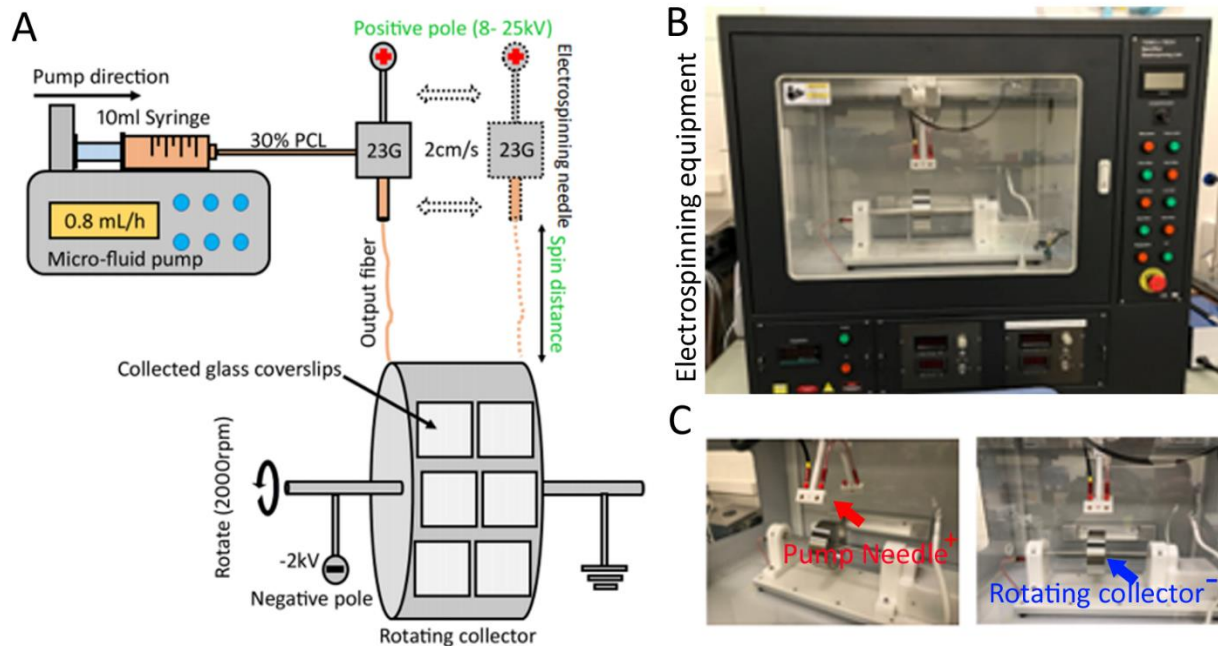
Figure 14. Electrospinning system for ASMFP fabrication. (A) Diagram of the electrospinning system for ASMFP fabrication. 30% PCL was loaded into the micro-fluid pump. The pump injected the solution into the electrospinning system with a fixed fluid rate (0.8 mL/h). The high voltage (8-25kV) was load into the system. The PCL solution pump needle in the electrospinning system moved from the left side to the right side at a fixed speed (2cm/s) to prevent the asymmetric thickness of the platform. The PCL fibers were pumped out of the needle and attached to the rotating metal collecting wheel, which was negatively charged. The wheel rotated at a fixed speed (2000 rpm) to ensure the fibers aligned well on the collecting wheel. (B) Overview of the electrospinning system from Tong Li Tech Co, China. (C) The fabrication unit (red arrow with a positive charge) and collecting wheel unit (blue arrow with a negative charge) in the electrospinning system. Electro spun system images were taken in Dr. Hu's Stem Cell Research Lab in the Department of Otolaryngology-HNS (Photo courtesy of Zhenjie Liu).

To study the functional size range for the fibers, the different sizes of the ASMFP needed to be fabricated. In the electrospinning system, many parameters are controllable to generate the different sizes of the ASMFP. Table 2 showed the controllable parameters in this system, including load voltage, spin distance, collector rotation speed, solution flow rate, and needle move speed. By testing, this system can generate fibers which diameter is from 0.7 μm to 3 μm. Three different fibers were chosen to study in this dissertation, which were 0.7 μm, 1.5 μm, and 3 μm. The detailed system parameters which used to fabricate three different sizes of ACMFPs were listed in the Table 2. The 0.7 μm ASMFP was fabricated with the 25kV load voltage and 12

cm spin distance. The 1.5 µm ASMFP was fabricated with the 15kV load voltage and 9 cm spin

distance. The 3 µm ASMFP was fabricated with the 8kV load voltage and 6 cm spin distance.

Table 2. System parameters for the ASMFP fabrication

Expected ASMFP fiber diameter (µm)	Voltage of positive pole (kV)	Voltage of negative pole (kV)	Spin distance (cm)	Collector rotation speed (rpm)	PCL flow rate (mL/h)	Needle move speed (cm/s)
0.7	25	-2	12	2000	0.8	2
1.5	15	-2	9	2000	0.8	2
3	8	-2	6	2000	0.8	2

PCL flat membrane fabrication

To fabricate the PCL flat membrane (control), a glass coverslip was used. 30% PCL of

Chloroform/THF solution was poured on this glass coverslip. The solution was dried at room

temperature overnight, following by 3 hours of distilled water rinsing to remove the residual

reagent. The PCL flat membrane was moved off from the glass coverslip and cut into the proper

size for the following experiments.

ASMFP hydrophilicity assay

PCL is a hydrophobic material, which limits cell attachment and growth (Shen et al., 2011).

The chemical treatment method was needed to improve the ASMFP surface hydrophilicity. The

ASMFPs were treated with Poly-D-Lysine (PDL) solution (Carlsbad, CA, Invitrogen) for 4 hours and

treated with Poly-L-ornithine (PLO) solution (Invitrogen) for another 12 hours in 37°C. After

treatment, the ASMFP was rinsed with PBS to remove the residual reagent (PDL and PLO). The

hydrophilicity assay was processed in the treated and non-treated (control) ASMFPs to identify

the material property as the previous report (Thomas et al., 2014; Zhao et al., 2015)(Figure 15).

40 µL distilled water was dripped on all groups of ASMFPs. The angle of the corner between the water droplet and substrate was used to evaluate the material hydrophilicity. When the angle is less than 90°C (acute angle), the material is hydrophilicity. When the angle is more than 90°C (obtuse angle), the material is hydrophobic.
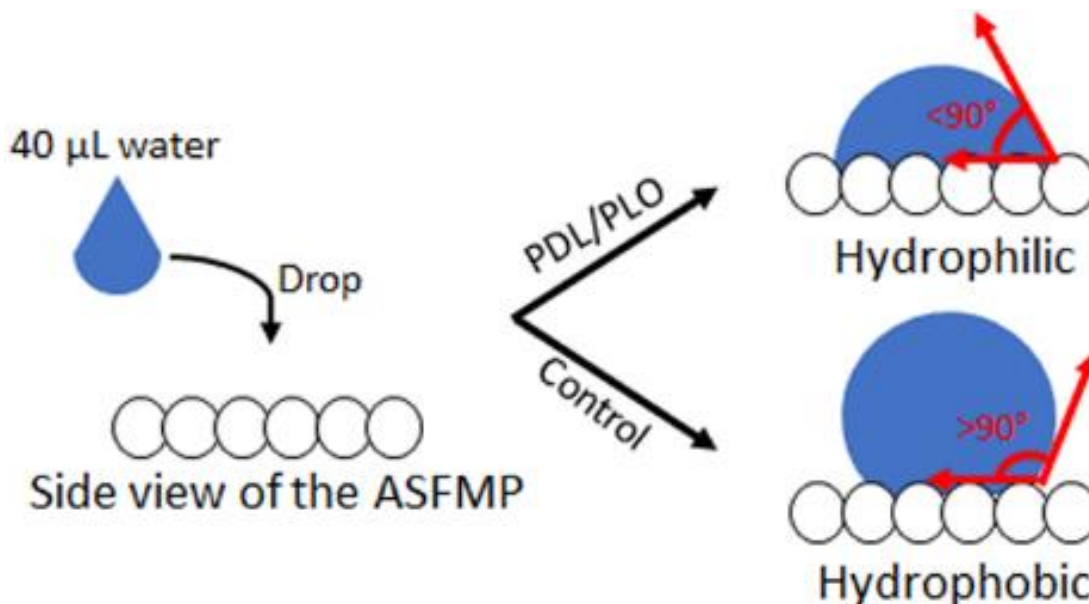
Figure 15. Diagram for the ASMFP hydrophilicity assay. To test the hydrophilic of the platform, 40 µL distilled water was dripped on PDL/PLO treated ASMFPs and control. The angle of the corner between the water droplet and substrate was used to evaluate the material hydrophilicity. When the angle is less than 90°C (acute angle), the material is hydrophilicity. When the angle is more than 90°C (obtuse angle), the material is hydrophobic.

ASMFP biocompatibility assay

PCL is a biocompatibility material. However, the biocompatibility of the ASMFP is not clear, which it suffered from Chloroform/THF solution and PDL/PLO treatment. To evaluate the biocompatibility, three groups of the ASMFPs were sterilized with 70% alcohol for 15 minutes, following by PBS 3-time rinsing. Next, the ASMFPs were coated with PDL/PLO and pre-treated with the 10% coverslip medium in the 37 °C and 5% CO_2 incubator for 30 minutes. Next, ESNs were seeded on the ASMFPs and cultured with the 10% coverslip culture medium in 37 °C and 5%

CO_2 incubator. After 24 hours, the samples were stained with the Calcein (1:2000; live-cell marker), PI (1:2000; dead cell marker), and H33342 (1:300, cell nuclei marker, Carlsbad, CA, Invitrogen) in the 37 °C and 5% CO_2 incubator for 20 minutes. The samples were observed and imaged by Leica DMI 3000B epifluorescence microscopy. The positive signal of the Calcein, PI, and H33342 were showed in each channel of the microscopy images. The cells which doubled labeled with the Calcein and H33342 indicated that they are live cells, while the cells doubled labeled with the PI and H33342 indicated that they are dead cells. The percentage of the live cells and dead cells were used to evaluate the biocompatibility of the ASMFP.

Quantification study and statistical analysis

The physical factors of the ACMFPs and ASMFPs were measured and analyzed, which included their fiber diameter and alignment value. For the diameter evaluation, all fibers in each ACMFP and ASMFP sample image were selected and measured via the ImageJ software length tool plugin (the total number of independent measurements between all treatment groups is 18; ACMFP samples (n) were from 3-6 independent experiments, ASMFP samples (n) were from 3 independent experiments). For the alignment test, the collecting rotator or collecting wheel rotating direction was chosen as the reference whose alignment value was equal to 0. The alignment value of each fiber was equal to the angle between the reference and the tested fiber. The angle was measured via the ImageJ software angle tool plugin (the total number of independent measurements between all treatment groups is 18; ACMFP samples (n) were from 3-6 independent experiments, ASMFP samples (n) were from 3 independent experiments).

The biocompatibility of the ACMFPs and ASMFPs were evaluated and analyzed. The positive cells of each protein marker (Calcein and PI) on the ACMFPs and ASMFPs (outcome factor

to evaluate the biocompatibility) were counted by the cell counter plugin module of Image J software (NIH). The percentage of the positive cells was equal to the number of Calcein or PI positive cells over the number of H33342 positive cells (the total number of independent measurements between all treatment groups is 3, ACMFP samples (n) were from 3 independent experiments; the total number of independent measurements between all treatment groups is 3, ASMFP samples (n) were from 3 independent experiments).

The hydrophilicity of the ASMFPs was evaluated and analyzed. The angle between the water droplet and platform in all ASMFPs groups was measured via the ImageJ software angle tool plugin (the total number of independent measurements between all treatment groups is 6, ASMFP samples (n) were from 3 independent experiments).

As mentioned in the previous parts separately, all the samples were collected from 3-6 independent experiments. Each independent experiment indicated the repeated experiment with independent platforms and cells. The number of n in each independent experiment means the number of the independent platforms or culturing wells. For example, "the total number of independent measurements between all treatment groups is 24 and samples (n) were from 3 independent experiments" indicated that the experiments were repeated 3 times with same protocol in different day. In each experiment, there were 8 separate samples in each group. A total 24 (3 x 8) experiments were used for the quantification study and statistical evaluation.

The data are represented as mean ± standard deviation. Student's t-test, a one-way ANOVA with post-hoc Tukey HSD Test and a two-way ANOVA test were used for statistical significance. The actual statistical power was calculated by G*power. The p-values smaller than 0.05 were considered significant (P<0.05, marked with *; P<0.01, marked with ** in the figures).

Results

Physical evaluation of the ACMFP

The ACMFPs with different diameters were fabricated, which were contiguous as expected. There were no observed gaps between the fibers (Figure 16). The quantification
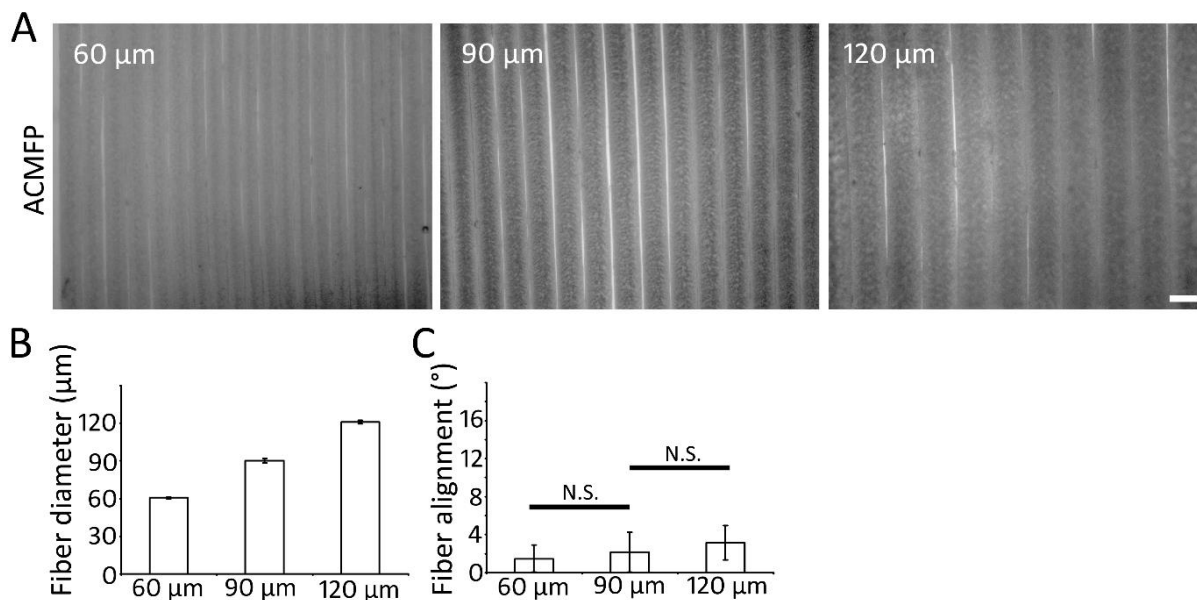
Figure 16. Physical factor evaluation of the ACMFP. (A) The bright-field image showed the 60 μm, 90 μm, and 120 μm ACMFPs. There were no observed gaps between the fibers in all three ACMFPs (B) Quantification studies of the ACMFPs' fiber diameter. The diameter of the 60 μm, 90 μm, and 120 μm ACMFPs' fibers were 60.61 ± 0.65 μm, 90.23 ± 1.75 μm, and 121.05 ± 1.23 μm (mean ± standard deviation, the total number of independent measurements between all treatment groups is 18; ACMFP samples (n) were from 6 independent experiments, (C) Quantification study of the ACMFPs' fiber alignment. The alignment values of 60 μm, 90 μm, and 120 μm groups were 1.47 ± 1.43°, 2.15 ± 2.10°, and 3.15 ± 1.79° (mean ± standard deviation, the total number of independent measurements between all treatment groups is 18; ACMFP samples (n) were from 6 independent experiments). All of them were smaller than 10° which were defined as high alignment. There was no significant difference (N.S.) between the 60 μm ACMFP and 90 μm ACMFP (P=0.28, actual statistical power= 0.80, Student's t-test) or between 90 μm ACMFP and 120 μm ACMFP (P=0.14, actual statistical power= 0.81, Student's t-test). Scale bar is 100 μm in A.

studies showed that the diameter of the 60 μm ACMFP's fiber was 60.61 ± 0.65 μm. The diameter of the 90 μm ACMFP's fiber was 90.23 ± 1.75 μm. The 120 μm ACMFP's fiber diameter was 121.05 ± 1.23 μm (mean ± standard deviation, the total number of independent measurements between

all treatment groups is 18; ACMFP samples (n) were from 6 independent experiments, Figure 16).

The alignment values of 60 μm, 90 μm, and 120 μm groups were 1.47 ± 1.43°, 2.15 ± 2.10°, and

3.15 ± 1.79° (mean ± standard deviation, the total number of independent measurements between

all treatment groups is 18; ACMFP samples (n) were from 6 independent experiments). All of them

were smaller than 10° which were defined as high alignment. The alignment value of the ACMFPs

seemed to increase as their diameter increase. However, there was no significant difference

between the 60 μm ACMFP and 90 μm ACMFP (P=0.28, actual statistical power= 0.80, Student's

t-test) or between 90 μm ACMFP and 120 μm ACMFP (P=0.14, actual statistical power= 0.81,

Student's t-test).

Shrinkage evaluation of the ACMFP

As the fiber shrinkage was caused by their material properties, only one group of ACMFP

(90 μm) as a representative was chosen to evaluate the fiber shrinkage (Figure 17). The ACMFP

was incubated from day 0 to day 2 at room temperature with different treatments and incubated

from day 3 to 12 at 37 °C. The condition of the ACMFPs was imaged to analyze the structure

change on day 1, 2, 3, 5, 7, and 12. There was no viewable structural change from day 0 to day 2

in control and Pluronic F127 treated groups. However, the fibers started to shrink, and the

alignment value showed a significant increase from day 3 to day 12. Several gaps were observed

between the fibers during this period (* area in Figure 17). The quantification studies showed

that the fiber of the ACMFPs shrink from 90.58 ± 3.27 μm (Day 2) to 53.05 ± 5.23 μm (Day 12)

little by little after they incubated in the 37°C, which showed a significant decrease (mean ±

standard deviation; P<0.0001, actual statistical power= 0.93, Student's t-test; the total number of

independent measurements between all treatment groups is 10, samples were (n) from 3

independent experiments). The fiber alignment value also increased
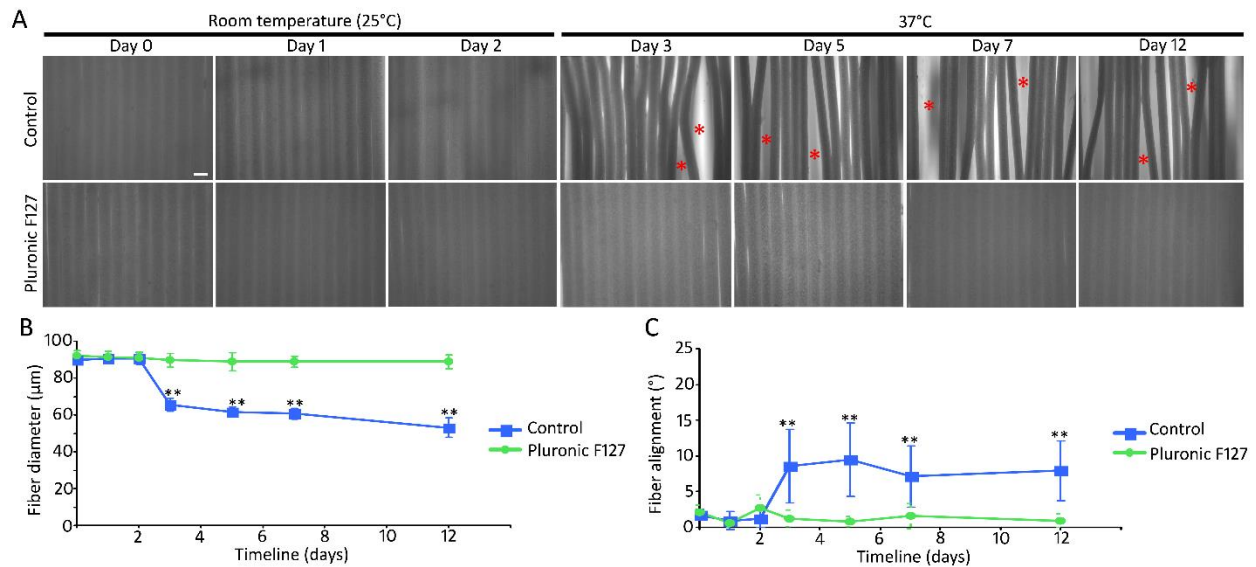
Figure 17. ACMFP anti-shrinkage evaluation. (A) Bright-field image for the ACMFPs treated and non-treated with Pluronic F127 from day 0 to day 2 at room temperature and from day 3 to day 12 at 37 °C. The Pluronic F127 treated group was treated with the chemical on day 1. Serval gaps (marked with red * symbol) were found in the control groups from day 3 to day 12, while there were no gaps found in all Pluronic F127 treated groups. (B) The quantification study for the fiber diameter changes in the groups. The diameter of the control groups started to have a significant decrease from day 3 (mean ± standard deviation; $F_{(6,63)}$= 230.53, P<0.0001, one-way ANOVA with post-hoc Tukey HSD Test; the total number of independent measurements between all treatment groups is 10, samples (n) were from 3 independent experiments), while the diameter of the Pluronic F127 treated groups did not have a significant difference between day 1 and day 12 (mean ± standard deviation; P=0.41, Student's t-test; the total number of independent measurements between all treatment groups is 10, samples (n) were from 3 independent experiments). (C) The quantification study for the fiber alignment changes in the groups. The alignment value of the control groups started to have a significant increase from day 3 (mean ± standard deviation; $F_{(6,63)}$= 10.00, P<0.0001, ne-way ANOVA with post-hoc Tukey HSD Test; the total number of independent measurements between all treatment groups is 10, samples were from 3 independent experiments), while the diameter of the Pluronic F127 treated groups did not have a significant difference between day 1 and day 12 (mean ± standard deviation; P=0.34, Student's t-test; the total number of independent measurements between all treatment groups is 10, samples (n) were from 3 independent experiments). Scale bar is 100 µm in A.

from 1.23 ± 1.27° to 7.92 ± 4.21° from day 2 to day 12, which showed significant different (mean

± standard deviation; P=0.0002, actual statistical power= 0.85, Student's t-test; the total number

of independent measurements between all treatment groups is 10, samples (n) were from 3

independent experiments). These results indicated that ACMFP could not maintain a stable structure in 37°C incubation. To overcome this problem, the Pluronic F127 was used to treat the ACMFP on day 1. The ACMFPs covered with Pluronic F127 were heated to 70°C for 3 hours, followed by PBS rinse at 4°C. The treated ACMFPs were incubated at 37°C from day 3 to day 12. There were no observable gaps found in the AMFSPs. The quantification study showed that the diameter of the ACMFPs was 91.22 ± 3.22 μm at Day 1, while the diameter of the ACMFPs was 89.93 ± 3.62 μm at Day 12. There was no significant difference between these two time points (mean ± standard deviation; P=0.41, actual statistical power= 0.81, Student's t-test; the total number of independent measurements between all treatment groups is 10, samples (n) were from 3 independent experiments). The alignment value also did not have significant change at Day 1 and Day 12, which were 0.61 ± 0.61° and 0.95 ± 0.94° (mean ± standard deviation; P=0.34, actual statistical power= 0.80, Student's t-test; the total number of independent measurements between all treatment groups is 10, samples (n) were from 3 independent experiments). These results showed that by treat with the Pluronic F127, the ACMFPs did not shrink during the 37°C incubation and keep in a stable stage as designed.

Biocompatibility evaluation of the ACMFP

PLGA is a good biocompatibility material (Zheng et al., 2018a). However, the biocompatibility of the ACMFP is not clear. 293T cells were used to evaluate the ACMFP biocompatibility as the previous method (Pospisil et al., 2016; Sun et al., 2014; Zhang et al., 2019). The 293T cells were seeded and cultured on the ACMFP. After two days, the cell viability staining kit was used on the ACMFP. The fluorescence staining showed that many cells located on the ACMPF were marked by H33342 (cell nucleus marker) and Calcein (live cell marker). Moreover,

some cells were marked by PI (dead cell marker). The quantification study showed that 88.46 ±

2.81% cells were marked by Calcein, and 11.54 ± 2.81% cells were marked by PI (mean ± standard

deviation; the total number of independent measurements between all treatment groups is 3,

samples (n) were from 3 independent experiments; Figure 18). The result showed that most of

the cells lived on the ACMFP (more than 80% live cells were considered as non-

cytotoxicity(Lopez-Garcia et al., 2014)), which indicated that ACMFP is not or less toxic for the

cell. In other words, the PLGA based ACMFP has good biocompatibility.
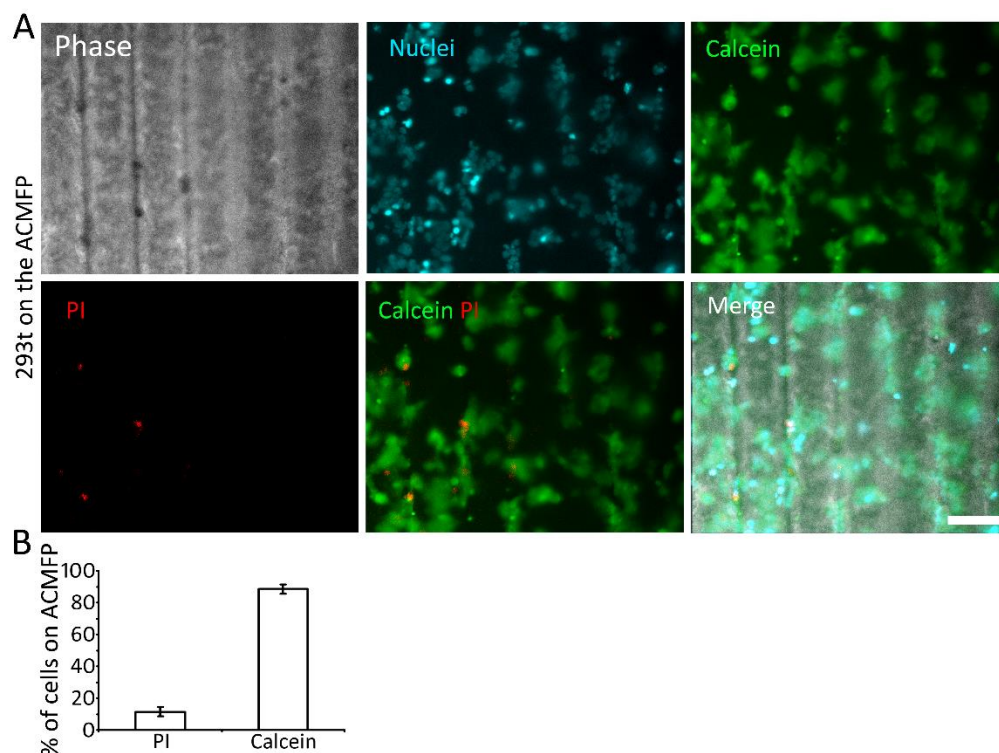
Figure 18. Cell viability evaluation of the ACMFP. (A) The phase and immunofluorescence images showed that cells were label by the H33342 (cell nuclei marker), Calcein (live cell marker), and PI (dead cell marker) on the ACMFPs. (B) The quantification study showed that the percentage of cells labeled with Calcein and PI on the ACMFPs were 88.46 ± 2.81% and 11.54 ± 2.81% (mean ± standard deviation; the total number of independent measurements between all treatment groups is 3, samples (n)were from 3 independent experiments). This figure was published in Liu and colleagues, 2018 (Liu and Hu, 2018). Scale bar is 100 μm in A.

***Physical factor evaluation of the ASMFP* (Pilot Data)**

The ASMFPs with different diameters were fabricated in different time points, including

3, 10, 15, 30, and 60 minutes (Figure 19). After 60 minutes of spinning, the fibers covered all the

surface, showing no observed blank in the platform. 60-minute spinning was used in the further
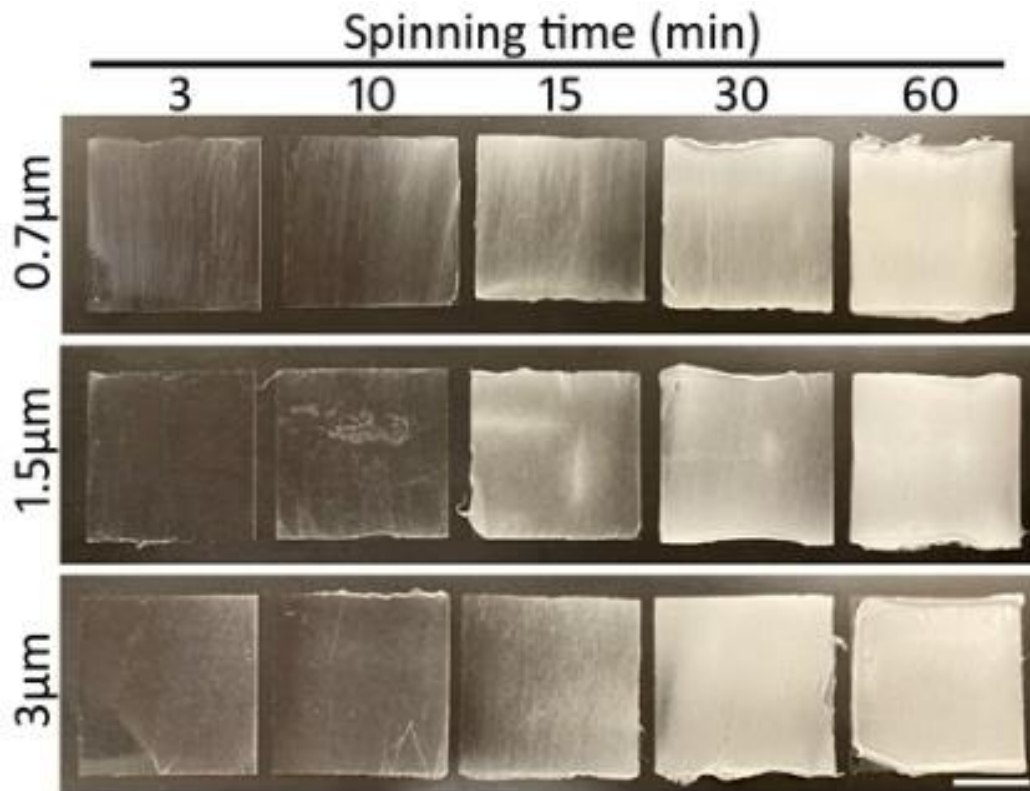
Figure 19. Fabricated ASMFPs in different time points and groups (Pilot data). The ASMFPs with different diameters were fabricated at different time points, including 3, 10, 15, 30, and 60 minutes. After 30 and 60 minutes of spinning, the fibers covered all the surface, showing no observed blank in the platform. The data is collected using ASMFP produced by the same batch of the PCL solution, which showed as the pilot data. Additional experiments are required to complete the project. Scale bar is 10 mm.

ASMFP fabrication. The three groups of the ASMFP, in which the expected diameter were 0.7 µm,

1.5 µm, and 3 µm, were fabricated as designed. The quantification studies showed that the

diameter of the 0.7 µm ASMFP's fiber was 0.70 ± 0.06 µm. The diameter of the 1.5 µm ACMFP's

fiber was 1.52 ± 0.08 µm. The 3 µm ACMFP's fiber diameter was 3.03 ± 0.23 µm (mean ± standard

deviation; the total number of independent measurements between all treatment groups is 9,

ASMFP samples (n) were from 3 independent experiments; Figure 20). The alignment values of

0.7 µm, 1.5 µm, and 3 µm groups were 6.41 ± 1.00°, 6.69 ± 1.14°, and 8.85 ± 1.59 ° (mean ±
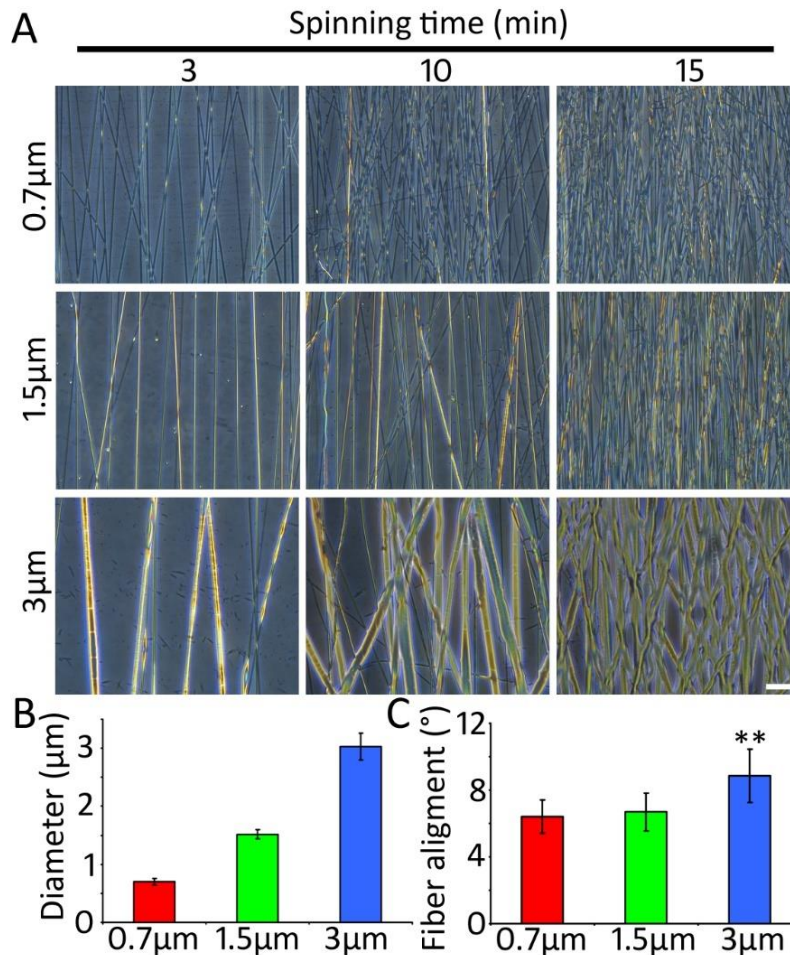
Figure 20. Physical factor evaluation of the ASMFP (Pilot data). (A) Bright-field images showed the 0.7 μm, 1.5 μm, and 3 μm ASMFPs present alignment structure after 3-, 10-, and 15-min spinning. (B) Quantification study of the ACMFPs' fiber diameter. The diameter of the 0.7 μm, 1.5 μm, and 3 μm ASMFPs' fibers were 0.70 ± 0.06 μm, 1.52 ± 0.08 μm, and 3.03 ± 0.23 μm (mean ± standard deviation, the total number of independent measurements between all treatment groups is 9; ASMFP samples (n) were from 3 independent experiments, (C) Quantification study of the ASMFPs' fiber alignment. The alignment values of 0.7 μm, 1.5 μm, and 3 μm groups were 6.41 ± 1.00°, 6.69 ± 1.14°, and 8.85 ± 1.59° (mean ± standard deviation, the total number of independent measurements between all treatment groups is 9; ASMFP samples (n) were from 3 independent experiments). All of them were smaller than 15° which showed good alignment. The alignment value of the 3 μm ASMFP group was significantly higher than the other two groups ($F_{(2,24)}$= 9.95, P=0.0007, one-way ANOVA with post-hoc Tukey HSD Test; the total number of independent measurements between all treatment groups is 9, samples (n) were from 3 independent experiments). The data is collected using ASMFP produced by the same batch of the PCL solution. Additional experiments are required to complete the project. Scale bar is 10 μm in A.

standard deviation; the total number of independent measurements between all treatment groups

is 9, ASMFP samples (n) were from 3 independent experiments). All of them were smaller than

15° which were considered as good alignment. 1.5 µm and 3 µm ASMFP's alignment value showed significant increase than 0.7 µm one ($F_{(2,24)}$= 9.95, P=0.0007, actual statistical power= 0.86, one-way ANOVA with post-hoc Tukey HSD Test; the total number of independent measurements between all treatment groups is 9, samples (n) were from 3 independent experiments). The data is collected using ASMFP produced by the same batch of the PCL solution, which showed as a pilot data. Additional experiments are required to complete the project.

***Hydrophilic evaluation of the ASMFP* (Pilot Data)**

       The hydrophilic of the platform plays a crucial role in cell attachment and growth (Shen et al., 2011). To achieve this aim, the ASMFPs need to be a hydrophilic platform for stem cell research. To check the ASMFPs' hydrophilic, the standard hydrophilic assay was used in this dissertation as the previous report (Thomas et al., 2014; Zhao et al., 2015). The result showed that the three ASMFP groups' hydrophilic angles were much larger than the right-angle, which suggested the surfaces were hydrophobic (Figure 21). To overcome this weakness, a PDL/PLO

Figure 21. Hydrophilic evaluation of the ASMFP (Pilot data). The image showed the condition of the water droplet on 0.7 µm, 1.5 µm, and 3 µm ASMFPs with and without PDL/PLO coated. For the hydrophilic assay, the angle of the corner between the water droplet and substrate was used to evaluate the material hydrophilicity. The angle in 0.7 µm, 1.5 µm, and 3 µm ASMFPs control groups showed obtuse angle, which indicated the platforms were hydrophobic. However, when the in 0.7 µm, 1.5 µm, and 3 µm ASMFPs coated with PDL/PLO, the angle was acute, indicating the platforms were hydrophilicity. The data is collected using ASMFP produced by the same batch of the PCL solution. Additional experiments are required to complete the project.
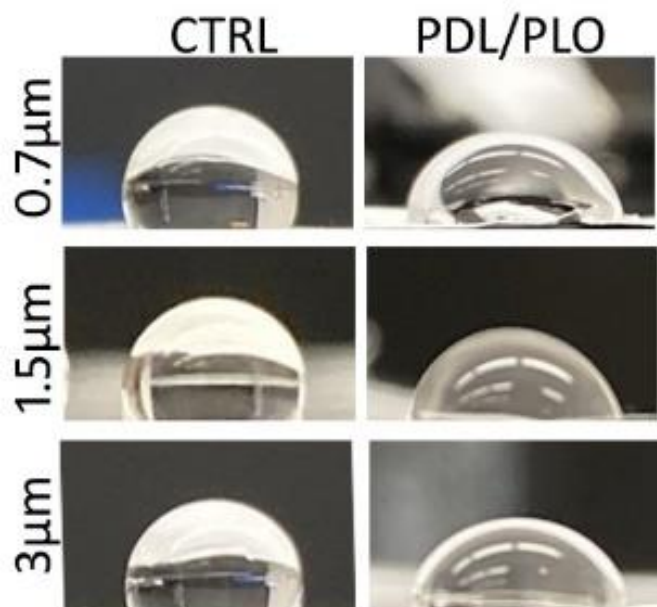
solution was used to coat the ASMFP. After coated, the water droplet showed a small angle (smaller than right-angle) between the water drop and three ASMFP groups, which suggested the surface was changed into hydrophilic.

PCL is a good biocompatibility material (Feng et al., 2019; O'Leary et al., 2020). However, the biocompatibility of the ASMFP is not clear. The biocompatibility assay was used to test the ACMFP via ESN cells. The ESN cells were seeded and cultured on the 0.7 µm, 1.5 µm, and 3 µm ASMFPs. After two days, the cell viability staining kit has treated the cells on the ASMFP. The fluorescence staining result showed that 97.31 ± 1.12%, 97.42 ± 1.36%, and 97.10 ± 1.86% of cells located on the 0.7 µm, 1.5 µm, and 3 µm ASMPF were marked by H33342 (cell nucleus marker) and Calcein (live cell marker) (Figure 22), suggested most of them were the live cells. 2.69 ± 1.12%, 2.58 ± 1.36%, and 2.90 ± 1.86% cells on the 0.7 µm, 1.5 µm, and 3 µm ASMPF were marked by PI (dead cell marker), suggested fewer cells died on the ASMFPs. Also, there was no significant difference among the three groups ($F_{R(7,14)}$= 0.91, P=0.527, $F_{C(2,14)}$= 0.095, P=0.910, actual statistical power= 0.80, two-way ANOVA; the total number of independent measurements between all treatment groups is 8, samples (n) were from 3 independent experiments). The result indicated that ASMFP is not toxic for the cell. In other words, the PCL-based ASMFP has good biocompatibility. The data is collected using ASMFP produced by the same batch of the PCL solution. Additional experiments are required to complete the project.
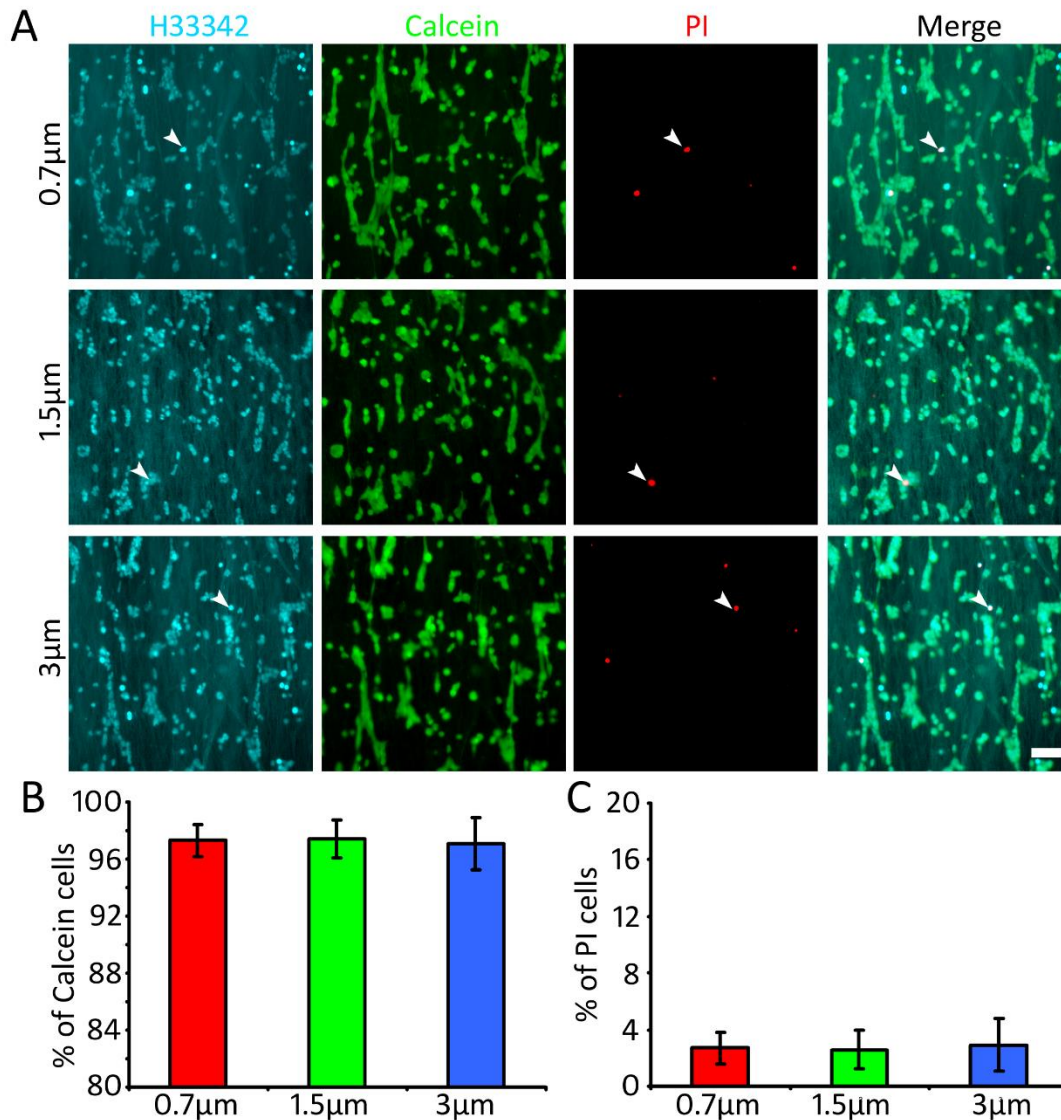
Figure 22. Biocompatibility evaluation of the ASMFPs (Pilot data). (A) The immunofluorescence images showed that cells were label by the H33342 (cell nuclei), Calcein (live cell), and PI (dead cell) on 0.7 μm, 1.5 μm, and 3 μm ASFMPs. (B) The quantification study showed that the percentage of cells labeled with Calcein on the 0.7 μm, 1.5 μm, and 3 μm ASMFPs were 97.31 ± 1.12%, 97.42 ± 1.36%, and 97.10 ± 1.86% (mean ± standard deviation; n=8, samples were from 3 independent experiments). (C) The quantification study showed that the percentage of cells were labeled with Calcein on the 0.7 μm, 1.5 μm, and 3 μm ASMFPs were 2.69 ± 1.12%, 2.58 ± 1.36%, and 2.90 ± 1.86% (mean ± standard deviation; n=8, samples were from 3 independent experiments). There was no significant difference among the three groups ($F_{R(7,14)}$= 0.91, P=0.527, $F_{C(2,14)}$= 0.095, P=0.910, actual statistical power= 0.80, two-way ANOVA; ; the total number of independent measurements between all treatment groups is 8, samples (n) were from 3 independent experiments). The data is collected using ASMFP produced by the same batch of the PCL solution. Additional experiments are required to complete the project. Scale bar is 20 μm in A.

Discussion

The purpose of this study was to fabricate the fiber platform to mimic the different sizes of the topography. During development, the cell lives in a complex micro-environment *in vivo*. The micro-environment includes topographical information, physiological cues, soluble factors, and cell-cell interactions. The micro-, submicro-, and nano-pattern topography of the micro-environment play a vital role in cell growth, proliferation, development, and differentiation *in vivo*(Govey et al., 2013; Keung et al., 2010; Lapointe et al., 2013). To mimic the different sizes of the topography, a novel platform was needed here. The most important findings of the current study were that two biomaterial-based fiber platforms were designed, fabricated, and evaluated.

To mimic the micro-level fiber topography, ACMFP were designed as contiguous, parallel, and fiber-based structure. The micro-fluid chip-based system was updated with a collecting unit to collect the PLGA-based fibers in a platform that kept them parallel and contiguous. As the plastically of the PLGA fibers, the ACMFP were fabricated into three different sizes, which were 60 μm, 90 μm, and 120 μm. The different sizes of the ACMFP could cover the micro-level fiber topography for further research. The alignment test and biocompatibility assay were evaluated for the ACMFP. The results showed that it was a good alignment and not toxic platform for the cell culture. However, the PLGA fiber showed an unstable stage in the body temperature, which limited the cell research. Therefore, the Pluronic F127 was treated for the ACMFP. It could help the ACMFP transfer into the glass stage (stable stage) to avoid shrinking body temperature. Overall, a good platform that has the micro-level topography was generated.

Besides the study of fiber sizes of ACMFPs, the microfibers' whole and local elasticity may also be critical physical factors that could influence cell growth and differentiation. However,

these properties did not evaluate in this dissertation, limiting the study of the other physical factors' role in cell growth and differentiation. What is more, the different sizes of fibers had different curvature topography. The specific role of the curvature topography in cell growth and differentiation was not involved in this dissertation. These factors would be considered and evaluated in the future with different types of evaluation methods and platforms.

To mimic the submicro- and nano-level fiber topography, ASMFP was designed as a parallel and fiber-based structure. The electrospinning system was used to fabricate the PCL-based fibers in a platform that kept them parallel. The long-time fabrication of the fibers (60 minutes) let the fibers fully cover the whole platform (no blank area). As the plastically of the PCL fibers, the ACMFP were fabricated into three different sizes, which were 0.7 μm (nano), 1.5 μm (submicron), and 3 μm (submicron). The different sizes of the ACMFP could cover the nano- and submicro-level fiber topography for further research. The alignment test and biocompatibility assay were evaluated for the ASMFP. The results showed it was a good alignment and not toxic for the cell culture. However, the PCL showed a hydrophobic surface which limited the cell attachment and growth. The PDL/PLO were used to coat the platforms, which led to the surface change into hydrophilicity. Overall, a good platform that had nano- and submicro-level topography was generated.

As the previous hypothesis in this chapter, one platform needed to be designed, fabricated, and evaluated, which can mimic the full-size fiber topography. However, as the biomaterials and fabrication technologies limit, no platform could be fabricated, which can be covered from the nano-level to the micro-level fiber. Thus, two different platforms were used to cover the different sizes of the topography separately. This technology limitation influenced the comparison of the

cell differentiation between the micro-topography and nano-topography.

For the nano-, submicro-, and micro-fiber platform fabrication, stamping technology and chemical etching technology were considered. These technologies can generate more specific fiber and platform. However, as their high cost, they did not use in this dissertation. They will be used as an alternative method in this dissertation or future studies to achieve other research aims.

In summary, two fiber-based platforms (ACMFP and ASMFP) were designed and fabricated with different size (60 μm, 90 μm, and 120 μm for the ACMFP; 0.7 μm, 1.5 μm, and 3 μm for the ASMFP). All of them showed good alignment, stability, hydrophilicity, and biocompatibility with specific treatment (Pluronic F127 for ACMFP and PDL/PLO for ASMFP). Thus, these platforms support a suitable matrix used on topography-induced cell research and clinical application. The data is collected using ASMFP produced by the same batch of the PCL solution. In the future, additional experiments are required to complete the project, and we will use these platforms to study the role of topography in stem cell differentiation.

CHAPTER 3 – NEURAL DIFFERENTIATION OF THE ESC ON THE ACMFP AND ASMFP

(This chapter contains previously published material. See Appendix B.)

Abstract

The topography of the ECM plays a crucial role in cell attachment, growth, proliferation, and differentiation. However, the different sizes of the topography in stem cell neural differentiation are not precise yet. To study the role of the topography in stem cell fate, the biomaterial platforms (ACMFPs and ASMFPs) were used to mimic the different sizes of the fiber topography, as the last chapter reported and studied the role in stem cell fate determination. The "step by step" method was used to induce the neural differentiation of the ESCs. The ESCs induced NBs were seeded and cultured on different sizes of the ACMFPs and ASMFPs. The immunofluorescence staining assay was used to identify the cell types on the platforms. The result showed that both ACMFPs and ASMFPs could stimulate neuron-like cell generation. The inhibition of the cell proliferation causes the stimulation of the ACMFPs induced neural differentiation. The ASMFPs and part of the ACMFPs (60 and 90 μm) can guide the neurite outgrowth. The different size of the fiber topography has a different level of the simulation in neural differentiation and maturation of the ESCs, which indicates that the topography seems to play a critical role in stem cell fate determination. The study and usage of biomaterial-induced neural differentiation will contribute to ECM-induced cell growth, differentiation, and maturation while it also contributes to future clinical application.

Introduction

Overview of the neural differentiation

As showed in Chapter 1, the ESC can be guided to differentiate into neural stem cells via

multiple methods (Alizadeh et al., 2019; Liu et al., 2018b; Malczynska et al., 2019). The neural stem cells, a tissue-specific stem cell, possess the ability to self-renew and have multi-pluripotency (Gonzalez et al., 2016; Grochowski et al., 2018). The definition of multi-pluripotency of neural stem cell can only differentiate into the neural lineage cells, including neurons, astrocytes, and oligodendrocytes(Gonzalez et al., 2016; Grochowski et al., 2018; Liu et al., 2018b). The neuron is an electrically excitable cell that can transmit a signal from other sensory cells or neurons. As it cannot proliferate, it cannot recover from damage, yet cell recovery is a primary area of research (Menorca et al., 2013; Tran et al., 2018).

Astrocytes are a sub-type of glia cells, which help maintain neuronal metabolism (Nutma et al., 2020). Oligodendrocytes are a type of large glial cell mainly located in the CNS. The primary function of oligodendrocytes is to produce the myelin sheath to enhance the speed of neuronal communication (Nutma et al., 2020; Stadelmann et al., 2019). In neural stem cell differentiation research, multiple protein markers were used to label neural stem cells and three neural lineage cells (Liu et al., 2018b). The generated yield of each type of lineage cell can be used to evaluate the amount neural differentiation of each. In this dissertation, the cells were identified on the ACMFP, ASMFP, and flat membrane groups to evaluate the role of the topography in stem cell differentiation.

Physical factors induced neural differentiation

During stem cell development and differentiation *in vivo* and *in vitro*, the stem cell fate is influenced by biophysical factors of the extracellular matrix (ECM) (Dong et al., 2017; Hu et al., 2019; Jain et al., 2020; Lau and Hudson, 2010; Li et al., 2016; Zhu et al., 2019; Zimmermann and Schaffer, 2019). The biophysical factors of ECM include micro/nano topography, matrix stiffness,

and mechanical forces. In this chapter, we mainly focus on the topography induced the stem cell research. There were currently two types of fiber platforms used for stem cell differentiation studies. For example, the micro-fiber platform can change the cell growth direction and morphology, while the nano-fiber platform can stimulate neural differentiation (Cheng and Kisaalita, 2010; Yang et al., 2005). However, the role of the micro-fiber in neural differentiation of the ESCs is not clear. Furthermore, the nano-fiber-based platform and micro-fiber function size for neural differentiation and neurite outgrowth are also unclear. Therefore, this chapter mainly focuses on the different sizes of the fiber-like topography in neural differentiation and neurite outgrowth.

Rationale and hypothesis for Chapter 3

ESC-derived NBs were seeded and cultured on the ACMFPs and ASMFPs to study the role of topography in neural differentiation. The neural stem cell and three neural lineage cells were identified on all the platforms and their flat membrane. We hypothesized that both ACMFP and ASMFP can stimulate neural stem cell differentiation and neural lineage cell differentiation while also guiding the neurite outgrowth. This stimulation will enhance as their fiber size decreases. If the ACMFP and ASFMP stimulate the differentiation, the mechanism would be explored.

Materials and methods

Neural differentiation of the ESC on the ACMFP and ASMFP

ESCs were differentiated into the NBs as a previously reported method(Liu et al., 2018b). The ESC cell line (Manassas, VA, American Type Culture Collection) were cultured with the ESC culture medium (Table 3) in the 37 °C and 5% CO_2 incubator for 48 hours. The ESCs were dissociated with TrypLE (Invitrogen) for 3 min in the 37 °C incubator and seeded into a 0.1%

Gelatin (Invitrogen) coated 24-well cell culture dish (Corning). Different batches and passages of

ESCs (cells samples were from at least 6 batches independent experiments) were used in these

experiments and support the sufficient cell source for the following differentiation experiments.

The ESCs were cultured with the RA neural differentiation medium for 3-4 days in the 37 °C and

5% CO_2 incubator named non-neural ectoderm (NNE). The NNE cells were dissociated with TrypLE

for 3 min in the 37 °C incubator and seeded into another 0.1% Gelatin coated 24-well cell culture

dish with RA neural differentiation medium for 3-4 days in the 37 °C and 5% CO_2 incubator, which

was named as otic placode and otocyst (OPO). The OPO cells were dissociated with TrypLE for 3

min in the 37 °C incubator and seeded into the 24-well suspension culture dish (Corning). The

OPO cells were cultured with the suspension culture medium for 3-4 days in the 37 °C and 5%

CO_2 incubator to form cell spheres named NB. ESC-derived NBs were dissociated, seeded, and

cultured on the different sizes of the ACMFPs, ASMFPs, and their flat membrane with 10%

coverslip medium in the 37 °C and 5% CO_2 incubator. After six days, the ESNs were fixed with the

4% paraformaldehyde (PFA) for 10 minutes at room temperature.

Table 3. List of chemicals for the cell culture medium and solution

Name	Ingredient (Company)
ESC culture medium	45% DMEM High glucose (Logan, UT, Hyclone), 45% DMEM/F12 GlutaMAX (Carlsbad, CA, Invitrogen), 10% Knockout FBS (Invitrogen), 1% MEM (Invitrogen), 1% NEAA (Invitrogen), 55 µM 2-ME (Invitrogen), and 1,000 unit/mL LIF (Millipore).
RA neural differentiation medium	45% DMEM High glucose (Hyclone), 45% DMEM/F12 GlutaMAX (Invitrogen), 10% FBS (Gaithersburg, MD, Gibco), 1% MEM (Invitrogen), 1% NEAA (Invitrogen), 55 µM 2-ME (Invitrogen), 100 µg/mL Ampicillin (Invitrogen), and 10-7 M all-trans RA (Sigma).
293T culture medium	90% DMEM High glucose (Hyclone), 10% FBS (Gibco), and 100 µg/mL Ampicillin (Invitrogen)
Suspension culture medium	97% DMEM/F12 GlutaMAX, 1% N-2 supplement 100x, 2% B-27 Supplement 50x, 55 µM 2-ME (Invitrogen), 20 ng/mL EGF, and 20 ng/mL FGF-2 (All from Invitrogen).
10% coverslips culture medium	45% DMEM/F12 GlutaMAX (Invitrogen), 45% Neurobasal (Invitrogen), 10% FBS (Gibco), 55 µM 2-ME (Invitrogen), 100 µg/mL Ampicillin (Invitrogen), and 20 ng/mL NGF (Invitrogen).
Blocking solution	5% Donkey serum (West Grove, PA, Jackson IR) and 0.2% Triton X-100 (St. Louis, MO, Sigma) of the DPBS (Sigma)
Working solution	1% Donkey serum (Jackson IR) and 0.04% Triton X-100 (Sigma) of the PBS (Sigma)

Evaluation of the NBs on the ACMFPs

To study the role of the ACMFP in neural stem cell differentiation, immunofluorescence staining assays were used for cell identification on each platform (Figure 23). The fixed ESNs (at least 3-6 independent ESNs differentiated from different batches of ESCs were used in the following experiments) with platforms were treated with blocking solution (Table 3) at room temperature for 1-2 hours. The ESNs were treated with the primary antibodies (Anti-NESTIN and anti-SOX2, Table 4; each antibody was used for 3-6 independent cells staining experiments) of the working solution (Table 3) in the 4 °C refrigerator overnight. ESNs were rinsed with PBS three times and treated with the related secondary antibodies (Table 5) and nuclei marker (DAPI, Invitrogen) at room temperature for 1-2 hours. The ESNs were rinsed with PBS three times to remove the residual reagent (working solution with left of secondary antibodies). The ESNs were observed and imaged by Leica SPE confocal microscopy. The number and percentage NESTIN, SOX2, and NESTIN & SOX2 positive cells in each image were counted for the following quantification studies.
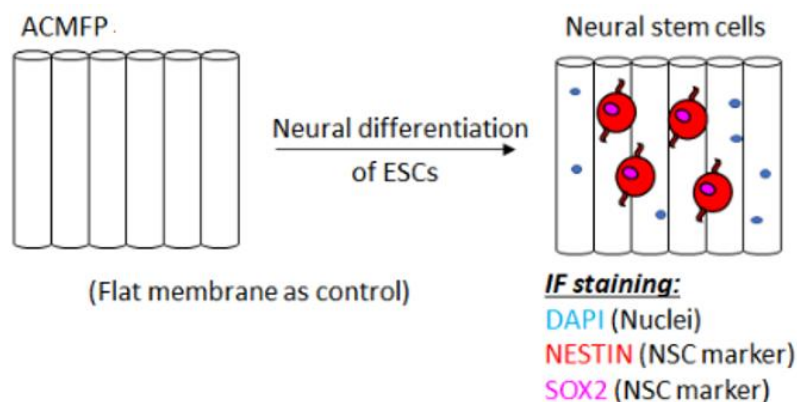
Figure 23. Diagram for the neural stem cell identification on the ACMFP. ESC-derived NBs were seeded and cultured on the 60 μm, 90 μm, 120 μm ACMFPs and PLGA flat membrane (control) for six days. The fixed ESNs with platforms were stained with the neural stem cell marker (NESTIN and SOX2) and cell nuclei marker (DAPI). The percentage of the NESTIN, SOX2, and NESTIN & SOX2 double-labeled cells in all groups were used to evaluate the role of the ACMCPs in neural stem cell differentiation.

Table 4. Primary antibody list for immunofluorescence in Chapter 3

Primary antibody	Company	Species	Catalog number	Dilution
SOX2	R&D	Goat	AF2018	1:200
NESTIN	DSHB	Mouse	RAT-401	1:100
GFAP	STCZ	Goat	SC-6170	1:200
TUJ1	AVES	Chicken	TUJ	1:500
MOG	Millipore	Mouse	AB5680	1:200
NF-L	AVES	Chicken	NFL	1:1500
KI-67	Thermofisher	Mouse	PA5-19462	1:400

Table 5. Secondary antibody list for immunofluorescence in Chapter 3

Secondary antibody	Company	Cat #	Combined primary antibody	Dilution
Alexa Fluor 488 Donkey anti-Mouse IgG	Jackson IR	715-546-150	MOG	1:500
Alexa Fluor 488 Donkey anti-Chicken IgY	Jackson IR	703-546-155	TUJ1	1:500
Cy3 Donkey anti-Chicken IgY	Jackson IR	703-166-155	TUJ1	1:500
Cy3 Donkey anti-Mouse IgG	Jackson IR	715-166-150	NESTIN; KI67	1:500
Cy3 Donkey anti-Goat IgG	Jackson IR	705-166-147	GFAP	1:500
Alexa Fluor 647 Donkey anti-Chicken IgY	Jackson IR	703-496-155	NF-L	1:500
Alexa Fluor 647 Donkey anti-Mouse IgG	Jackson IR	715-496-150	MOG	1:500
Alexa Fluor 647 Donkey anti-Goat IgG	Jackson IR	705-496-147	SOX2; GFAP	1:500

Evaluation of the ESNs on the ACMFPs and ASMFPs

To study the role of the ACMFP and ASMFP in neural differentiation, the immunofluorescence staining assays were used for cell identification on the platforms (Figure 24). The fixed ESNs (at least 3-6 independent ESNs differentiated from different batches of ESCs were used in the following experiments) were treated with blocking solution (Table 3) at room temperature for 1-2 hours. The ESNs were treated with the primary antibodies (Anti-MOG, anti-TU1J, and anti-GFAP, Table 4; each antibody was used for 3-6 independent cells staining

experiments) of the working solution (Table 3) in the 4 °C refrigerator overnight. ESNs were rinsed

with PBS three times and treated with the related secondary antibodies (Table 5) and nuclei

marker (DAPI, Invitrogen) at room temperature for 1-2 hours. The ESNs were rinsed with PBS

three times to remove the residual reagent (working solution with left second antibodies). The

ESNs were observed and imaged by Leica SPE confocal microscopy. The number and percentage

of MOG, TUJ1, and GFAP positive cells in each image were counted for the following

quantification studies.
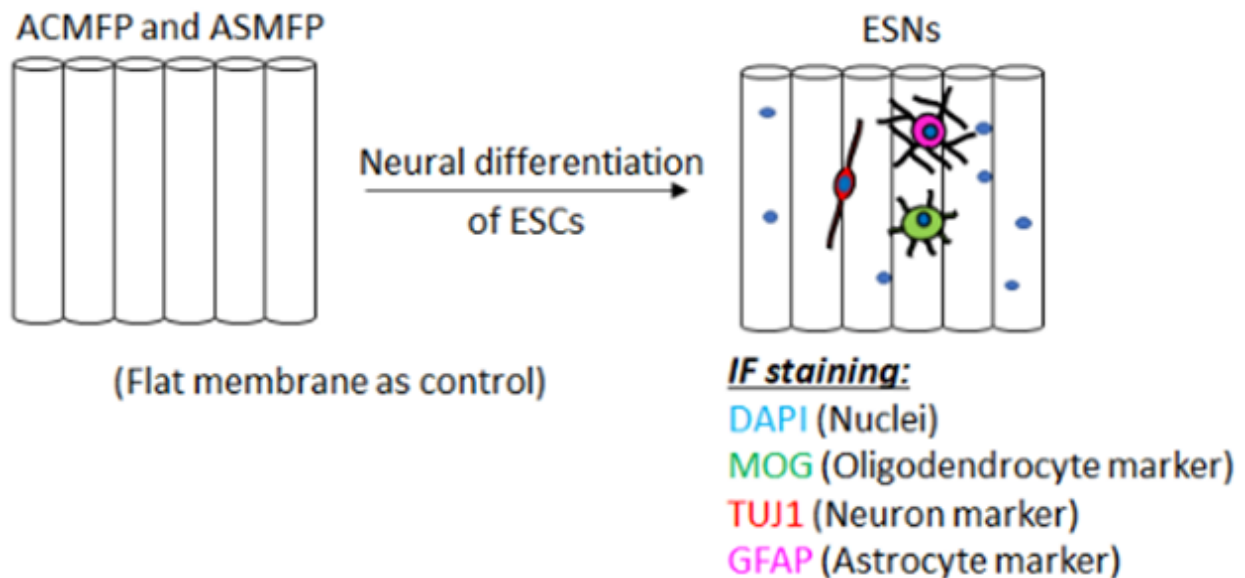
Figure 24. Diagram for the neural lineage cells identification on the ACMFP and ASMFP. ESC-derived NBs were seeded and cultured on the 0.7 μm, 1.5 μm, and 3 μm ACMFPs, ASMFPs, and their flat membrane (control) for six days. The fixed ESNs with platforms were stained with the MOG (oligodendrocyte marker), TUJ1 (neuron marker), GFAP (astrocyte marker), and cell nuclei marker (DAPI). The percentage of the MOG, TUJ1, and GFAP positive cells in all groups were used to evaluate the role of the ACMCPs in neural differentiation.

Initial cell attachment assay

The initial attachment needed to be tested on the ACMFPs to clarify whether the ACMFPs

stimulated neural differentiation by influence the cell attachment. The same volume and

concentration of the dissociated NBs (NBs were from 3 independent batches cell differentiation)

were seeded and cultured on the ACMFPs and PLGA flat membrane with 10% coverslip medium

in the 37 °C and 5% CO_2 incubator for 4 hours (Figure 25). After the cell attached, the samples

were stained with DAPI (1:500) in the 37 °C and 5% CO_2 incubator for 20 minutes. The samples

were imaged by Leica DMI 3000B epifluorescence microscopy. The number of the DAPI positive

cells were counted in the images to evaluate the cell initial attachment on the ACMFP.
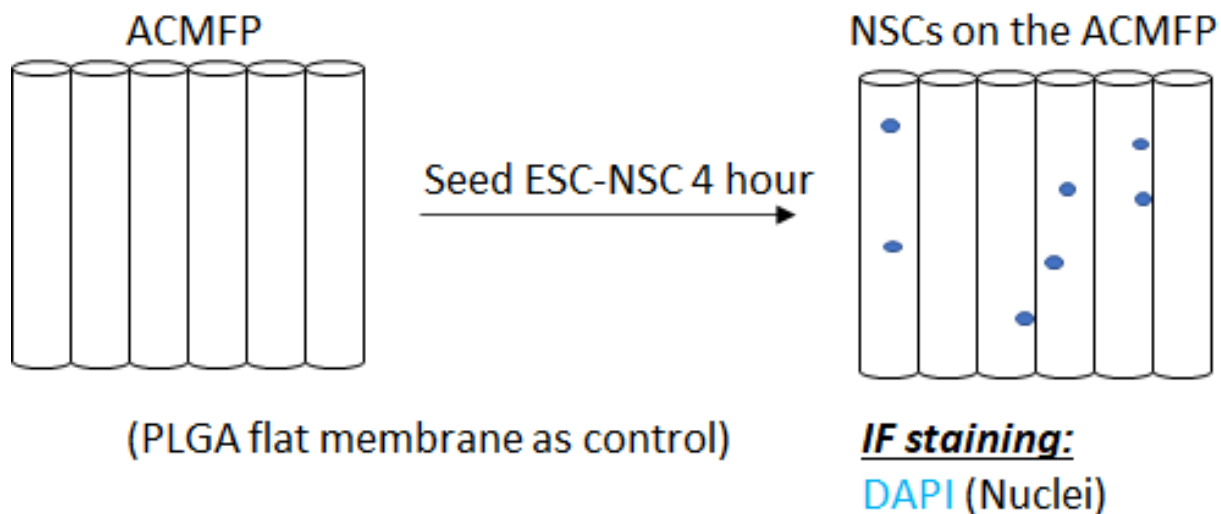
Figure 25. Diagram for the initial cell attachment evaluation. The same volume and concentration neural stem cells were seeded and cultured on the ACMFP and PLGA flat membrane (control) for 4 hours. After that, the cells attached on the platforms were stained with DAPI (cell nuclei marker). The number of the DAPI positive cells were counted in the images to evaluate the cell initial attachment on the ACMFP.

Cell proliferation test

The cell proliferation needed to be tested on the ACMFPs to clarify whether the ACMFPs

stimulated neural differentiation by influencing cell proliferation. The same volume and

concentration of the dissociated NBs were seeded and cultured on the ACMFPs and PLGA flat

membrane with 10% coverslip medium in the 37 °C and 5% CO_2 incubator (Figure 26). After 6

days, the fixed samples (3 independent cells differentiated from different batches of ESCs) were

treated with blocking solution (Table 3) at room temperature for 1-2 hours. The cells were

treated with the primary antibodies (Table 4; anti-KI67 was used for 3 independent cells staining

experiments) of the working solution (Table 3) in the 4 °C overnight. Cells were rinsed with PBS

three times and treated with the related secondary antibodies (Table 5) and nuclei marker (DAPI,

Invitrogen) at room temperature for 1-2 hours. The cells were rinsed with PBS three times to

remove the residual reagent (working solution with left second antibody). The cells were

observed and imaged by Leica SPE confocal microscopy. The percentage of KI67 positive cells in

each image was counted for the following quantification study.
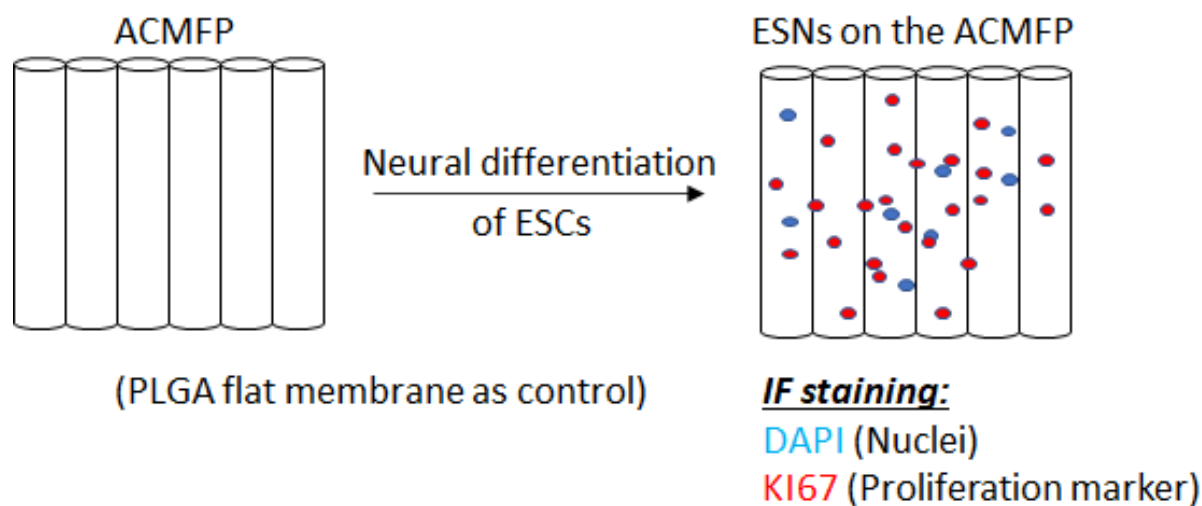
Figure 26. Diagram for the cell proliferation evaluation. The same volume and concentration neural stem cells were seeded and cultured on the ACMFP and PLGA flat membrane (control) for 6 days. After that, the cells were stained with KI-67 (proliferating cell marker) and DAPI (cell nuclei marker). The percentage of the KI67 positive cells were counted in the images to evaluate the cell proliferation on the ACMFP.

Neurite outgrowth of the ESNs on the ACMFPs and ASMFPs

To study the role of the ACMFP in neurite outgrowth, immunofluorescence staining

assays were used for cell identification on the platforms. The fixed ESNs (at least 3-6 independent

ESNs differentiated from different batches of ESCs were used in the following experiments) with

platforms treated with blocking solution (Table 3) at room temperature for 1-2 hours. The ESNs

were treated with primary antibodies (Anti-NF-L or anti-TU1J, Table 4; each antibody was used

for 3-6 independent cells staining experiments) of the working solution (Table 3) in the 4 °C

refrigerator overnight. ESNs were rinsed with PBS three times and treated with the related secondary antibodies (Table 5) and nuclei marker (DAPI, Invitrogen) at room temperature for 1-2 hours. The ESNs were rinsed with PBS three times to remove the residual reagent (working solution with second antibodies). The ESNs were observed and imaged by Leica SPE confocal microscopy. The length and direction of the NF-L or TUJ1 positive cells' neurite in each image were measured for the following quantification studies.

Quantification study and statistical analysis

To identify and quantify the neural stem cell yield on the ACMFPs, the immunofluorescence images of the NBs on the 60 µm, 90 µm, 120 µm ACMFPs and PLGA flat membrane were collected and analyzed. The positive cells of NESTIN, SOX2, and DAPI (samples (n) were from 3 independent experiments with same immunofluorescence staining) in the ESNs on the 60 µm, 90 µm, 120 µm ACMFPs and PLGA flat membrane were counted by the cell counter plugin module of Image J software (NIH). The percentage of the positive cells was equal to the number of SOX2, NESTIN, and SOX2 & NESTIN double-labeled cells over the number of DAPI positive cells (the total number of independent measurements between all treatment groups is 6, samples (n) were from 3 independent experiments).

To identify and quantify the new generated neural lineage cell types on the ACMFPs and ASMFPs, the immunofluorescence images of the ESNs on the 60 µm, 90 µm, 120 µm ACMFPs (the total number of independent measurements between all treatment groups is 12, samples (n) were from 4 independent experiments), 0.7 µm, 1.5, µm, 3 µm ASMFPs (the total number of independent measurements between all treatment groups is 24, samples (n) were from 3 independent experiments) and their flat membranes (control) were collected and analyzed. The

positive cells of MOG, TUJ1, GFAP, and DAPI (samples (n) were from 3-4 independent experiments with immunofluorescence staining) in the ESNs on the 60 μm, 90 μm, 120 μm ACMFPs and their flat membrane were counted by the cell counter plugin module of Image J software (NIH). The percentage of the positive cells was equal to the number of MOG, TUJ1, and GFAP cells over the number of DAPI positive cells (the total number of independent measurements between all treatment groups is 12, samples (n) were from 4 independent experiments for ACMFPs; the total number of independent measurements between all treatment groups is 24, samples (n) were from 3 independent experiments for ASMFPs).

To identify and quantify the initial cell attachment on the ACMFPs, the immunofluorescence images of the NBs on the ACMFPs (the total number of independent measurements between all treatment groups is 8, samples (n) were from 3 independent experiments) and PLGA flat membranes (control) were collected and analyzed. The DAPI positive cells (samples (n) were from 3 independent experiments with immunofluorescence staining) on the ACMFPs and PLGA flat membrane were counted by the cell counter plugin module of ImageJ software (NIH). The number of the DAPI positive cells were used to evaluate initial cell attachment (the total number of independent measurements between all treatment groups is 8, samples (n) were from 3 independent experiments).

To identify and quantify the cell proliferation on the ACMFPs, the immunofluorescence images of the NBs on the ACMFPs (the total number of independent measurements between all treatment groups is 8, samples (n) were from 3 independent experiments) and PLGA flat membranes (control) were collected and analyzed. The positive cells of KI67 and DAPI (samples (n) were from 3 independent experiments with immunofluorescence staining) on the ACMFPs

and PLGA flat membrane were counted by the cell counter plugin module of ImageJ software (NIH). The percentage of the KI67 positive cells was used to evaluate cell proliferation (the total number of independent measurements between all treatment groups is 8, samples (n) were from 3 independent experiments).

To study whether ACMFPs and ASMFPs can guide the neurite outgrowth direction, the immunofluorescence images of the ESNs on the 60 μm, 90 μm, 120 μm ACMFPs (the total number of independent measurements between all treatment groups is 10, samples (n) were from 3 independent experiments), 0.7 μm, 1.5, μm, 3 μm ASMFPs (the total number of independent measurements between all treatment groups is 24, samples (n) were from 3 independent experiments) and their flat membrane were collected and analyzed. The alignment value of the neurite on the 60 μm, 90 μm, 120 μm ACMFPs 0.7 μm, 1.5 μm, 3 μm ASMFPs and their flat membrane was measured by the angle plugin module of the Image J software (NIH). The alignment value of each fiber was equal to the angle between the neurite and the fiber direction. The low alignment value and low standard derivation mean that the neurite was considered as a high parallel stage. The high alignment value or high standard derivation means that the neurite was considered as random growth stage.

As mentioned in the previous parts separately, all the samples were collected from 3-6 independent experiments. Each independent experiment indicated the repeated experiment with independent platforms and cells. The number of n in each independent experiment means the number of the independent platforms or culturing wells. For example, "the total number of independent measurements between all treatment groups is 24 and samples (n) were from 3 independent experiments" indicated that the experiments were repeated 3 times with same

protocol in different day. In each experiment, there were 8 separate samples in each group. A total 24 (3 x 8) experiments were used for the quantification study and statistical evaluation.

The data are represented as mean ± standard deviation. Student's t-test, a one-way ANOVA with post-hoc Tukey HSD Test, and a two-way ANOVA test were used for statistical significance. The actual statistical power was calculated by G*power. The *p*-values smaller than 0.05 were considered significant (P<0.05, marked with *; P<0.01, marked with ** in the figures).

Results

Neural stem cell differentiation on the ACMFPs

A previous report showed that the ESC would differentiate into the neural stem cells by RA, EGF, FGF-2, and NGF treatments (Liu et al., 2018b). To study the role of the ACMSPs in the neural stem cell generation, the cells on the 60 μm, 90 μm, 120 μm ACMFPs, and PLGA flat membrane were double-labeled with two different types of neural stem cells marker (NESTIN and SOX2) as previously reported (Hu et al., 2017; Liu et al., 2018b). The immunofluorescence staining showed that 50.30 ± 6.84%, 44.18 ± 6.47%, 53.10 ± 7.29%, and 62.87 ± 5.60% cells on the 60 μm, 90 μm, 120 μm, and PLGA flat membrane were labeled with the NESTIN. 47.63 ± 6.27%, 45.09 ± 9.04%, 43.76 ± 4.95%, and 56.87 ± 3.70% cells on the 60 μm, 90 μm, 120 μm, and PLGA flat membrane were labeled with the SOX2. 42.07 ± 1.92%, 39.73 ± 3.38%, 38.75± 4.69%, and 44.23 ± 6.79% cells on the 60 μm, 90 μm, 120 μm, and PLGA flat membrane were double-labeled with the NESTIN & SOX2 (Figure 27). Quantification showed that the percentages of the NESTIN & SOX2 positive cells in 60 μm, 90 μm, and 120 μm ACMFPs did not have significantly difference with PLGA flat membrane ($F_{R (5,15)}$ = 2.489, P= 0.0784, $F_{C (3,15)}$= 2.385, P= 0.1100 for NESTIN & SOX2, actual statistical power = 1, two-way ANOVA; the total number of independent

measurements between all treatment groups is 6, samples (n) were from 3 independent

experiments). The results indicate that the ACMFPs did not influence neural stem cell generation.
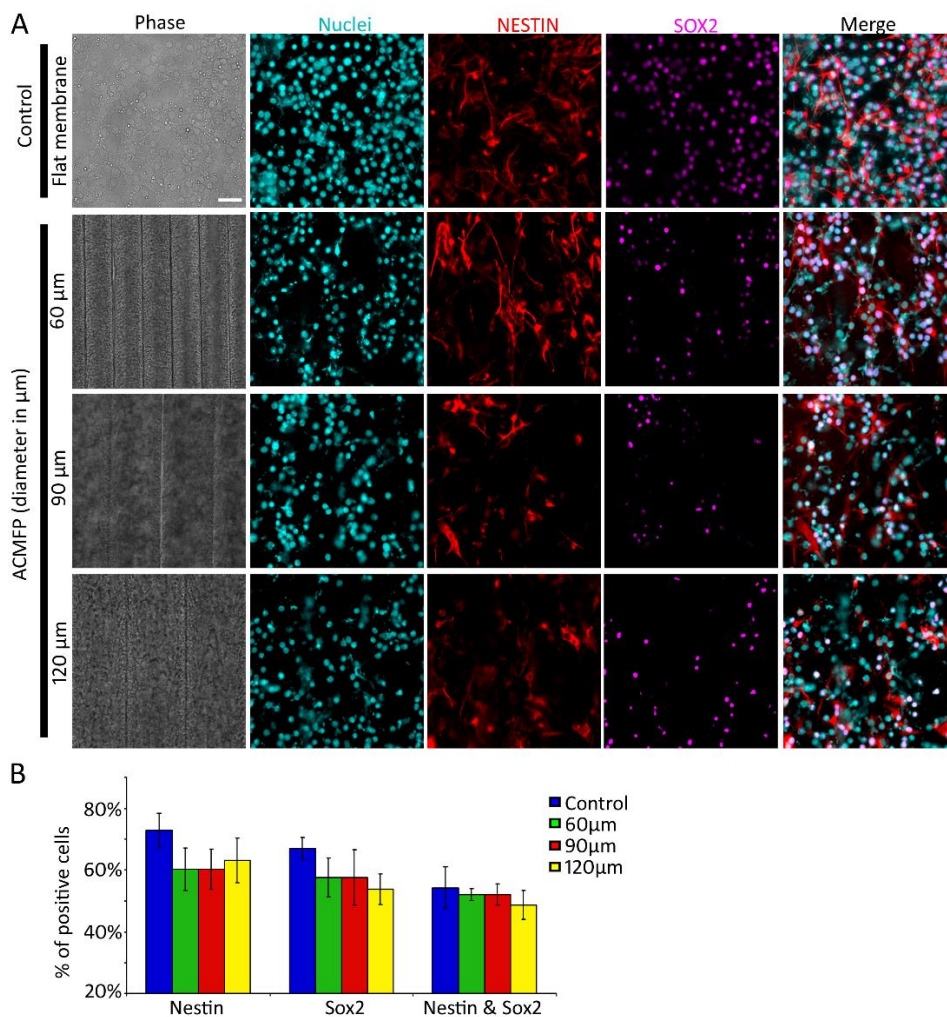
Figure 27. Neural stem cell differentiation on the ACMFP. (A) The ESCs derived NBs were cultured on the flat membrane and three groups of the ACMFPs for six days. The immunofluorescence staining $50.30 \pm 6.84\%$, $44.18 \pm 6.47\%$, $53.10 \pm 7.29\%$, and $62.87 \pm 5.60\%$ cells on the 60 µm, 90 µm, 120 µm, and PLGA flat membrane were labeled with the NESTIN. $47.63 \pm 6.27\%$, $45.09 \pm 9.04\%$, $43.76 \pm 4.95\%$, and $56.87 \pm 3.70\%$ cells on the 60 µm, 90 µm, 120 µm, and PLGA flat membrane were labeled with the SOX2. $42.07 \pm 1.92\%$, $39.73 \pm 3.38\%$, $38.75 \pm 4.69\%$, and $44.23 \pm 6.79\%$ cells on the 60 µm, 90 µm, 120 µm, and PLGA flat membrane were double-labeled with the NESTIN & SOX2 (neural stem cell markers) (B) The quantification study showed that the percentage of the Sox2/Nestin double-label cells on the flat membrane and three ACMSPs groups which showed not significant difference among them ($F_{R(5,15)}= 2.489$, P= 0.0784, $F_{C(3,15)}= 2.385$, P= 0.1100 for NESTIN & SOX2, actual statistical power = 1, two-way ANOVA; the total number of independent measurements between all treatment groups is 6, samples (n) were from 3 independent experiments). Figure published in Liu and colleagues, 2018 (Liu and Hu, 2018). Scale bar is 50 µm in A.

Neural differentiation on the ACMFPs

A previous report showed that the ESCs would differentiate into neural lineage cells (neuron and glia cells) by RA, EGF, FGF-2, and NGF treatments (Liu et al., 2018b). The neural lineage cells included three different types, which are neuron, astrocyte, and oligodendrocyte (Liang et al., 2020; Liu et al., 2018b; Tang et al., 2017). To study the role of the ACMSPs in the neural lineage cell differentiation, the cells on the 60 μm, 90 μm, 120 μm ACMFPs and PLGA flat membrane were labeled with different cell markers (MOG, marker for the oligodendrocyte; TUJ1, marker for the neuron; GFAP, marker for the astrocyte) as previously reported (Li et al., 2016; Liu et al., 2018b). Each antibody was used to label each type of neural lineage cell on the ACMFPs and flat membrane. The results showed that 8.08 ± 2.13%, 8.82 ± 2.29%, 9.67 ± 2.38%, and 2.62 ± 0.90 % cells on the 60 μm, 90 μm, 120 μm, and PLGA flat membrane were labeled with the TUJ1. 22.26 ± 4.56%, 21.69 ± 4.86%, 22.58 ± 5.31%, and 16.30 ± 2.85% cells on the 60 μm, 90 μm, 120 μm, and PLGA flat membrane were labeled with the GFAP (Figure 28). However, fewer MOG positive cells were found in 60 μm, 90 μm, 120 μm ACMFPs, and PLGA flat membrane (data showed the same result as the previous report (Liu et al., 2018b)). The quantification study showed that the percentage of the TUJ1 or GFAP positive cells in 60 μm, 90 μm, 120 μm ACMFPs were significantly higher than the PLGA flat membrane one ($F_{(3,44)}$= 20.62, P<0.0001, and actual statistical power= 0.99 for TUJ1, $F_{(3,44)}$= 5.09, P=0.0041, and actual statistical power= 0.99 for GFAP, one-way ANOVA with post-hoc Tukey HSD Test; the total number of independent measurements between all treatment groups is 12, samples (n) were from 4 independent experiments), while there was no significant difference among the 60
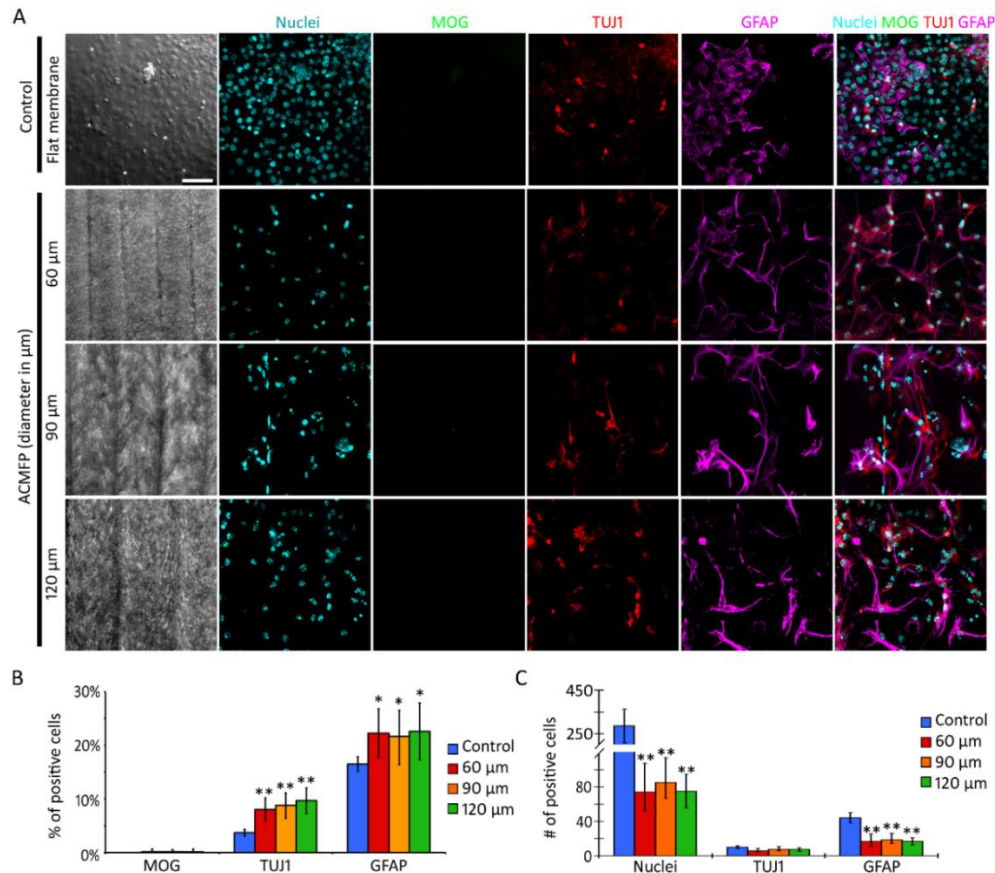
Figure 28. Neural differentiation on the ACMFP. (A) The ESCs derived NBs were cultured on the flat membrane and three groups of the ACMFPs for six days. The immunofluorescence staining images show that 8.08 ± 2.13%, 8.82 ± 2.29%, 9.67 ± 2.38%, and 2.62 ± 0.90 % cells on the 60 µm, 90 µm, 120 µm, and PLGA flat membrane were labeled with the TUJ1 (neuron marker). 22.26 ± 4.56%, 21.69 ± 4.86%, 22.58 ± 5.31%, and 16.30 ± 2.85% cells on the 60 µm, 90 µm, 120 µm, and PLGA flat membrane were labeled with the GFAP (astrocyte marker). Fewer cells were labeled with MOG (oligodendrocyte marker). (B) Quantification showed the percentage of the MOG, TUJ1, and GFAP positive cells on the flat membrane and three ACMSPs groups. The percentage of the TUJ1 or GFAP positive cells in 60 µm, 90 µm, 120 µm ACMFPs were significantly higher than the PLGA flat membrane one ($F_{(3,44)}$= 20.62, P<0.0001 for TUJ1, $F_{(3,44)}$= 5.09, P=0.0041 for GFAP), while there was no significant difference among the 60 µm, 90 µm, and 120 µm ACMFPs ($F_{R(11,22)}$= 1.204, P=0.340, $F_{C(2,22)}$= 1.536, P=0.2375 for TUJ1, $F_{R(11,22)}$= 1.481, P= 0.208, $F_{C(2,22)}$= 0.1135, P=0.8932 for GFAP, two-way ANOVA; the total number of independent measurements between all treatment groups is 12, samples (n) were from 4 independent experiments, * means P<0.05, ** means P<0.01). (C) Quantification showed that the number of the nuclei, TUJ1, and GFAP positive cells on the flat membrane and three ACMSPs groups. The number of the TUJ1 positive cells did not have a significant difference among all groups ($F_{(3,44)}$= 2.00, P=0.1264), while the number of the DAPI positive cells in the ACMFPs were significantly higher than the PLGA flat membrane ($F_{(3,44)}$= 55.38, P<0.0001, one-way ANOVA with post-hoc Tukey HSD Test; the total number of independent measurements between all treatment groups is 12, samples (n) were from 4 independent experiments, * means P<0.05, ** means P<0.01). Figure published in Liu and colleagues, 2018 (Liu and Hu, 2018). Scale bar is 50 µm in A.

μm, 90 μm, and 120 μm ACMFPs ($F_{R\,(11,22)}$ = 1.204, P=0.340, $F_{C(2,22)}$= 1.536, P=0.2375 for TUJ1, $F_{R(11,22)}$= 1.481, P= 0.208, $F_{C(2,22)}$= 0.1135, P=0.8932 for GFAP , and actual statistical power= 0.82 for GFAP, two-way ANOVA; the total number of independent measurements between all treatment groups is 12, samples (n) were from 4 independent experiments). These results indicate that ACMFPs seem to stimulate the neural lineage cell generation, especially for generation of neurons. However, the quantification study also showed that the number of the TUJ1 positive cells did not have a significant difference among all groups ($F_{(3,44)}$= 2.00, P= 0.1264, actual statistical power= 1, one-way ANOVA with post-hoc Tukey HSD Test; the total number of independent measurements between all treatment groups is 12, samples (n) were from 4 independent experiments), while the number of the DAPI and GFAP positive cells in the ACMFPs were significantly higher than the PLGA flat membrane ($F_{(3,44)}$= 55.38 for DAPI, $F_{(3,44)}$= 15.66 for GFAP, P<0.0001 and actual statistical power=1, one-way ANOVA with post-hoc Tukey HSD Test; the total number of independent measurements between all treatment groups is 12, samples (n) were from 4 independent experiments). These results indicate that the increasing neural yield on the ACMFPs was led by a reduction of total cells.

Mechanism of the ACMFPs induced neural differentiation

The neural yield increasing on the ACMFPs was led by the reduction of the total cell. Two reasons may induce fewer cells on the ACMFP after 6 days of culture: the ACMFPs limiting cell attachment or limiting cell proliferation. To prove these two hypotheses, the initial cell attaches assay and cell proliferation assay was processed separately.

For the initial cell attachment evaluation, the dissociated NBs were seeded and cultured on the ACMFP and PLGA flat membrane for 4 hours, followed by cell nuclei staining and

quantification. The staining images showed 32.46 ± 7.83 and 38.87 ± 2.67 DAPI positive cells per image attached to the ACMFP and PLGA flat membrane after 4 hours (Figure 29). However, the quantification study showed that the number of the DAPI positive cells did not significantly differ between the ACMFP group and PLGA flat membrane group (P=0.063, actual statistical power= 0.72, Student's t-test; the total number of independent measurements between all treatment groups is 8, samples (n) were from 3 independent experiments). This result indicated that the ACMFPs did not influence the cell attachment.
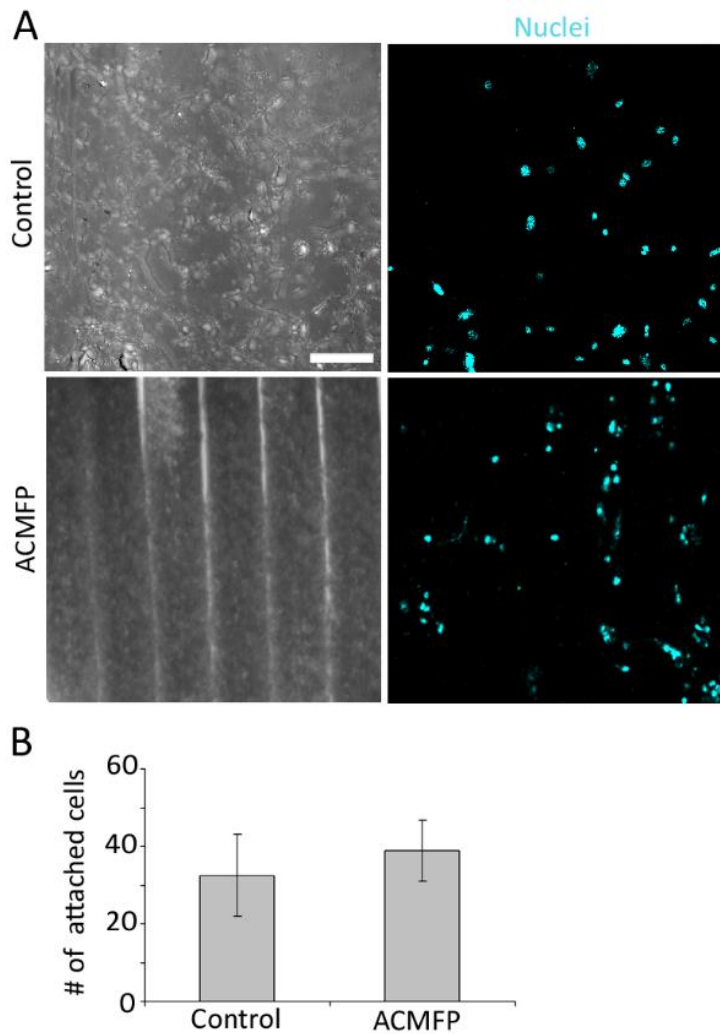
Figure 29. Cell attachment evaluation on the ACMFP. (A) The ESCs derived NBs were cultured on the flat membrane and ACMFPs for 4 hours. The immunofluorescence images show that the 32.46 ± 7.83 and 38.87 ± 2.67 DAPI positive cells per image were labeled in two groups (B) The quantification study showed that the number of the DAPI positive cells did not have a significant difference between the ACMFP group and PLGA flat membrane group (P=0.063, Student's t-test; the total number of independent measurements between all treatment groups is 8, samples (n) were from 3 independent experiments). Figure published in Liu and colleagues, 2018 (Liu and Hu, 2018). Scale bar is 100 μm in A.

For the cell proliferation evaluation, the dissociated NBs were seeded and cultured on the ACMFP and PLGA flat membrane for 6 days, followed by KI67 (proliferating cell marker) and DAPI (cell nuclei marker) staining and quantification. The staining images showed that 53.00 ± 8.94% and 68.52 ± 5.46% KI67 positive cells were on the ACMFP and PLGA flat membrane (Figure 30). Quantification showed that the percentage of the KI67 positive cells on the ACMFPs was significantly lower than the PLGA flat membrane one (P=0.0009, actual statistical power= 0.95, Student's t-test; the total number of independent measurements between all treatment groups is 8, samples (n) were from 3 independent experiments). This result indicates that the ACMFPs limit cell proliferation. These results suggest that the ACMFP might stimulate neural differentiation by limiting cell proliferation.
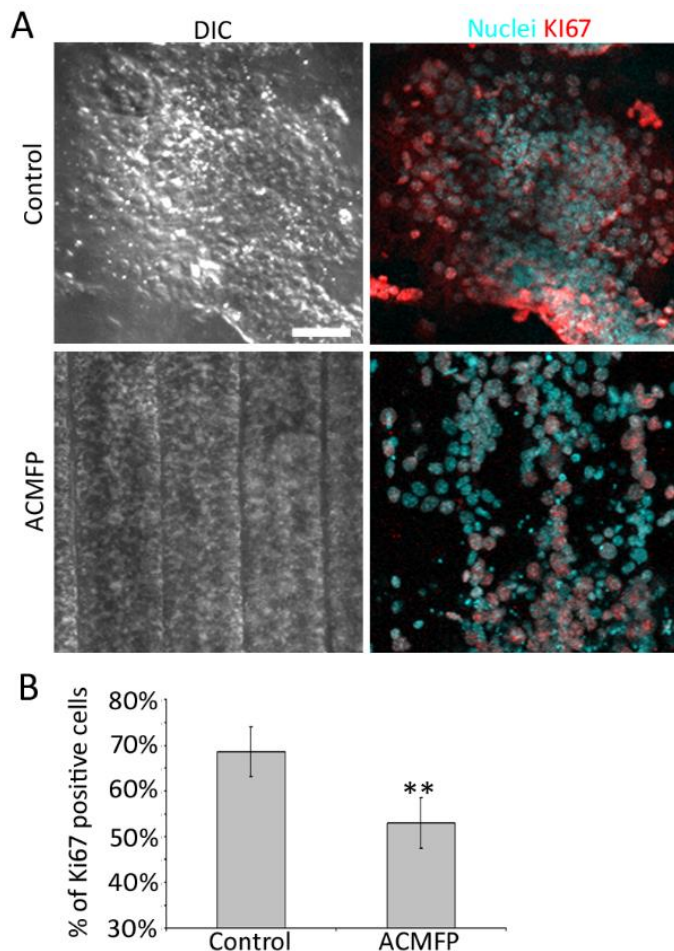
Figure 30. Cell proliferation evaluation on the ACMFP. (A) The ESCs derived NBs were cultured on the flat membrane and ACMFPs for 6 days. The immunofluorescence images show that the 53.00 ± 8.94% and 68.52 ± 5.46% cells were labeled with Ki67 in two groups (B) The quantification study showed that the percentage of the KI67 cells on the flat membrane and the ACMSP groups, which shows the significant decrease in the ACMFP group (P=0.0009, Student's t-test; the total number of independent measurements between all treatment groups is 8, samples (n) were from 3 independent experiments; ** means P<0.01). Figure published in Liu and colleagues, 2018 (Liu and Hu, 2018). Scale bar is 50 µm in A.

Neurite outgrowth on the ACMFP

The growth direction of the neurites in the flat membrane and ACMFPs groups were used to evaluate the role of the ACMFP in the neurite outgrowth. The ESNs on the 60 μm, 90 μm, 120 μm ACMFPs and PLGA flat membrane were labeled with NF-L (marker for the neuron and show the direction of the neurite(Li et al., 2016; Liu et al., 2018b)). The result showed that lots of cells were labeled by NF-L on the 60 μm, 90 μm, 120 μm ACMFPs and PLGA flat membrane (Figure 31).
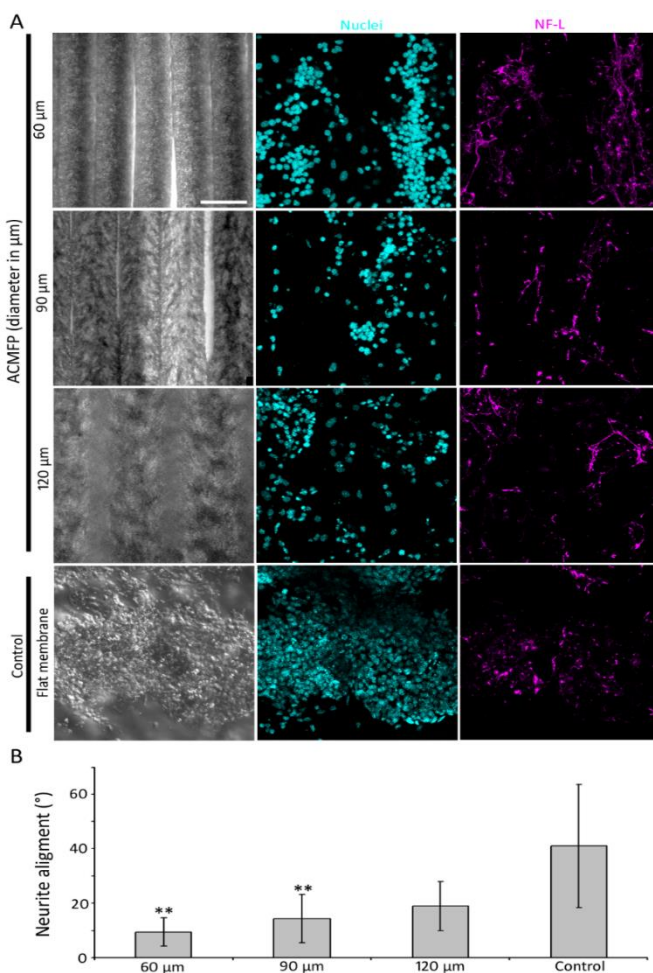
Figure 31. Neurite outgrowth evaluation on the ACMFP. (A) The ESCs derived NBs were cultured on the flat membrane and ACMFPs for 6 days. The immunofluorescence images show that the neurites of the ESNs were labeled with NF-L in flat membrane and all ACMFP groups (B) The quantification study showed that the neurites alignment value on the flat membrane and the ACMSP groups, which shows the significant decrease in the 60 and 90 μm ACMFP group ($F_{(3,36)}$= 38.50, P<0.0001, one-way ANOVA with post-hoc Tukey HSD Test; the total number of independent measurements between all treatment groups is 10, samples (n) were from 3 independent experiments; ** means P<0.01,). Figure published in Liu and colleagues, 2018 (Liu and Hu, 2018). Scale bar is 100 μm in A.

The quantification study showed that the alignment value of the ESNs on 60 μm and 90 μm ACMFPs were significantly lower than the 120 μm ACMFPs and PLGA flat membrane one ($F_{(3,36)}$= 38.50, P<0.0001, actual statistical power= 1, one-way ANOVA with post-hoc Tukey HSD

Test; the total number of independent measurements between all treatment groups is 10, samples (n) were from 3 independent experiments). The lower alignment value of the neurites on the 60 µm and 90 µm ACMFPs indicated that the neurite on these ACMFPs were considered as a high parallel stage. The results indicated that 60 µm and 90 µm ACMFPs seem to guide the neurite-aligned growth.

***Neural differentiation on the ASMFPs* (Pilot Data)**

The previous results showed that ACMFPs could stimulate neural differentiation (Liu and Hu, 2018). However, the role of the ASMFPs in neural differentiation is not clear. To study the role of the ASMFPs in the neural lineage cell differentiation, the cells on the 0.7 µm, 1.5, µm, 3 µm ASMFPs and flat membrane (PCL and glass) were labeled with different cell markers (MOG, marker for the oligodendrocyte; TUJ1, marker for the neuron; GFAP, marker for the astrocyte) as previously reported (Li et al., 2016; Liu et al., 2018b). Each antibody was used to label each type of neural lineage cell on the ASMFPs and flat membrane. The result showed 50.91 ± 5.90%, 47.05 ± 6.13 %, 40.37 ± 7.58%, 10.44 ± 3.12%, and 7.36 ± 2.48% cells were labeled by TUJ1 on the 0.7 µm, 1.5 µm, 3 µm ACMFPs and flat membrane (PCL and glass, Figure 32). 7.92 ± 2.35%, 8.05 ± 3.49%, 20.61 ± 7.04%, 17.35 ± 6.72%, and 17.18 ± 4.08% cells were labeled by GFAP on the 60 µm, 90 µm, 120 µm ACMFPs and flat membrane (PCL and glass, Figure 32). However, fewer MOG positive cells were found in 0.7 µm, 1.5 µm, 3 µm ASMFPs, and flat membrane (data showed the same result as the previous report (Liu et al., 2018b)).

The quantification study showed that the percentage of the TUJ1 positive cells in 0.7 µm, 1.5, µm, 3 µm ASMFPs were significantly higher than the glass and PCL flat membrane one ($F_{(4,115)}$= 353.84, P<0.0001, actual statistical power= 1, one-way ANOVA with post-hoc Tukey HSD

Figure 32. Neural differentiation on the ASMFP (Pilot data). (A) The ESCs derived NBs were cultured on the glass coverslip, flat membrane, and three groups of the ASMFPs for six days. The immunofluorescence staining images show that 50.91 ± 5.90%, 47.05 ± 6.13 %, 40.37 ± 7.58%, 10.44 ± 3.12%, and 7.36 ± 2.48% cells were labeled by TUJ1 on the 0.7 μm, 1.5 μm, 3 μm ACMFPs and flat membrane (PCL and glass). 7.92 ± 2.35%, 8.05 ± 3.49%, 20.61 ± 7.04%, 17.35 ± 6.72%, and 17.18 ± 4.08% cells were labeled by GFAP on the 60 μm, 90 μm, 120 μm ACMFPs and flat membrane (PCL and glass). Fewer cells were labeled with MOG. (B) The quantification study showed that the
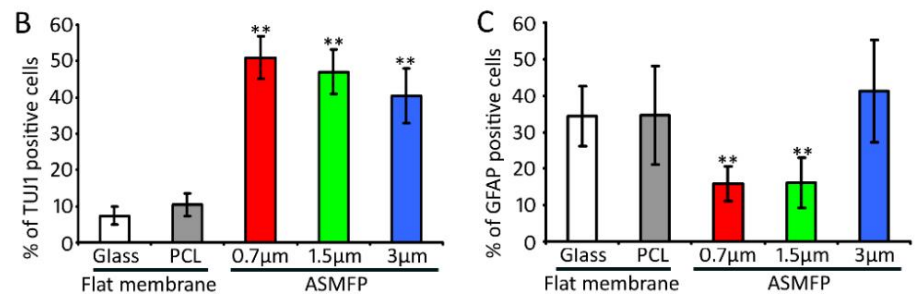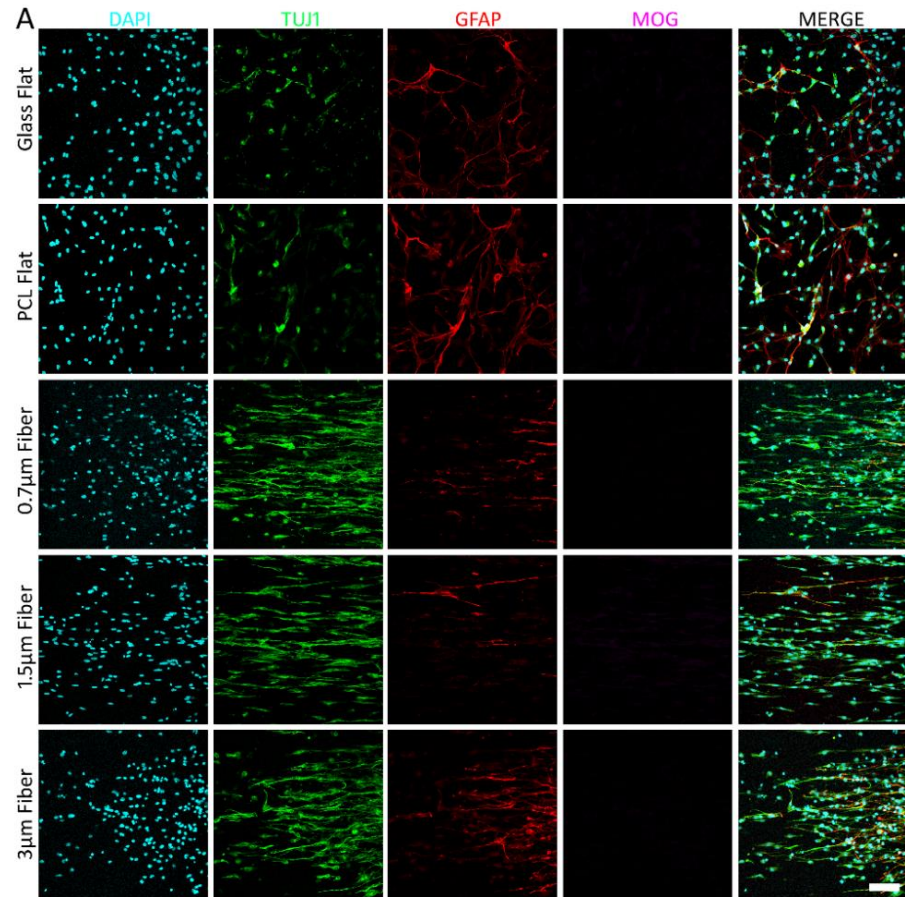
percentage of the TUJ1 positive cells in 0.7 μm, 1.5, μm, 3 μm ASMFPs were significantly higher than the glass and PCL flat membrane one ($F_{(4,115)}$= 353.84, P<0.0001), while the percentage of the 0.7 μm, 1.5, μm ASMFPs were significantly higher than 3 μm ASMFP one ($F_{(2,69)}$= 15.77, P=0.002, one-way ANOVA with post-hoc Tukey HSD Test; the total number of independent measurements between all treatment groups is 24, samples (n) were from 3 independent experiments). (C) The percentage of the GFAP positive cells in 0.7 μm and 1.5 μm ASMFPs were significantly lower than the 3 μm ASMFPs, and glass or PCL flat membrane one ($F_{(4,115)}$= 31.87, P<0.0001), while there was no significant among the 3 μm ASMFPs, glass, and PCL flat membrane one ($F_{(2,69)}$= 2.41, P=0.0977, one-way ANOVA with post-hoc Tukey HSD Test; the total number of independent measurements between all treatment groups is 24, samples (n) were from 3 independent experiments). The data is collected using ASMFP produced by the same batch of the PCL solution. Scale bar is 50 μm.

Test; the total number of independent measurements between all treatment groups is 24, samples (n) were from 3 independent experiments), while the percentage of the 0.7 µm, 1.5, µm ASMFPs were significantly higher than 3 µm ASMFP one ($F_{(2,69)}$= 15.77, P=0.002, actual statistical power= 0.99, one-way ANOVA with post-hoc Tukey HSD Test; the total number of independent measurements between all treatment groups is 24, samples (n) were from 3 independent experiments). On the other hand, the percentage of the GFAP positive cells in 0.7 µm and 1.5 µm ASMFPs were significantly lower than the 3 µm ASMFPs, and glass or PCL flat membrane one ($F_{(4,115)}$= 31.87, P<0.0001, actual statistical power= 1, one-way ANOVA with post-hoc Tukey HSD Test; the total number of independent measurements between all treatment groups is 24, samples (n) were from 3 independent experiments), while there was no significant among the 3 µm ASMFPs, glass, and PCL flat membrane one ($F_{(2,69)}$= 2.41, P= 0.0977, actual statistical power= 1, one-way ANOVA with post-hoc Tukey HSD Test; the total number of independent measurements between all treatment groups is 24, samples (n) were from 3 independent experiments). Thus, all the results indicated that the ASMFPs could stimulate neural differentiation, while the small size of the ASMFPs showed the best performance. In addition, the small size of the ASMFPs can limit glia differentiation.

***Neurite outgrowth on the ASMFP* (Pilot Data)**

The previous report showed that nano-fibers also could guide neurite outgrowth. The neurite direction evaluation was analyzed in the glass, flat membrane, and all three ASMFPs groups to evaluate these. The immunofluorescence staining showed that the TUJ1 positive cells, which grew on the glass, flat membrane, and 3 µm ASMFP, showed direction randomly, while the TUJ1 positive cells, which grew on the 0.7 µm and 1.5 µm ASMFPs showed the parallel

morphology. It indicated that the small size of the ASMFPs seems to guide neurite outgrowth, while it showed that the ASMFPs played a vital role in neurite outgrowth. As previously reported, the small size of the ACMFPs can guide the neurite outgrowth direction. However, the role of the ASMFPs in neurite outgrowth is not clear. To study this point, the growth direction of the neurites in the flat membrane and ASMFPs groups were used to evaluate the role of the ASMFP in the neurite outgrowth. The ESNs on the 0.7 µm, 1.5 µm, 3 µm ACMFPs and flat membrane were labeled with TUJ1 (marker for the neuron and show the direction of the neurite (Hackelberg et al., 2017; Liu et al., 2018b)). The result showed that lots of cells were labeled by TUJ1 on the 0.7 µm, 1.5 µm, 3 µm ASMFPs and flat membrane (Figure 33). The quantification study showed that

Figure 33. Neurite outgrowth evaluation on the ASMFP (Pilot data). (A) The ESCs derived NBs were cultured on the flat membrane and ASMFPs for 6 days. The immunofluorescence images show the TU1J positive neurons' neurites' growth direction in glass flat, PCL flat, 0.7 µm, 1.5 µm, and 3 µm ASMFP groups. The
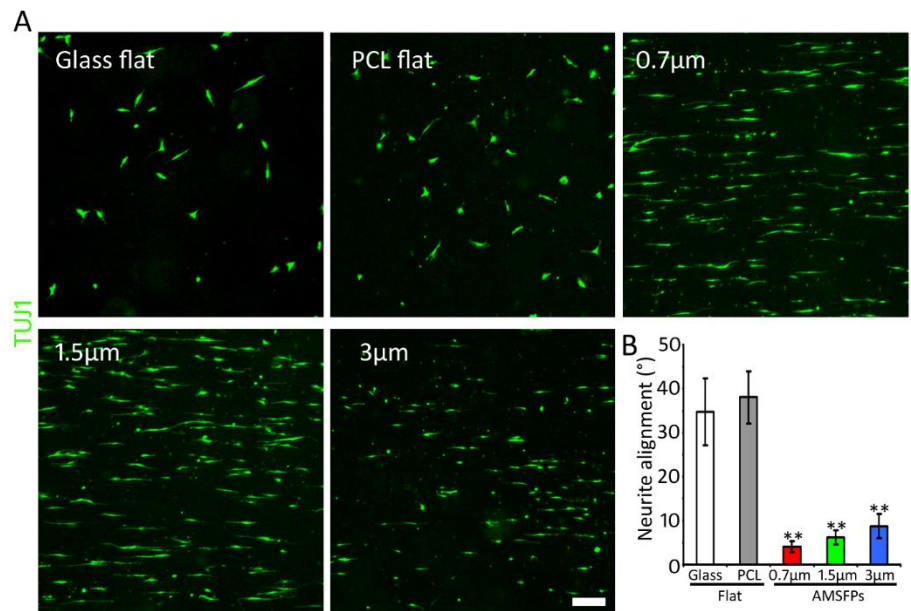
quantification study showed that the alignment value of the ESNs' neurites on the 0.7 µm, 1.5 µm, 3 µm ASMFPs were significantly lower than the flat membrane one ($F_{(4,115)}$ = 313.31, P<0.0001, one-way ANOVA with post-hoc Tukey HSD Test; the total number of independent measurements between all treatment groups is 24, samples (n) were from 3 independent experiments). The lower alignment value of the neurites on the 0.7 µm, 1.5 µm, and 3 µm ASMFPs indicated that the neurite on these ASMFPs were considered as a high parallel stage. The alignment value of the 0.7 µm, 1.5 µm, and 3 µm ASMFPs showed an increasing tendency significantly ($F_{(2,69)}$ = 34.41, P<0.0001, one-way ANOVA with post-hoc Tukey HSD Test; n=24, samples were from 3 independent experiments). The data is collected using ASMFP produced by the same batch of the PCL solution. Scale bar is 100 µm in A.

the alignment value of the ESNs neurites on the 0.7 μm, 1.5 μm, 3 μm ASMFPs was significantly lower than the flat membrane one ($F_{(4,115)}$ = 313.31, P<0.0001, actual statistical power= 1, one-way ANOVA with post-hoc Tukey HSD Test; the total number of independent measurements between all treatment groups is 24, samples (n) were from 3 independent experiments). The lower alignment value of the neurites on the 0.7 μm, 1.5 μm, and 3 μm ASMFPs indicated that the neurite on these ASMFPs were considered as a high parallel stage. The alignment value of the 0.7 μm, 1.5 μm, and 3 μm ASMFPs showed an increasing tendency significantly ($F_{(2,69)}$= 34.41, P<0.0001, actual statistical power= 1, one-way ANOVA with post-hoc Tukey HSD Test; the total number of independent measurements between all treatment groups is 24, samples (n) were from 3 independent experiments). The data is collected using ASMFP produced by the same batch of the PCL solution. Additional experiments are required to complete the project.

Discussion

The purpose of this study was to identify the role of topography in neural differentiation. The previous papers showed that the nano-pattern platform stimulated neural differentiation while the micro-pattern platform guided the neurite outgrowth (Cheng and Kisaalita, 2010; Yang et al., 2005). However, the detailed role of the topography in neural differentiation is not clear. To study this aim, the ESC was guided to differentiate to the neural stem cell and neural linage cells as previous "step by step" method (Liu et al., 2018b).

To study the role of the micro-topography in neural differentiation, the ESC-derived NBs were seeded and cultured on the different sizes of the ACMFPs and the PLGA flat membrane (control for the topography). The multiply protein markers were labeled the cells on the platforms for the neural stem cell and neural lineage cell identification (Liu et al., 2018b). The

results showed that the ACMFP could not influence neural stem cell differentiation, while it could stimulate neural differentiation and glial differentiation. The mechanism testing results showed that the affection of this simulation was caused by the limitation of the cell proliferation on the ACMFPs. Otherwise, the small size (60 μm and 90 μm) of the ACMFP could guide the neurite outgrowth, while the large size (120 μm) of the ACMFP could not.

To study the role of the nano- and submicro-topography in the neural differentiation, the ESC-derived NBs were seeded and cultured on the different sizes of the ASMFPs and the flat membrane (control for the topography). The multiply protein markers were labeled the cells on the platforms for neural lineage cell identification (Liu et al., 2018b). The results showed that the ASMFP could stimulate neural differentiation, while the small size (0.7 μm and 1.5 μm) of the ASFMP could inhibit the glia differentiation. Otherwise, the ASMFP could guide the neurite outgrowth. Smaller ASMFP showed better guidance for the neurite outgrowth.

This dissertation hypothesizes the fiber pattern active the Integrin receptor to decide the stem cell differentiation. Different types of Integrins were expressed on the ESN cell membrane (data not shown). However, these integrins' role in the topography-induced stem cell differentiation and neurite outgrowth was not clear. Moreover, the specific intracellular pathway for this affection was not clear yet. The specific experiments, which included receptor knock-out, overexpression, and inhibitor treatment, will be processed in the system in future research. These future studies may clarify the mechanism for the topography-induced stimulation.

In this chapter, we hypothesis that ACMFP and ASMFP could stimulate neural stem cell differentiation and neural lineage cell differentiation. However, the result showed that the

ACMFP could not influence the neural stem cell differentiation, while the part of the ASMFP could inhibit the glial differentiation. As a limitation of the technologies, only four groups of protein markers can be labeled in one group of samples (Liu et al., 2018b). The cell identification from the one or two protein markers is weak. Otherwise, the cell function assay was not used for the neural differentiation evaluation, limiting the study of the role of the topography in stem cell differentiation.

In summary, the ESC-derived NBs were cultured on the ACMFP and ASMFP. Both ACMFP and ASMFP could stimulate neural differentiation and guide the neurite outgrowth. It indicated that the topography played a vital role in neural differentiation. The multiply cell identify experiments, cell function evaluation and mechanism would be tested in the future. The study and usage of biomaterial-induced neural differentiation will contribute to ECM-induced cell growth, differentiation, and maturation, while it also contributes to future clinical application.

CHAPTER 4 – SYNAPTOGENESIS OF THE ESN ON THE DIFFERENT SIZE OF THE ASMFP

Abstract

The micro-environment of the ECMs plays a crucial role in neuron maturation and synaptogenesis. However, the role of topography in the synaptogenesis between stem cell differentiated neurons is not precise. The ESCs induced NBs were seeded and cultured on the submicro- and nano-fiber platforms (ASMFPs). After six days, the ESNs generated and formed a connection with other ESNs. The different synaptic markers (SV2, PSD93, and Syn1) were used to label and evaluate the newly generated synapses between the ESNs as in previous reports. The staining and quantification showed that the ESNs on the 0.7 µm and 1.5 µm ASMFPs expressed more synaptic markers than the 3 µm ASMFP or the flat membrane. The results indicate that the submicro- and nano-fiber platforms could stimulate the formation of the synapse *in vitro*. These studies about the topography-induced ESNs synaptogenesis contribute importantly to stem cell-based research and future clinical therapy.

Introduction

Synaptogenesis of the ESN in vitro

Overview of the synaptogenesis

During development, neurons connect and form a functional structure at the end of the neurites or axon, called the synapse (Palay, 1956; Perea et al., 2009). The synapse can transmit the electro-chemical signal via the release and binding of neurotransmitters (Perea et al., 2009). Several studies have focused on the study of synaptogenesis, synapse maturation, and synaptic plasticity (Blanco-Suarez et al., 2018; Li et al., 2016; Liu et al., 2018b; Schafer et al., 2012; Varoqueaux et al., 2006). In this dissertation, we mainly focused on synaptogenesis. Typically,

synaptogenesis between two neurons can be divided into three steps: (1) the axon or neurite of the neuron targets into other neurons; (2) synapse-like structure form at the end of the neurites; (3) the new synapse expresses several synaptic protein markers, release of neurotransmitter and electrophysiology activity. The auditory neuron, for example (Carricondo and Romero-Gomez, 2019), will target its upstream sensory cells (hair cells) and downstream cells (CN neurons) at the end of SGNs development. The mature synapse will then form among these three cells and transfer the signal from the hair cells to CN neurons *in vivo*.

Synaptogenesis between the stem cell-derived neurons

As previously reported, the ESC could differentiate into the ESNs, which expressed the neuron-specific gene, protein, iron channel, and electrophysiological activity (Liu et al., 2018b). In addition, synaptogenesis is also an index to evaluate a newly generated neuron. To study the ability of the synaptogenesis between the ESN and native neurons, the co-culture assay or tri-culture assay was used (Chen et al., 2018; Liu et al., 2018b). The ESN were cultured with native neurons for several days, following with synaptogenesis evaluation. Several methods could be used for synaptogenesis evaluation (Chen et al., 2018; Liu et al., 2018b). Firstly, the physical connection and morphology of synapses between neurons were observed and evaluated. Secondly, the multiply synapse protein markers were used to label the synapse between the connections. Lastly, the signal transmission between the connected neurons was tested by patch-clamp assays *in vitro*. Our previous report showed that ESNs could make the synapse-like structure with the native neurons in the co-culture assay *in vitro* (Liu et al., 2018b). However, the connected ESNs expressed fewer synapse protein markers and showed low electrophysiological activity. Bio-chemical treatment method was used to stimulate synaptogenesis with good results

(Liu et al., 2018b). However, this method was only suitable for the *in vitro* culturing system, suggesting another type of method needs to be considered.

Physical factor-induced synaptogenesis

During development, synaptogenesis of native neurons happens in a complex micro-environment *in vivo* (Govey et al., 2013; Keung et al., 2010; Lapointe et al., 2013). The micro-environment includes topographical information, physiological cues, soluble factors, and cell-cell interactions. A previous report showed that a soft matrix could stimulate synaptogenesis (Zhang et al., 2014). However, fewer reports show that the topography can stimulate the synaptogenesis between the stem cell-derived neurons. In this dissertation, the ASMFPs were used to mimic the submicro- and nano-topography and evaluate their role in the ESNs' synaptogenesis.

Rationale and hypothesis for Chapter 4

The ESC-derived NBs were seeded and cultured on the ASMFPs to study the role of the topography in synaptogenesis. The neuronal connection and synapse-specific protein markers were identified and evaluated on the different platforms and a flat membrane. We hypothesized that ASMFP can stimulate synaptogenesis between the ESNs. The stimulation will increase as their fiber size decreases.

Materials and methods

Evaluation of synaptogenesis on the ASMFPs

The previous report showed that the ESC-derived ESNs have fewer synapses between neural connections, as fewer synaptic markers were expressed along the connection (Liu et al., 2018b). There has been no report that showed that the topography could stimulate the ESNs synaptogenesis. To study this role of the topography in neural synaptogenesis, the NBs were

seeded and cultured for 6 days on all the ASMFP groups and flat membranes (glass and PCL) (Figure 34). The fixed ESNs on the platforms were treated with blocking solution (Table 3) at room temperature for 1-2 hours. The ESNs on the platforms were treated with the primary antibodies (Anti-SV2, anti-SYN1, anti-PSD93, AND anti-TUJ1; Table 6; each antibody was used for 3 independent cells staining experiment) the working solution (Table 3) 4 °C refrigerator overnight. ESNs were rinsed with PBS three times and treated with the related secondary antibodies (Table 7) and nuclei marker (DAPI, Invitrogen) at room temperature for 1-2 hours. The ESNs were rinsed with PBS three times to remove the residual reagent (secondary antibodies and working solution). The ESNs were observed and imaged by Leica SPE confocal microscopy. The number and area of the SV2, PSD93, and SYN1 positive puncta in each image were counted for the following quantification studies.
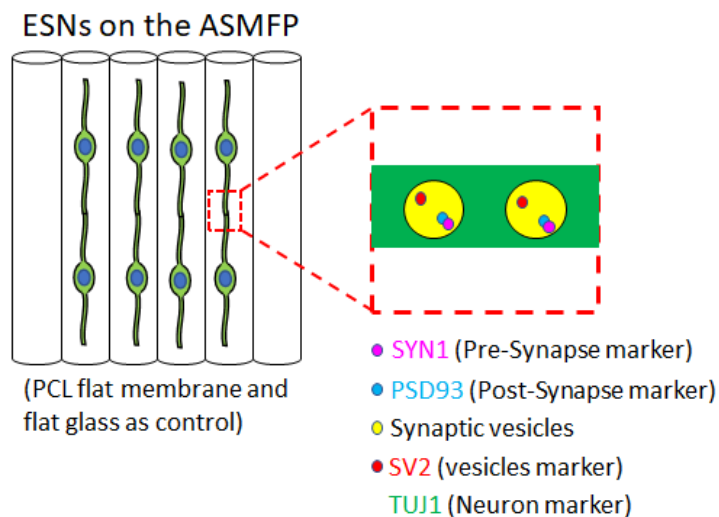
Figure 34. Diagram of the synaptogenesis evaluation on the ASMFP. The ESC-derived NBs were seeded and cultured on the 0.7 μm, 1.5 μm, and 3 μm ACMFPs, ASMFPs, and their flat membrane (control) for six days. The fixed ESNs with platforms were stained with the SYN1 (pre-synapse marker), PSD93 (post-synapse marker), SV2 (synaptic vesicle marker), and TUJ1 (neuron marker). The number and area of the SV2, PSD93, and SYN1 positive puncta in each image were counted for the following quantification studies.

Table 6. Primary antibody list for immunofluorescence in Chapter 4

Primary antibody	Company	Species	Catalog number	Dilution
SV2	DSHB	Mouse	SV2-A	1:50
SYN1	STCZ	Goat	SC-8295-R	1:200
PSD93	SYSY	Rabbit	124102	1:200
TUJ1	AVES	Chicken	TUJ	1:500

Table 7. Secondary antibody list for immunofluorescence in Chapter 4

Secondary antibody	Company	Cat #	Combined primary antibody	Dilution
AMCA Donkey anti-Rabbit IgG	Jackson IR	711-156-152	PSD93	1:500
Alexa Fluor 488 Donkey anti-Chicken IgY	Jackson IR	703-546-155	TUJ1	1:500
Cy3 Donkey anti-Mouse IgG	Jackson IR	711-166-150	SV2	1:500
Alexa Fluor 647 Donkey anti-Goat IgG	Jackson IR	705-496-147	SYN1	1:500

Quantification study and statistical analysis

To identify and quantify the newly generated synapses on the ASMFPs, the immunofluorescence images of the ESNs on the 0.7 μm, 1.5 μm, 3 μm ACMFPs and flat membranes (glass and PCL) (the total number of independent measurements between all treatment groups is 24, samples (n) were from 3 independent experiments) were collected and analyzed. Each connected TUJ1 positive cells were collected in each immunofluorescence image, which was considered a connected neuron-like cell and could form a synapse. The number and total area of the SV2 and PSD93 & SYN1 colocalized puncta along one TUJ1 positive connection were analyzed by the analyze particles plugin module of Image J software (each puncta size was chosen as 0.4-3 μm^2; the total number of independent measurements between all treatment groups is 24, samples (n) were from 3 independent experiments for ASMFPs) as previously reported (Liu et al., 2018b).

As mentioned in the previous parts separately, all the samples were collected from 3-6 independent experiments. Each independent experiment indicated the repeated experiment with independent platforms and cells. The number of n in each independent experiment means the number of the independent platforms or culturing wells. For example, "the total number of independent measurements between all treatment groups is 24 and samples (n) were from 3 independent experiments" indicated that the experiments were repeated 3 times with same protocol in different day. In each experiment, there were 8 separate samples in each group. A total 24 (3 x 8) experiments were used for the quantification study and statistical evaluation.

The data are represented as mean ± standard deviation. Student's t-test, a one-way ANOVA with post-hoc Tukey HSD Test, and a two-way ANOVA test were used for statistical significance. The actual statistical power was calculated by G*power. The p-values smaller than 0.05 were considered significant (P<0.05, marked with *; P<0.01, marked with ** in the figures).

Results

A previous report showed that the ESC-derived ESNs have less synapse, which showed an immature condition for signal transmission [ref]. To stimulate synaptogenesis between the ESNs, the ASMFPs were used as a platform for the ESNs, which studied the role of the ASMFPs in synaptogenesis. The ESCs derived NBs were seeded and cultured on the different sizes of the ASMFPs to study the role of the ASMFPs in the stem cell-derived neuron's synaptogenesis. The immunofluorescence images showed several TUJ1 positive cells connected in all ASMFPs groups and flat membrane (glass and PCL) (Figure 35). In addition, the SV2 (synaptic vesicle marker), SYN1 (pre-synaptic marker), PSD93 (post-synaptic marker) were also labeled along the TUJ1 positive connection in the 0.7 μm, 1.5 μm, 3 μm ASMFPs groups, and flat membranes groups

(Figure 34).
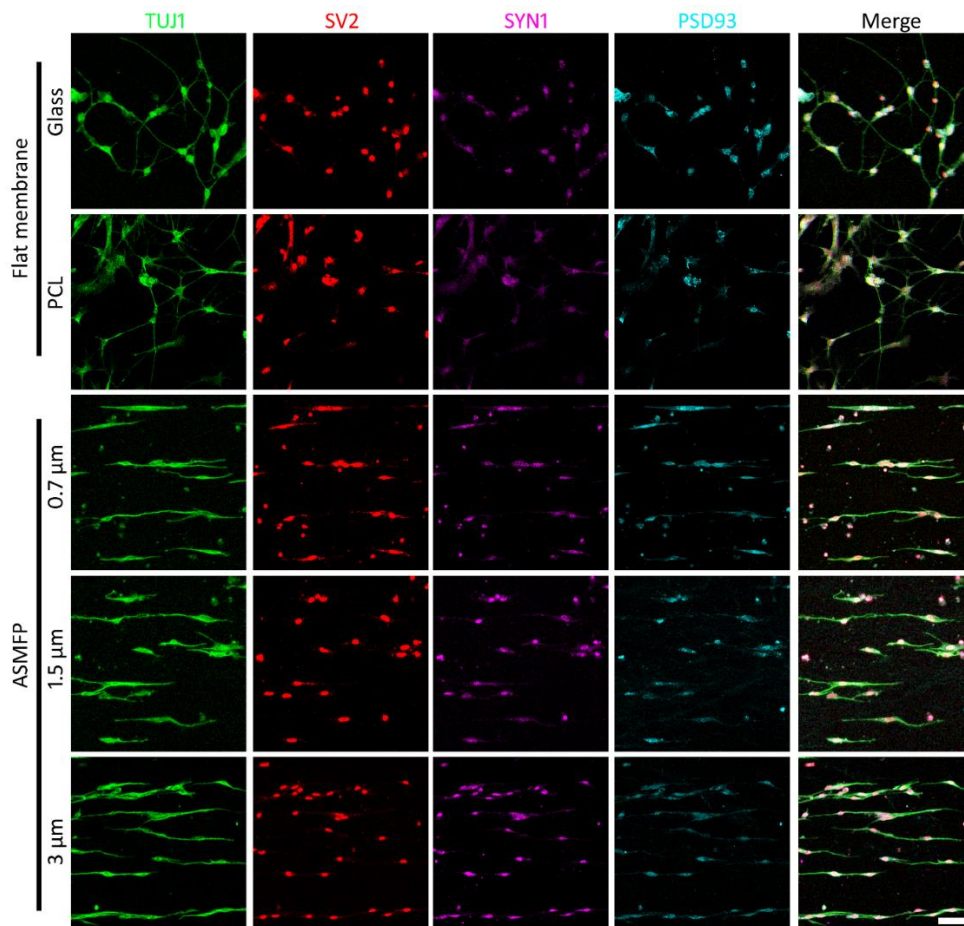
Figure 35. Connected ESNs from synapse on the ASMFP (Pilot data). The ESCs derived NBs were seeded and cultured on the different sizes of the ASMFPs to study the role of the ASMFPs in the stem cell-derived neuron's synaptogenesis. The immunofluorescence images showed several TUJ1 positive cells connected in all ASMFPs groups and flat membrane (glass and PCL). The SV2 (synaptic vesicle marker), SYN1 (pre-synaptic marker), PSD93 (post-synaptic marker) were also labeled along the TUJ1 positive connection in the 0.7 μm, 1.5 μm, 3 μm ASMFPs groups, and flat membranes groups. The data is collected using ASMFP produced by the same batch of the PCL solution. Scale bar is 20 μm.

The quantification study showed that the number and total area of the SV2 positive puncta along the connection in 0.7 μm and 1.5 μm ASMFPs were significantly higher than the 3 μm ASMFP, glass and PCL flat membrane one (Figure 36; $P<0.0001$, $F_{(4,115)}=50.22$ and actual statistical power= 0.95 for puncta number and total area, $F_{(4,115)}=44.84$ and actual statistical power= 0.88 for puncta number, actual statistical power= 0.98 for puncta area, one-way ANOVA

with post-hoc Tukey HSD Test; n=24, samples were from 3 independent experiments).

Figure 36. Evaluation of the synaptogenesis of the ASMFP (Pilot data). (A) High magnificent images of Figure 24 showed that the SV2 (arrowhead), SYN1 & PSD93 colocalization (red arrow) were also labeled along the TUJ1 positive connection in the 0.7 μm, 1.5 μm, 3 μm ASMFPs groups, and flat membranes groups. (B) The quantification study showed that the number and total area of the SV2 positive puncta along the connection in 0.7 μm and 1.5 μm ASMFPs were significantly higher than the 3 μm ASMFP, glass and PCL flat membrane one ($F_{(4,115)}$= 50.22, P<0.0001 for puncta number, $F_{(4,115)}$= 44.84, P<0.0001 for total area, one-way ANOVA with post-hoc Tukey HSD Test; the total number of independent measurements between all treatment groups is 24, samples (n) were from 3 independent experiments). The number and total area of the PSD93 & SYN1 colocalization positive puncta along the connection in 0.7 μm and 1.5 μm ASMFPs were also significantly higher than the 3 μm ASMFP, glass and PCL flat membrane one ($F_{(4,115)}$= 41.88 P<0.0001 for puncta number, $F_{(4,115)}$= 39.71, P<0.0001 for total area, one-way ANOVA with post-hoc Tukey HSD Test; the total number of independent measurements between all treatment groups is 24, samples (n) were from 3 independent experiments). The data is collected using ASMFP produced by the same batch of the PCL solution. Scale bar is 10 μm in A.

In addition, the number and total area of the PSD93 & SYN1 colocalization positive puncta along the connection in 0.7 μm and 1.5 μm ASMFPs were also significantly higher than the 3 μm ASMFP, glass, and PCL flat membrane one (Figure 36; $F_{(4,115)}$= 41.88 for puncta number, $F_{(4,115)}$= 39.71 for puncta area, P<0.0001 for puncta number and total area, one-way ANOVA with post-hoc Tukey HSD Test; the total number of independent measurements between all treatment groups is 24, samples (n) were from 3 independent experiments). The result indicated that the

parts of the ASMFPs could simulate the synaptogenesis of the ESNs. The data is collected using ASMFP produced by the same batch of the PCL solution. Additional experiments are required to complete the project.

Discussion

The purpose of this study was to identify the role of topography in synaptogenesis. Previous papers showed that the ESC-derived ESNs contained immature synapses, which showed fewer synaptic markers along with the neural connection (Liu et al., 2018b). A biochemical method was used to simulate synaptogenesis (Liu et al., 2018b). However, the role of the topography in synaptogenesis is not clear. To study this aim, the ESC-derived NBs were seeded and cultured on the different sizes of the ASMFPs and their flat membrane (control for the topography). The multiply synapse protein markers were labeled the cells on the platforms for synapse identification and evaluation (Liu et al., 2018b). The results showed that the small size of the (0.7 μm and 1.5 μm) ASMFPs could stimulate the synaptogenesis between the ESNs connection, while the large size (3 μm) of the ASMFP could not.

In this chapter, we hypothesis that ASMFP could stimulate synaptogenesis between the ESNs connection. However, the result showed that only part of the ASMFP could stimulate synaptogenesis. The functional size was less than 1.5 μm ASFMPs. The average diameter of the ESN's neurite was also 1.5 μm (data do not show) (Liu et al., 2018b). It is not clear whether the size of neurite and fibers decided this simulation level. In addition, as the limitation of the technologies, the electrophysical activity of the new synapse were not evaluated on the platforms, which is a limitation in our conclusion regarding the role of the ASMFP in the synapse maturation.

In this dissertation, the submicro-fiber platform, which incorporated the TSP1 protein, were considered to stimulate the synaptogenesis between ESNs. However, the experiments showed that the small size ASMFPs (0.7 µm and 1.5 µm) could stimulate the synaptogenesis between ESNs. So, the TSP1 did not involve in the dissertation. The protein incorporated fiber system will be processed on the stem cell differentiation experiments to achieve other specific aims in future research.

In summary, the ESC-derived NBs were cultured on the ASMFP. Part of the ASMFP could stimulate synaptogenesis between the ESNs, suggesting that topography played a vital role in synaptogenesis. The electrophysiology evaluation would be processed on the ASMFP groups to test the synapse maturation in the future. In addition, the mechanism and intracellular pathway could be tested in the future experiments. The study and usage of biomaterial-induced neural differentiation will contribute to ECM-induced cell growth, differentiation, and maturation, while it also contributes to future clinical application.

CHAPTER 5 – CONCLUSIONS

This dissertation was mainly focused on the topography-induced the stem cell fate determination. Two similar types of fiber platforms, ACMFP and ASMFP, were designed, fabricated, and evaluated to achieve these aims. These fiber platforms have several advantages for use in stem cell research. Firstly, they have good biocompatibility showing little or no toxicity. Secondly, they are high or good in alignment. The fibers in the platform showed a parallel pattern that can use to build the parallel nerve tissue. Thirdly, their fiber size is controllable in different scale ranges. To mimic the whole size range from the micro-meter to the nano-meter, the ACMFP were designed into three size types: 60 μm, 90 μm, and 120 μm, while the ASMFP were also designed into three size-types which are 0.7 μm 1.5 μm, and 3 μm. Lastly, the platform's fibers show no gaps or no blank, which support an intact platform for cell attachment and growth. Moreover, Pluronic F127 and PDL/PLO were used to treat and overcome the ACMFP's shrinkage and ASMFP's hydrophobic. Overall, two good platforms were available for the topography-induced stem cell differentiation study. All ASMFP experiments were performed using ASMFP produced by the same batch of the PCL solution, so additional experiments are required to complete the project.

The ESCs derived NBs were cultured on the ACMFP and ASMFP to evaluate the role of the topography in neural differentiation, neurite outgrowth, and synaptogenesis (Table 8 &9). The results suggested that the micro-pattern fiber did not influence the neural stem cell differentiation. All the fiber platforms could stimulate neural differentiation. The micro-pattern made this effect by inhibiting cell proliferation. Small submicro- & nano-fiber pattern could inhibit the glia differentiation. In addition, the small micro-fiber pattern and submicro- & nano-fiber

pattern could guide the neurite outgrowth direction. The effect of this stimulation was decrease as the fiber size increase, which showed a linear tendency. Lastly, small size of the submicro- & nano-fiber pattern could simulate the synaptogenesis between the ESNs. In conclusion, the fiber-pattern topography seems to contribute the neural differentiation and maturation, which play a crucial role in stem cell fate determination.

Table 8. Conclusion for the stem cell fate on the ACMFPs

Group	Neural stem cell differentiation	Neural differentiation	Glia differentiation	Cell attachment	Cell proliferation	Neurite outgrowth direction
PLGA flat	----	----	----	----	----	----
60 μm	----	↑↑	↑	N/A	N/A	↑↑
90 μm	----	↑↑	↑	----	↓↓	↑↑
120 μm	----	↑↑	↑	N/A	N/A	----

(---- means no significant difference; ↑means significant increase; ↓means significant decrease; N/A means not test).

Table 9. Conclusion for the stem cell fate on the ASMFPs (Pilot data)

Group	Neural differentiation	Glia differentiation	Neurite outgrowth direction	Synaptogenesis
Glass flat	----	----	----	----
PCL flat	----	----	----	----
0.7 μm	↑↑↑	↓↓	↑↑↑	↑↑
1.5 μm	↑↑↑	↓↓	↑↑	↑↑
3 μm	↑↑	----	↑	----

(---- means no significant difference; ↑means significant increase; ↓means significant decrease).

APPENDIX A

Copyright License Agreement for Chapter 1

Copyright Clearance Center | RightsLink®

Home | Help | Email Support | Sign in | Create Account

Embryonic Stem Cell-Derived Peripheral Auditory Neurons Form Neural Connections with Mouse Central Auditory Neurons In Vitro via the α2δ1 Receptor

Author: Zhenjie Liu,Yiyun Jiang,Xiaoyang Li,Zhengqing Hu

Publication: Stem Cell Reports

Publisher: Elsevier

Date: 10 July 2018

© 2018 The Author(s).

Journal Author Rights

BACK | CLOSE WINDOW

APPENDIX B

Copyright License Agreement for Chapters 2 & 3

APPENDIX C

IACUC Protocol Approval Letter

WAYNE STATE UNIVERSITY

Institutional Animal Care and Use Committee

87 East Canfield, Second Floor
Detroit, MI 48201
Phone: (313) 577-1629
www.research.wayne.edu/iacuc/

ANIMAL WELFARE ASSURANCE # D16-00198 (A3310-01)

TO: Zhengqing Hu
Otolaryngology, Head & Neck Surgery

FROM: Institutional Animal Care and Use Committee

DATE: January 31, 2018

SUBJECT: Approval of Protocol IACUC-17-11-0387

TITLE: Dr. Hu's lab stem cell research core project

Protocol Effective Period: January 31, 2018 - January 30, 2021

Your animal research protocol has been approved by the Wayne State University Institutional Animal Care and Use Committee (IACUC).

Be advised that this protocol must be reviewed by the IACUC on an annual basis to remain active. Any changes (e.g. procedures, lab personnel, strains, additional numbers of animals) must be submitted as amendments and require prior approval by the IACUC. Any animal work on this research protocol beyond the expiration date will require the submission of a new IACUC protocol application for committee review and approval.

The *Guide for the Care and Use of Laboratory Animals* (the Guide, NRC 2011) is the primary reference used for standards of animal care at Wayne State University. The University has submitted an appropriate assurance statement to the Office for Laboratory Animal Welfare (OLAW) of the National Institutes of Health. The animal care program at Wayne State University is accredited by the Association for Assessment and Accreditation of Laboratory Animal Care International (AAALAC).

REFERENCES

1.   Aamodt, J.M., and Grainger, D.W. (2016). Extracellular matrix-based biomaterial scaffolds and the host response. Biomaterials *86*, 68-82.

2.   Alexander, J.K., Fuss, B., and Colello, R.J. (2006). Electric field-induced astrocyte alignment directs neurite outgrowth. Neuron Glia Biol *2*, 93-103.

3.   Alizadeh, R., Zarrintaj, P., Kamrava, S.K., Bagher, Z., Farhadi, M., Heidari, F., Komeili, A., Gutierrez, T.J., and Saeb, M.R. (2019). Conductive hydrogels based on agarose/alginate/chitosan for neural disorder therapy. Carbohydr Polym *224*, 115-161.

4.   Ashammakhi, N., Kim, H.J., Ehsanipour, A., Bierman, R.D., Kaarela, O., Xue, C., Khademhosseini, A., and Seidlits, S.K. (2019). Regenerative Therapies for Spinal Cord Injury. Tissue Eng Part B Rev *25*, 471-491.

5.   Ashe, S., Behera, S., Dash, P., Nayak, D., and Nayak, B. (2020). Gelatin carrageenan sericin hydrogel composites improves cell viability of cryopreserved SaOS-2 cells. Int J Biol Macromol *154*, 606-620.

6.   Astete, C.E., and Sabliov, C.M. (2006). Synthesis and characterization of PLGA nanoparticles. J Biomater Sci Polym Ed *17*, 247-289.

7.   Bagno, L., Hatzistergos, K.E., Balkan, W., and Hare, J.M. (2018). Mesenchymal Stem Cell-Based Therapy for Cardiovascular Disease: Progress and Challenges. Mol Ther *26*, 1610-1623.

8.   Baldwin, T. (2009). Morality and human embryo research. Introduction to the Talking Point on morality and human embryo research. EMBO Rep *10*, 299-300.

9.   Bax, D.V., Davidenko, N., Hamaia, S.W., Farndale, R.W., Best, S.M., and Cameron, R.E.

(2019). Impact of UV- and carbodiimide-based crosslinking on the integrin-binding properties of collagen-based materials. Acta Biomater *100*, 280-291.

10.   Belzner, K.A., and Seal, B.C. (2009). Children with cochlear implants: a review of demographics and communication outcomes. Am Ann Deaf *154*, 311-333.

11.   Bhardwaj, N., Chouhan, D., and Mandal, B.B. (2017). Tissue Engineered Skin and Wound Healing: Current Strategies and Future Directions. Curr Pharm Des *23*, 3455-3482.

12.   Bhardwaj, N., and Kundu, S.C. (2010). Electrospinning: a fascinating fiber fabrication technique. Biotechnol Adv *28*, 325-347.

13.   Biswas, A., and Hutchins, R. (2007). Embryonic stem cells. Stem Cells Dev *16*, 213-222.

14.   Blanco-Suarez, E., Liu, T.F., Kopelevich, A., and Allen, N.J. (2018). Astrocyte-Secreted Chordin-like 1 Drives Synapse Maturation and Limits Plasticity by Increasing Synaptic GluA2 AMPA Receptors. Neuron *100*, 1116-1132.

15.   Cacabelos, R., Torrellas, C., Fernandez-Novoa, L., and Lopez-Munoz, F. (2016). Histamine and Immune Biomarkers in CNS Disorders. Mediators Inflamm *2016*, 1-10.

16.   Carricondo, F., and Romero-Gomez, B. (2019). The Cochlear Spiral Ganglion Neurons: The Auditory Portion of the VIII Nerve. Anat Rec (Hoboken) *302*, 463-471.

17.   Cha, B.H., Shin, S.R., Leijten, J., Li, Y.C., Singh, S., Liu, J.C., Annabi, N., Abdi, R., Dokmeci, M.R., Vrana, N.E.*, et al.* (2017). Integrin-Mediated Interactions Control Macrophage Polarization in 3D Hydrogels. Adv Healthc Mater *6*, 1-22.

18.   Chen, J., Hong, F., Zhang, C., Li, L., Wang, C., Shi, H., Fu, Y., and Wang, J. (2018). Differentiation and transplantation of human induced pluripotent stem cell-derived otic epithelial progenitors in mouse cochlea. Stem Cell Res Ther *9*, 230, 1-15

19.   Chen, P., Cui, L., Fu, S.C., Shen, L., Zhang, W., You, T., Ong, T.Y., Liu, Y., Yung, S.H., and Jiang, C. (2020a). The 3D-Printed PLGA Scaffolds Loaded with Bone Marrow-Derived Mesenchymal Stem Cells Augment the Healing of Rotator Cuff Repair in the Rabbits. Cell Transplant *29*, 1-18.

20.   Chen, S., Galuskova, D., Kankova, H., Zheng, K., Michalek, M., Liverani, L., Galusek, D., and Boccaccini, A.R. (2020b). Electrospun PCL Fiber Mats Incorporating Multi-Targeted B and Co Co-Doped Bioactive Glass Nanoparticles for Angiogenesis. Materials (Basel) *13*, 1-15.

21.   Cheng, K., and Kisaalita, W.S. (2010). Exploring cellular adhesion and differentiation in a micro-/nano-hybrid polymer scaffold. Biotechnol Prog *26*, 838-846.

22.   Chew, S.A., and Danti, S. (2017). Biomaterial-Based Implantable Devices for Cancer Therapy. Adv Healthc Mater *6*, 1-13.

23.   Cohen, B.E., Durstenfeld, A., and Roehm, P.C. (2014). Viral causes of hearing loss: a review for hearing health professionals. Trends Hear *18*, 1-17.

24.   Contrera, K.J., Wallhagen, M.I., Mamo, S.K., Oh, E.S., and Lin, F.R. (2016). Hearing Loss Health Care for Older Adults. J Am Board Fam Med *29*, 394-403.

25.   Craff, M.N., Zeballos, J.L., Johnson, T.S., Ranka, M.P., Howard, R., Motarjem, P., Randolph, M.A., and Winograd, J.M. (2007). Embryonic stem cell-derived motor neurons preserve muscle after peripheral nerve injury. Plast Reconstr Surg *119*, 235-245.

26.   Dietrich, M., Le Roy, H., Bruckner, D.B., Engelke, H., Zantl, R., Radler, J.O., and Broedersz, C.P. (2018). Guiding 3D cell migration in deformed synthetic hydrogel microstructures. Soft Matter *14*, 2816-2826.

27.   Dong, J., Zhu, G., Wang, T.C., and Shi, F.S. (2017). Ginsenoside Rg1 promotes neural

differentiation of mouse adipose-derived stem cells via the miRNA-124 signaling pathway. J Zhejiang Univ Sci B *18*, 445-448.

28. Du, B., Yin, H., Chen, Y., Lin, W., Wang, Y., Zhao, D., Wang, G., He, X., Li, J., Li, Z*., et al.* (2020). A waterborne polyurethane 3D scaffold containing PLGA with a controllable degradation rate and an anti-inflammatory effect for potential applications in neural tissue repair. J Mater Chem B *8*, 4434-4446.

29. Epstein, S., and Reilly, J.S. (1989). Sensorineural hearing loss. Pediatr Clin North Am *36*, 1501-1520.

30. Fang, X., Zhang, C., Yu, Z., Li, W., Huang, Z., and Zhang, W. (2019). GDNF pretreatment overcomes Schwann cell phenotype mismatch to promote motor axon regeneration via sensory graft. Exp Neurol *318*, 258-266.

31. Feng, B., Wang, S., Hu, D., Fu, W., Wu, J., Hong, H., Domian, I.J., Li, F., and Liu, J. (2019). Bioresorbable electrospun gelatin/polycaprolactone nanofibrous membrane as a barrier to prevent cardiac postoperative adhesion. Acta Biomater *83*, 211-220.

32. Fisher, O.Z., Khademhosseini, A., Langer, R., and Peppas, N.A. (2010). Bioinspired materials for controlling stem cell fate. Acc Chem Res *43*, 419-428.

33. Fleischmann, G., Muller, T., Blasczyk, R., Sasaki, E., and Horn, P.A. (2009). Growth characteristics of the nonhuman primate embryonic stem cell line cjes001 depending on feeder cell treatment. Cloning Stem Cells *11*, 225-233.

34. Gao, L., Xu, W., Li, T., Chen, J., Shao, A., Yan, F., and Chen, G. (2018). Stem Cell Therapy: A Promising Therapeutic Method for Intracerebral Hemorrhage. Cell Transplant *27*, 1809-1824.

35.   Gao, X., Fraulob, M., and Haiat, G. (2019). Biomechanical behaviours of the bone-implant interface: a review. J R Soc Interface *16*, 20190259, 1-20.

36.   Golafshan, N., Kharaziha, M., and Alehosseini, M. (2018). A three-layered hollow tubular scaffold as an enhancement of nerve regeneration potential. Biomed Mater *13*, 065005.

37.   Gonzalez, R., Hamblin, M.H., and Lee, J.P. (2016). Neural Stem Cell Transplantation and CNS Diseases. CNS Neurol Disord Drug Targets *15*, 881-886.

38.   Goodwin, D.G., Jr., Boyer, I., Devahif, T., Gao, C., Frank, B.P., Lu, X., Kuwama, L., Gordon, T.B., Wang, J., Ranville, J.F.*, et al.* (2018). Biodegradation of Carbon Nanotube/Polymer Nanocomposites using a Monoculture. Environ Sci Technol *52*, 40-51.

39.   Govey, P.M., Loiselle, A.E., and Donahue, H.J. (2013). Biophysical regulation of stem cell differentiation. Curr Osteoporos Rep *11*, 83-91.

40.   Grijalvo, S., Nieto-Diaz, M., Maza, R.M., Eritja, R., and Diaz, D.D. (2019). Alginate Hydrogels as Scaffolds and Delivery Systems to Repair the Damaged Spinal Cord. Biotechnol J *14*, e1900275, 1-8.

41.   Grochowski, C., Radzikowska, E., and Maciejewski, R. (2018). Neural stem cell therapy-Brief review. Clin Neurol Neurosurg *173*, 8-14.

42.   Grossemy, S., Chan, P.P.Y., and Doran, P.M. (2019). Electrical stimulation of cell growth and neurogenesis using conductive and nonconductive microfibrous scaffolds. Integr Biol (Camb) *11*, 264-279.

43.   Gu, Q., Tomaskovic-Crook, E., Lozano, R., Chen, Y., Kapsa, R.M., Zhou, Q., Wallace, G.G., and Crook, J.M. (2016). Functional 3D Neural Mini-Tissues from Printed Gel-Based Bioink and Human Neural Stem Cells. Adv Healthc Mater *5*, 1429-1438.

44.   Hackelberg, S., Tuck, S.J., He, L., Rastogi, A., White, C., Liu, L., Prieskorn, D.M., Miller, R.J., Chan, C., Loomis, B.R.*, et al.* (2017). Nanofibrous scaffolds for the guidance of stem cell-derived neurons for auditory nerve regeneration. PLoS One *12*, e0180427, 1-26.

45.   Haldar, S., Sharma, A., Gupta, S., Chauhan, S., Roy, P., and Lahiri, D. (2019). Bioengineered smart trilayer skin tissue substitute for efficient deep wound healing. Mater Sci Eng C Mater Biol Appl *105*, 110-140.

46.   Han, F., and Hu, B. (2020). Stem Cell Therapy for Parkinson's Disease. Adv Exp Med Biol *1266*, 21-38.

47.   He, S., Nakada, D., and Morrison, S.J. (2009). Mechanisms of stem cell self-renewal. Annu Rev Cell Dev Biol *25*, 377-406.

48.   Hu, Z., Liu, Z., Li, X., and Deng, X. (2017). Stimulation of synapse formation between stem cell-derived neurons and native brainstem auditory neurons. Sci Rep *7*, 13843, 1-12.

49.   Hu, Z., Tao, L., Liu, Z., Jiang, Y., and Deng, X. (2019). Identification of Neural Stem Cells from Postnatal Mouse Auditory Cortex In Vitro. Stem Cells Dev *28*, 860-870.

50.   Huang, L., and Zhang, L. (2019). Neural stem cell therapies and hypoxic-ischemic brain injury. Prog Neurobiol *173*, 1-17.

51.   Hwang, C.M., Khademhosseini, A., Park, Y., Sun, K., and Lee, S.H. (2008). Microfluidic chip-based fabrication of PLGA microfiber scaffolds for tissue engineering. Langmuir *24*, 6845-6851.

52.   Jain, D., Mattiassi, S., Goh, E.L., and Yim, E.K.F. (2020). Extracellular matrix and biomimetic engineering microenvironment for neuronal differentiation. Neural Regen Res *15*, 573-585.

53.   Kapoor, D.N., Bhatia, A., Kaur, R., Sharma, R., Kaur, G., and Dhawan, S. (2015). PLGA: a unique polymer for drug delivery. Ther Deliv *6*, 41-58.

54.   Keung, A.J., Healy, K.E., Kumar, S., and Schaffer, D.V. (2010). Biophysics and dynamics of natural and engineered stem cell microenvironments. Wiley Interdiscip Rev Syst Biol Med *2*, 49-64.

55.   Kim, I.A., Park, S.A., Kim, Y.J., Kim, S.H., Shin, H.J., Lee, Y.J., Kang, S.G., and Shin, J.W. (2006). Effects of mechanical stimuli and microfiber-based substrate on neurite outgrowth and guidance. J Biosci Bioeng *101*, 120-126.

56.   Kim, M., Park, S.R., and Choi, B.H. (2014). Biomaterial scaffolds used for the regeneration of spinal cord injury (SCI). Histol Histopathol *29*, 1395-1408.

57.   Kuhn, L.T., Liu, Y., Boyd, N.L., Dennis, J.E., Jiang, X., Xin, X., Charles, L.F., Wang, L., Aguila, H.L., Rowe, D.W.*, et al.* (2014). Developmental-like bone regeneration by human embryonic stem cell-derived mesenchymal cells. Tissue Eng Part A *20*, 365-377.

58.   Kuhn, M., Heman-Ackah, S.E., Shaikh, J.A., and Roehm, P.C. (2011). Sudden sensorineural hearing loss: a review of diagnosis, treatment, and prognosis. Trends Amplif *15*, 91-105.

59.   Lai, Y., Li, Y., Cao, H., Long, J., Wang, X., Li, L., Li, C., Jia, Q., Teng, B., Tang, T.*, et al.* (2019). Osteogenic magnesium incorporated into PLGA/TCP porous scaffold by 3D printing for repairing challenging bone defect. Biomaterials *197*, 207-219.

60.   Lanzoni, G., Linetsky, E., Correa, D., Messinger Cayetano, S., Alvarez, R.A., Kouroupis, D., Alvarez Gil, A., Poggioli, R., Ruiz, P., Marttos, A.C.*, et al.* (2021). Umbilical cord mesenchymal stem cells for COVID-19 acute respiratory distress syndrome: A double-blind, phase 1/2a, randomized controlled trial. Stem Cells Transl Med *10*, 660-673.

61. Lapointe, V.L., Fernandes, A.T., Bell, N.C., Stellacci, F., and Stevens, M.M. (2013). Nanoscale topography and chemistry affect embryonic stem cell self-renewal and early differentiation. Adv Healthc Mater *2*, 1644-1650.

62. Lau, P., and Hudson, L.D. (2010). MicroRNAs in neural cell differentiation. Brain Res *1338*, 14-19.

63. Leach, D.G., Young, S., and Hartgerink, J.D. (2019). Advances in immunotherapy delivery from implantable and injectable biomaterials. Acta Biomater *88*, 15-31.

64. Li, X., Aleardi, A., Wang, J., Zhou, Y., Andrade, R., and Hu, Z. (2016). Differentiation of Spiral Ganglion-Derived Neural Stem Cells into Functional Synaptogenetic Neurons. Stem Cells Dev *25*, 803-813.

65. Liang, X., Kristiansen, C.K., Vatne, G.H., Hong, Y., and Bindoff, L.A. (2020). Patient-specific neural progenitor cells derived from induced pluripotent stem cells offer a promise of good models for mitochondrial disease. Cell Tissue Res *380*, 15-30.

66. Lieu, J.E.C., Kenna, M., Anne, S., and Davidson, L. (2020). Hearing Loss in Children: A Review. JAMA *324*, 2195-2205.

67. Lim, T.C., and Spector, M. (2017). Biomaterials for Enhancing CNS Repair. Transl Stroke Res *8*, 57-64.

68. Lin, Y., Gil, C.H., and Yoder, M.C. (2017). Differentiation, Evaluation, and Application of Human Induced Pluripotent Stem Cell-Derived Endothelial Cells. Arterioscler Thromb Vasc Biol *37*, 2014-2025.

69. Liu, L., Michowski, W., Kolodziejczyk, A., and Sicinski, P. (2019). The cell cycle in stem cell proliferation, pluripotency and differentiation. Nat Cell Biol *21*, 1060-1067.

70.   Liu, P., Sun, L., Liu, P., Yu, W., Zhang, Q., Zhang, W., Ma, J., Liu, P., and Shen, J. (2018a). Surface modification of porous PLGA scaffolds with plasma for preventing dimensional shrinkage and promoting scaffold-cell/tissue interactions. J Mater Chem B *6*, 7605-7613.

71.   Liu, Z., and Hu, Z. (2018). Aligned contiguous microfiber platform enhances neural differentiation of embryonic stem cells. Sci Rep *8*, 60-87.

72.   Liu, Z., Jiang, Y., Li, X., and Hu, Z. (2018b). Embryonic Stem Cell-Derived Peripheral Auditory Neurons Form Neural Connections with Mouse Central Auditory Neurons In Vitro via the alpha2delta1 Receptor. Stem Cell Reports *11*, 157-170.

73.   Long, K.R., and Huttner, W.B. (2019). How the extracellular matrix shapes neural development. Open Biol *9*, 180-216.

74.   Lopez-Garcia, J., Lehocky, M., Humpolicek, P., and Saha, P. (2014). HaCaT Keratinocytes Response on Antimicrobial Atelocollagen Substrates: Extent of Cytotoxicity, Cell Viability and Proliferation. J Funct Biomater *5*, 43-57.

75.   Ludwig, T., and J, A.T. (2007). Defined, feeder-independent medium for human embryonic stem cell culture. Curr Protoc Stem Cell Biol *Chapter 1*, Unit 1C 2, 1-2.

76.   Lv, H., Wang, H., Zhang, Z., Yang, W., Liu, W., Li, Y., and Li, L. (2017). Biomaterial stiffness determines stem cell fate. Life Sci *178*, 42-48.

77.   Malczynska, P., Piotrowicz, Z., Drabarek, D., Langfort, J., and Chalimoniuk, M. (2019). [The role of the brain-derived neurotrophic factor (BDNF) in neurodegenerative processes and in the neuroregeneration mechanisms induced by increased physical activity]. Postepy Biochem *65*, 2-8.

78.   Mantecon-Oria, M., Diban, N., Berciano, M.T., Rivero, M.J., David, O., Lafarga, M., Tapia,

O., and Urtiaga, A. (2020). Hollow Fiber Membranes of PCL and PCL/Graphene as Scaffolds with Potential to Develop In Vitro Blood-Brain Barrier Models. Membranes (Basel) *10*.

79.   Martello, G., and Smith, A. (2014). The nature of embryonic stem cells. Annu Rev Cell Dev Biol *30*, 647-675.

80.   Mashinchian, O., Turner, L.A., Dalby, M.J., Laurent, S., Shokrgozar, M.A., Bonakdar, S., Imani, M., and Mahmoudi, M. (2015). Regulation of stem cell fate by nanomaterial substrates. Nanomedicine (Lond) *10*, 829-847.

81.   McCaig, C.D., Sangster, L., and Stewart, R. (2000). Neurotrophins enhance electric field-directed growth cone guidance and directed nerve branching. Dev Dyn *217*, 299-308.

82.   Mead, B., Berry, M., Logan, A., Scott, R.A., Leadbeater, W., and Scheven, B.A. (2015). Stem cell treatment of degenerative eye disease. Stem Cell Res *14*, 243-257.

83.   Menorca, R.M., Fussell, T.S., and Elfar, J.C. (2013). Nerve physiology: mechanisms of injury and recovery. Hand Clin *29*, 317-330.

84.   Michels, T.C., Duffy, M.T., and Rogers, D.J. (2019). Hearing Loss in Adults: Differential Diagnosis and Treatment. Am Fam Physician *100*, 98-108.

85.   Mo, X., Weber, H.J., and Ramakrishna, S. (2006). PCL-PGLA composite tubular scaffold preparation and biocompatibility investigation. Int J Artif Organs *29*, 790-799.

86.   Moran, M.C., Ruano, G., Cirisano, F., and Ferrari, M. (2019). Mammalian cell viability on hydrophobic and superhydrophobic fabrics. Mater Sci Eng C Mater Biol Appl *99*, 241-247.

87.   Morelli, S., Piscioneri, A., Salerno, S., and De Bartolo, L. (2021). Hollow Fiber and Nanofiber Membranes in Bioartificial Liver and Neuronal Tissue Engineering. Cells Tissues Organs, 1-30.

88. Mulwafu, W., Kuper, H., and Ensink, R.J. (2016). Prevalence and causes of hearing impairment in Africa. Trop Med Int Health *21*, 158-165.

89. Narayanan, G., Shen, J., Boy, R., Gupta, B.S., and Tonelli, A.E. (2018). Aliphatic Polyester Nanofibers Functionalized with Cyclodextrins and Cyclodextrin-Guest Inclusion Complexes. Polymers (Basel) *10*, 1-26.

90. Neto, E., Leitao, L., Sousa, D.M., Alves, C.J., Alencastre, I.S., Aguiar, P., and Lamghari, M. (2016). Compartmentalized Microfluidic Platforms: The Unrivaled Breakthrough of In Vitro Tools for Neurobiological Research. J Neurosci *36*, 11573-11584.

91. Nutma, E., van Gent, D., Amor, S., and Peferoen, L.A.N. (2020). Astrocyte and Oligodendrocyte Cross-Talk in the Central Nervous System. Cells *9*, 1-21.

92. O'Leary, C., Soriano, L., Fagan-Murphy, A., Ivankovic, I., Cavanagh, B., O'Brien, F.J., and Cryan, S.A. (2020). The Fabrication and in vitro Evaluation of Retinoic Acid-Loaded Electrospun Composite Biomaterials for Tracheal Tissue Regeneration. Front Bioeng Biotechnol *8*, 190, 1-12.

93. Ong, W., Lin, J., Bechler, M.E., Wang, K., Wang, M., Ffrench-Constant, C., and Chew, S.Y. (2018). Microfiber drug/gene delivery platform for study of myelination. Acta Biomater *75*, 152-160.

94. Onoe, H., Kato-Negishi, M., Itou, A., and Takeuchi, S. (2016). Differentiation Induction of Mouse Neural Stem Cells in Hydrogel Tubular Microenvironments with Controlled Tube Dimensions. Adv Healthc Mater *5*, 1104-1111.

95. Ouyang, L., Yao, R., Mao, S., Chen, X., Na, J., and Sun, W. (2015). Three-dimensional bioprinting of embryonic stem cells directs highly uniform embryoid body formation.

Biofabrication *7*, 044-101.

96.   Palay, S.L. (1956). Synapses in the central nervous system. J Biophys Biochem Cytol *2*, 193-202.

97.   Pan, L., North, H.A., Sahni, V., Jeong, S.J., McGuire, T.L., Berns, E.J., Stupp, S.I., and Kessler, J.A. (2014). beta1-Integrin and integrin linked kinase regulate astrocytic differentiation of neural stem cells. PLoS One *9*, e104335, 1-12.

98.   Perea, G., Navarrete, M., and Araque, A. (2009). Tripartite synapses: astrocytes process and control synaptic information. Trends Neurosci *32*, 421-431.

99.   Pospisil, T., Ferhatovic Hamzic, L., Brkic Ahmed, L., Lovric, M., Gajovic, S., and Frkanec, L. (2016). Synthesis, characterization and in vitro biocompatibility assessment of a novel tripeptide hydrogelator, as a promising scaffold for tissue engineering applications. Biomater Sci *4*, 1412-1416.

100.   Rabinovsky, E.D., Gelir, E., Gelir, S., Lui, H., Kattash, M., DeMayo, F.J., Shenaq, S.M., and Schwartz, R.J. (2003). Targeted expression of IGF-1 transgene to skeletal muscle accelerates muscle and motor neuron regeneration. FASEB J *17*, 53-55.

101.   Saveh-Shemshaki, N., L, S.N., and Laurencin, C.T. (2019). Nanofiber-based matrices for rotator cuff regenerative engineering. Acta Biomater *94*, 64-81.

102.   Schafer, D.P., Lehrman, E.K., Kautzman, A.G., Koyama, R., Mardinly, A.R., Yamasaki, R., Ransohoff, R.M., Greenberg, M.E., Barres, B.A., and Stevens, B. (2012). Microglia sculpt postnatal neural circuits in an activity and complement-dependent manner. Neuron *74*, 691-705.

103.   Shen, Y., Wang, G., Shen, N., Wu, J., and Liu, X. (2011). [Advances of research of

hydrophilic/hydrophobic surface effect on cell biologic behaviors in vitro]. Sheng Wu Yi Xue Gong Cheng Xue Za Zhi *28*, 1237-1241.

104. Shparberg, R.A., Glover, H.J., and Morris, M.B. (2019). Embryoid Body Differentiation of Mouse Embryonic Stem Cells into Neurectoderm and Neural Progenitors. Methods Mol Biol *2029*, 273-285.

105. Silantyeva, E.A., Nasir, W., Carpenter, J., Manahan, O., Becker, M.L., and Willits, R.K. (2018). Accelerated neural differentiation of mouse embryonic stem cells on aligned GYIGSR-functionalized nanofibers. Acta Biomater *75*, 129-139.

106. Sitt, A., Soukupova, J., Miller, D., Verdi, D., Zboril, R., Hess, H., and Lahann, J. (2016). Microscale Rockets and Picoliter Containers Engineered from Electrospun Polymeric Microtubes. Small *12*, 1432-1439.

107. Smith, M.J., Webber, B.R., Mohtashami, M., Stefanski, H.E., Zuniga-Pflucker, J.C., and Blazar, B.R. (2015). In Vitro T-Cell Generation From Adult, Embryonic, and Induced Pluripotent Stem Cells: Many Roads to One Destination. Stem Cells *33*, 3174-3180.

108. Stadelmann, C., Timmler, S., Barrantes-Freer, A., and Simons, M. (2019). Myelin in the Central Nervous System: Structure, Function, and Pathology. Physiol Rev *99*, 1381-1431.

109. Sun, Y., Jiao, Y., Wang, Y., Lu, D., and Yang, W. (2014). The strategy to improve gene transfection efficiency and biocompatibility of hyperbranched PAMAM with the cooperation of PEGylated hyperbranched PAMAM. Int J Pharm *465*, 112-119.

110. Tang, Y., Yu, P., and Cheng, L. (2017). Current progress in the derivation and therapeutic application of neural stem cells. Cell Death Dis *8*, e3108, 1-12.

111. Thomas, M., Arora, A., and Katti, D.S. (2014). Surface hydrophilicity of PLGA fibers governs

in vitro mineralization and osteogenic differentiation. Mater Sci Eng C Mater Biol Appl *45*, 320-332.

112. Thomson, J.A., Itskovitz-Eldor, J., Shapiro, S.S., Waknitz, M.A., Swiergiel, J.J., Marshall, V.S., and Jones, J.M. (1998). Embryonic stem cell lines derived from human blastocysts. Science *282*, 1145-1147.

113. Tran, A.P., Warren, P.M., and Silver, J. (2018). The Biology of Regeneration Failure and Success After Spinal Cord Injury. Physiol Rev *98*, 881-917.

114. Vanhee, S., De Mulder, K., Van Caeneghem, Y., Verstichel, G., Van Roy, N., Menten, B., Velghe, I., Philippe, J., De Bleser, D., Lambrecht, B.N.*, et al.* (2015). In vitro human embryonic stem cell hematopoiesis mimics MYB-independent yolk sac hematopoiesis. Haematologica *100*, 157-166.

115. Varoqueaux, F., Aramuni, G., Rawson, R.L., Mohrmann, R., Missler, M., Gottmann, K., Zhang, W., Sudhof, T.C., and Brose, N. (2006). Neuroligins determine synapse maturation and function. Neuron *51*, 741-754.

116. Vivi, V.K., Martins-Franchetti, S.M., and Attili-Angelis, D. (2019). Biodegradation of PCL and PVC: Chaetomium globosum (ATCC 16021) activity. Folia Microbiol (Praha) *64*, 1-7.

117. Wang, B., Zou, X., Zhang, H., Duan, D., Ju, L., Jiang, X., Sun, X., Zhao, C., Zhao, H., Guo, J.*, et al.* (2008). Establishment of an immortalized GABAergic neuronal progenitor cell line from embryonic ventral mesencephalon in the rat. Brain Res *1210*, 63-75.

118. Wang, Q., Shen, M., Li, W., Li, W., and Zhang, F. (2019). Controlled-release of fluazinam from biodegradable PLGA-based microspheres. J Environ Sci Health B *54*, 810-816.

119. Wei, J., Fan, Z., Yang, Z., Zhou, Y., Da, F., Zhou, L., Tao, W., and Wang, D. (2018). Leukemia

Inhibitory Factor Is Essential for the Self-Renewal of Embryonic Stem Cells from Nile Tilapia (Oreochromis niloticus) Through Stat3 Signaling. Stem Cells Dev *27*, 123-132.

120.   Xu, K., Zhu, C., Xie, J., Li, X., Zhang, Y., Yao, F., Gu, Z., and Yang, J. (2018). Enhanced vascularization of PCL porous scaffolds through VEGF-Fc modification. J Mater Chem B *6*, 4474-4485.

121.   Xue, J., Wu, T., Dai, Y., and Xia, Y. (2019). Electrospinning and Electrospun Nanofibers: Methods, Materials, and Applications. Chem Rev *119*, 5298-5415.

122.   Yan, Q., Fang, L., Wei, J., Xiao, G., Lv, M., Ma, Q., Liu, C., and Wang, W. (2017). Silicon nanowires enhanced proliferation and neuronal differentiation of neural stem cell with vertically surface microenvironment. J Biomater Sci Polym Ed *28*, 1394-1407.

123.   Yang, F., Murugan, R., Wang, S., and Ramakrishna, S. (2005). Electrospinning of nano/micro scale poly(L-lactic acid) aligned fibers and their potential in neural tissue engineering. Biomaterials *26*, 2603-2610.

124.   Yang, K., Yu, S.J., Lee, J.S., Lee, H.R., Chang, G.E., Seo, J., Lee, T., Cheong, E., Im, S.G., and Cho, S.W. (2017). Electroconductive nanoscale topography for enhanced neuronal differentiation and electrophysiological maturation of human neural stem cells. Nanoscale *9*, 18737-18752.

125.   Yang, L., Soonpaa, M.H., Adler, E.D., Roepke, T.K., Kattman, S.J., Kennedy, M., Henckaerts, E., Bonham, K., Abbott, G.W., Linden, R.M.*, et al.* (2008). Human cardiovascular progenitor cells develop from a KDR+ embryonic-stem-cell-derived population. Nature *453*, 524-528.

126.   Yeung, E., Fukunishi, T., Bai, Y., Bedja, D., Pitaktong, I., Mattson, G., Jeyaram, A., Lui, C.,

Ong, C.S., Inoue, T.*, et al.* (2019). Cardiac regeneration using human-induced pluripotent stem cell-derived biomaterial-free 3D-bioprinted cardiac patch in vivo. J Tissue Eng Regen Med *13*, 2031-2039.

127. Zhang, C., Li, H., Guo, Z., Xue, B., and Zhou, C. (2017). Fabrication of Hydroxyapatite Nanofiber via Electrospinning as a Carrier for Protein. J Nanosci Nanotechnol *17*, 1018-1024.

128. Zhang, L., Yang, P., Guo, R., Sun, J., Xie, R., and Yang, W. (2019). Multifunctional Mesoporous Polydopamine With Hydrophobic Paclitaxel For Photoacoustic Imaging-Guided Chemo-Photothermal Synergistic Therapy. Int J Nanomedicine *14*, 8647-8663.

129. Zhang, Q.Y., Zhang, Y.Y., Xie, J., Li, C.X., Chen, W.Y., Liu, B.L., Wu, X.A., Li, S.N., Huo, B., Jiang, L.H.*, et al.* (2014). Stiff substrates enhance cultured neuronal network activity. Sci Rep *4*, 6215, 1-8.

130. Zhang, S., Chen, X., Yu, J., Hong, B., Lei, Q., and Fang, W. (2016). Hydrophobic fractal surface from glycerol tripalmitate and the effects on C6 glioma cell growth. Colloids Surf B Biointerfaces *142*, 377-384.

131. Zhao, Z.B., An, S.S., Xie, H.J., Han, X.L., Wang, F.H., and Jiang, Y. (2015). The Relationship between the Hydrophilicity and Surface Chemical Composition Microphase Separation Structure of Multicomponent Silicone Hydrogels. J Phys Chem B *119*, 9780-9786.

132. Zheng, B., Bai, Y., Chen, H., Pan, H., Ji, W., Gong, X., Wu, X., Wang, H., and Chang, J. (2018a). Targeted delivery of tungsten oxide nanoparticles for multifunctional anti-tumor therapy via macrophages. Biomater Sci *6*, 1379-1389.

133. Zheng, Z., Liu, Y., Huang, W., Mo, Y., Lan, Y., Guo, R., and Cheng, B. (2018b). Neurotensin-

loaded PLGA/CNC composite nanofiber membranes accelerate diabetic wound healing. Artif Cells Nanomed Biotechnol *46*, 493-501.

134.   Zhu, Y., Li, X., Janairo, R.R.R., Kwong, G., Tsou, A.D., Chu, J.S., Wang, A., Yu, J., Wang, D., and Li, S. (2019). Matrix stiffness modulates the differentiation of neural crest stem cells in vivo. J Cell Physiol *234*, 7569-7578.

135.   Zimmermann, J.A., and Schaffer, D.V. (2019). Engineering biomaterials to control the neural differentiation of stem cells. Brain Res Bull *150*, 50-60.

ABSTRACT

THE ROLE OF BIOMATERIAL SUBSTRATE IN STEM CELL FATE DETERMINATION

by

ZHENJIE LIU

August 2021

Advisor: Dr. Zhengqing Hu

Major: Physiology

Degree: Doctor of Philosophy

The physical cues, which included topography, stiffness, and mechanical forces, can influence the stem cell renewal, differentiation, and maturation *in vivo* and *in vitro*. The nano-topography of the ECM can stimulate the neural differentiation of the stem cells, while the micro-topography of the ECM can guide the neurite outgrowth. However, the role and functional size of the micro- and nano-topography in the stem cell fate determination is not clear yet. To study this aim, two biomaterial based aligned fiber platforms (ACMFP and ASMFP) were designed, fabrication and evaluated to cover the micro-, submicro-, and nano-fiber topography, which used to study the neural differentiation and maturation of the ESCs. All these platforms were showed good alignment, contiguous, and biocompatibility via the physical factor assay, biocompatibility assay evaluation. The results showed three different gradient sizes of the platforms were fabricated in two type of platforms, which are 60 μm, 90 μm, 120 μm in ACMFPs and 0.7 μm, 1.5 μm, 3 μm in ASFMPs. The ESCs derived NBs were cultured on all platforms and their control flat membranes for six days, which followed with immunofluorescence staining. The result showed that all the ACMFPs and ASMFPs could stimulate the neural lineage cell differentiation. The

affection of the ACMFPs induced the neural differentiation stimulate may cause by limit the cell proliferation. Part of the ACMFPs and ASMFPs can guide the neurite outgrowth direction. Part of the ASMFPs can stimulate the synaptogenesis. Overall, the micro-, submicro-, and nano-fiber pattern platforms seem to play a key role in the stem cell determination with different stimulation levels and types. The study of the topography induced stem cell differentiation may contribute the stem cell research and open a new way for clinical therapy in the future.

AUTOBIOGRAPHICAL STATEMENT

ZHENJIE LIU

EDUCATION

2009- 2013   B.S. in Biotechnology and bioinformation, Tianjin Medical University

2013- 2015   M.S. in Biological Engineering, Illinois Institute of Technology

2016- 2021   Ph.D. in Physiology, Wayne State University, School of Medicine

HONORS & AWARDS

2017- 2018 Association for Research in Otolaryngology Travel Award.

2017- 2018 Marion I. Barnhart Graduate Student Award.

2017- 2018 Thomas C. Rumble University Graduate Fellowship.

2018- 2019 Association for Research in Otolaryngology Travel Award.

2018- 2019 Three-minute thesis competition in Dept of Physiology 3rd place.

2020- 2021 IBS Discretionary Fellowship award- AY.

PUBLICATIONS

1. Qin L, Niu Q, Li X, **Liu Z**, Xu Z, Ma Z, Liu Z. (2013). CTCF mediates long-range interaction between silencer Sis and enhancer Ei and inhibits VJ rearrangement in pre-B cell. Central European Journal of Immunology 38(3): 349-354.

2. Hu Z, **Liu Z**, Li X, and Deng X. (2017). Stimulation of synapse formation between stem cell-derived neurons and native brainstem auditory neurons. Sci Rep 7, 13843.

3. **Liu Z** and Hu Z. (2018). Aligned contiguous microfiber platform enhances neural differentiation of embryonic stem cells. Sci Rep 8, 6087. (Data involved in this thesis)

4. **Liu Z**, Jiang Y, Li X, and Hu Z. (2018). Embryonic Stem Cell-Derived Peripheral Auditory Neurons Form Neural Connections with Mouse Central Auditory Neurons In Vitro via the alpha2delta1 Receptor. Stem Cell Reports. 2018 Jul 10;11(1):157-170. doi: 10.1016/j.stemcr.2018.05.006. Epub 2018 Jun 7. (Data involved in this thesis)

5. Hu Z, Tao L, **Liu Z**, Jiang Y, Deng X. Identification of Neural Stem Cells from Postnatal Mouse. Stem Cells Dev. 2019 May 29. doi: 10.1089/scd.2018.0247.

6. Deng X, **Liu Z**, Li X, Zhou Y, Hu Z. Generation of new hair cells by DNA methyltransferase (Dnmt) inhibitor 5-azacytidine in a chemically-deafened mouse model. Sci Rep. 2019 May 29;9(1):7997. doi: 10.1038/s41598-019-44313-0. PMID: 31142766